7

Analysis of Laminates

7.1 Introduction

While an understanding of lamina mechanical behavior is essential to the development of theories for the analysis of composite structures, the unidirectional lamina alone is generally not very useful as a structural element because of its poor transverse properties. Composite structures are more likely to be in the form of laminates consisting of multiple laminae or plies oriented in the desired directions and bonded together in a structural unit. The virtually limitless combinations of ply materials, ply orientations, and ply-stacking sequences offered by laminated construction considerably enhance the design flexibility inherent in composite structures.

In this chapter, the analysis of laminates will be introduced by considering a simplified theory of laminated beams in pure flexure. This will be followed by a discussion of the more general Classical Lamination Theory (CLT), which makes it possible to analyze the complex coupling effects that may occur in laminates. Other aspects of laminate analysis, such as prediction of thermal and residual stresses, interlaminar stresses, and laminate strength are also discussed.

Because of the need for adequate description of many possible combinations of ply orientations and stacking sequences in laminates, a laminate orientation code has evolved in the composites literature. The basis of the code is that ply angles, separated by slashes, are listed in order from the top surface to the bottom surface and enclosed in square brackets, as shown by the examples in figure 7.1. Note that symmetric laminates can be described by listing only the ply angles for the top half of the laminate and by using the subscript "s" outside the brackets, and that adjacent plies having the same orientations can be described by using a numerical subscript on the appropriate ply angle. In the case of symmetric laminates having an odd number of plies, the center ply angle is denoted by an overbar. Sets of ply angles that are repeated in the laminate are identified by enclosing the set of angles in parentheses. The examples shown in figure 7.1 are for laminates consisting of plies of the same material. For

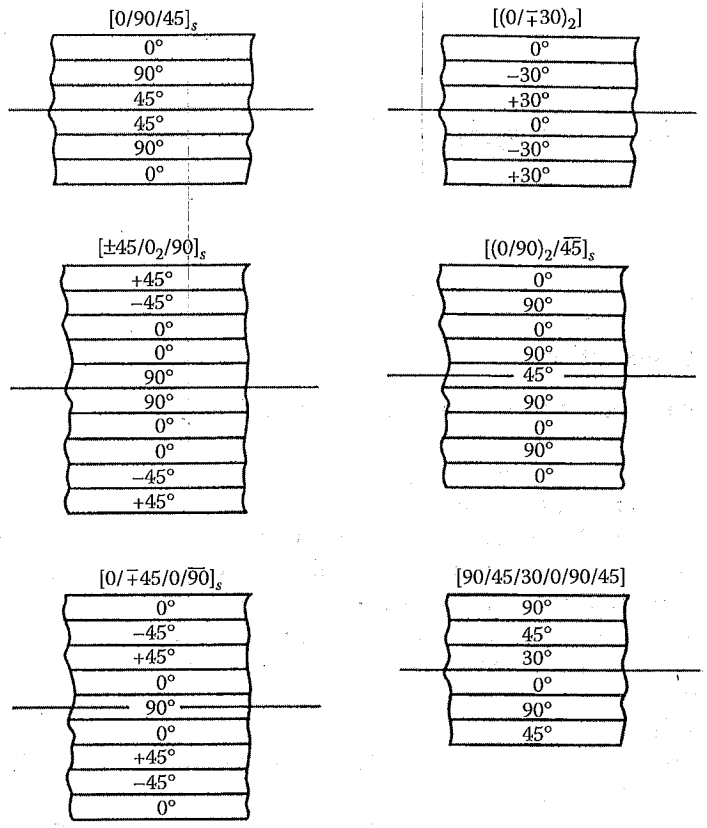

FIGURE 7.1
Examples of laminate stacking sequences and the corresponding laminate orientation codes.

hybrid laminates having plies of different materials, additional subscripts on the ply angles may be used to identify the ply material.

7.2 Theory of Laminated Beams in Pure Flexure

For the purpose of analysis, the simplest laminated structure is a laminated beam that is subjected to pure bending. A theory of laminated beams in pure flexure can be developed from the Bernoulli–Euler theory of elementary mechanics of materials. Although the application of this theory is quite restricted, it yields considerable insight into the analysis of

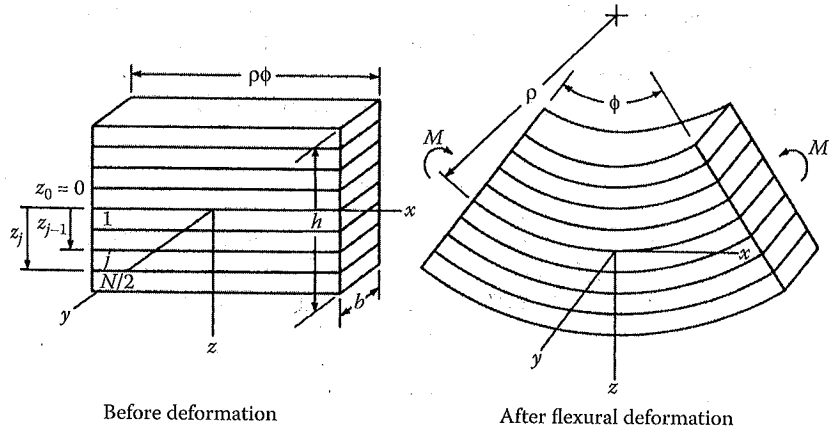

FIGURE 7.2
An element of a laminated beam before and after the application of a bending moment.

laminated structures and provides a natural introduction to the more general CLT, which is described in the next section. The theory described here is based on the analysis of Pagano [1].

A section of a rectangular laminated beam of depth h and width b is shown in figure 7.2 before and after the application of a bending moment M. The assumptions used in developing the analysis are as follows:

1. Plane sections that are initially normal to the longitudinal axis of the beam remain plane and normal during flexure.
2. The beam has both geometric and material property symmetry about the neutral surface (i.e., the plies are symmetrically arranged about the xy plane).
3. Each ply is linearly elastic with no shear coupling (i.e., ply orientations are either 0° or 90°).
4. The plies are perfectly bonded together, so that no slip occurs at ply interfaces.
5. The only stress components present are σ_x and τ_{xz}.

As a result of assumption 1, the longitudinal normal strain at a distance z from the neutral surface is given by the familiar equation

$$\varepsilon_x = \frac{(\rho + z)\phi - \rho\phi}{\rho\phi} = \frac{z}{\rho} \tag{7.1}$$

where ρ is the radius of curvature of the neutral surface during flexure, ϕ the angle defined in figure 7.2, and z the distance from neutral surface defined by the xy plane.

From assumption 3, the longitudinal stress in the jth ply is given by

$$(\sigma_x)_j = (E_x)_j(\varepsilon_x) \tag{7.2}$$

where $(E_x)_j$ is the Young's modulus of jth ply along the x direction and $(\varepsilon_x)_j$ is the longitudinal strain in the jth ply along the x direction. From equation (7.1) and equation (7.2), the longitudinal stress is seen to be

$$(\sigma_x)_j = (E_x)_j \frac{z}{\rho} \tag{7.3}$$

Static equilibrium requires that the applied bending moment M must be related to the longitudinal stresses by

$$M = 2\int_0^{h/2} \sigma_x z b \, dz \tag{7.4}$$

where the symmetry assumption 2 has been used. Substitution of equation (7.3) in equation (7.4) gives

$$M = \frac{2b}{3\rho}\sum_{j=1}^{N/2}(E_x)_j\left(z_j^3 - z_{j-1}^3\right) \tag{7.5}$$

where N is the total number of plies and z_j is the distance from the neutral surface to the outside of the jth ply. For an even number of plies of uniform thickness $z_j = jh/N$ and equation (7.5) becomes

$$M = \frac{2bh^3}{3\rho N^3}\sum_{j=1}^{N/2}(E_x)_j(3j^2 - 3j + 1) \tag{7.6}$$

Equation (7.6) can also be used for an odd number of plies if we simply divide each ply into two identical plies having half the thickness of the original ply, so that the total number of plies is now even.

Recall that for a homogeneous, isotropic beam, the moment–curvature relation is given by

$$M = \frac{E_f I_{yy}}{\rho} = \frac{E_f b h^3}{12\rho} \tag{7.7}$$

where $I_{yy} = \int z^2 dA = bh^3/12$ is the moment of inertia of the cross section about the neutral axis (y axis), A the cross-sectional area, and E_f the effective flexural modulus of the beam (which is same as Young's modulus of the beam material for a homogeneous, isotropic beam).

Combining equation (7.5) and equation (7.7), we find that the effective flexural modulus of the laminated beam can be expressed as

$$E_f = \frac{8}{h^3}\sum_{j=1}^{N/2}(E_x)_j\left(z_j^3 - z_{j-1}^3\right) \tag{7.8}$$

or for an even number of plies we can combine equation (7.6) and equation (7.7) to get

$$E_f = \frac{8}{N^3}\sum_{j=1}^{N/2}(E_x)_j(3j^2 - 3j + 1) \tag{7.9}$$

Thus, the flexural modulus of the laminated beam, unlike the Young's modulus of the homogeneous isotropic beam, depends on the ply-stacking sequence and the ply moduli. That is, if the properties do not change through the thickness of a beam, the flexural modulus is the same as the Young's modulus.

The deflections of laminated beams can now be calculated by using the flexural modulus in place of the Young's modulus in the beam deflection equations from elementary mechanics of materials. For example, the differential equation for the transverse deflection, w, of a laminated beam would be of the form

$$E_f I_{yy}\frac{d^2w}{dx^2} = M \tag{7.10}$$

and the maximum deflection at the tip of the laminated cantilever beam in figure 7.3 would be given by the familiar equation

$$w_{max} = \frac{PL^3}{3E_f I_{yy}} \quad \text{at} \quad x = L \tag{7.11}$$

where P is the applied tip load and L is the beam length. The Euler buckling load, P_{cr}, for a laminated beam can be estimated by the formula

$$P_{cr} = \frac{\pi^2 E_f I_{yy}}{L^2} \tag{7.12}$$

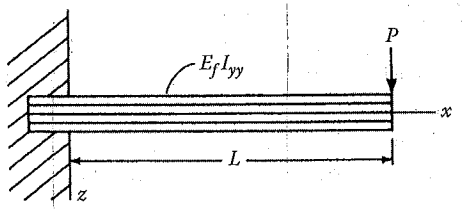

FIGURE 7.3
Cantilevered laminated beam under a concentrated tip load.

where L_e is the effective length that includes the effect of end conditions. Similarly, other beam equations involving the Young's modulus can now be modified for use with laminated beams.

An alternative expression for the stress in the jth ply can be obtained by combining equation (7.3) and equation (7.7) and by eliminating the radius of curvature:

$$(\sigma_x)_j = \frac{M}{E_f I_{yy}}(E_x)_j z = \frac{Mz}{I_{yy}}\left[\frac{(E_x)_j}{E_f}\right] \tag{7.13}$$

Thus, the term in square brackets can be thought of as a correction term, which when multiplied by the familiar homogeneous isotropic beam stress, Mz/I_{yy} gives the stress in the jth ply of the laminated beam. Another important observation is that the maximum stress in the laminated beam does not always occur on the outer surface as it does in the homogeneous, isotropic beam. At each section in a laminated beam, the ratio $M/E_f I_{yy}$ is constant, and the remaining term $(E_x)_j z$ determines the maximum stress. The maximum stress in the laminated beam therefore occurs in the ply having the greatest product of modulus $(E_x)_j$ and distance from the neutral axis, z. For the homogeneous isotropic beam, the stress at a given point in the cross section depends only on the distance z, and the maximum stress occurs at the outer surface where z is the greatest. The stress distributions in homogeneous isotropic beams and laminated beams are compared schematically in figure 7.4.

Failure of laminated beams can be estimated by using the stress from equation (7.13) in one of the failure criteria that was discussed in chapter 4. For example, if the jth ply is a longitudinal (0°) ply in compression, failure in this ply according to the Maximum Stress Criterion will occur when $(\sigma_{xmax})_j = s_L^{(-)}$, where $(\sigma_{xmax})_j$ is the maximum stress in the jth ply at $z = z_j$.

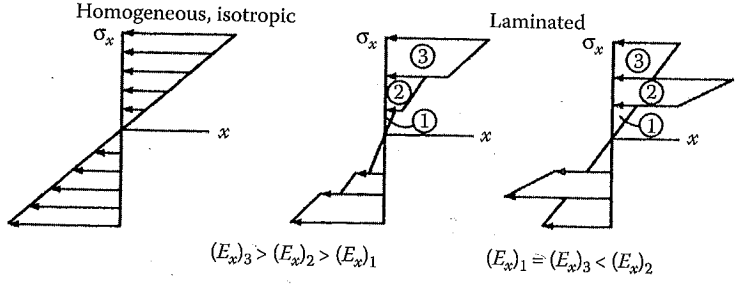

FIGURE 7.4
Stress distributions in homogeneous, isotropic beams and in laminated beams.

From equation (7.13), the applied bending moment that would cause this condition is

$$M_{max} = \frac{E_f I_{yy} s_L^{(-)}}{(E_1)_j z_j} \tag{7.14}$$

where $(E_1)_j$ is the longitudinal modulus of the jth ply. Similarly, for a transverse (90°) ply in tension the maximum bending moment is:

$$M_{max} = \frac{E_f I_{yy} s_T^{(+)}}{(E_2)_j z_j} \tag{7.15}$$

Laminate failure would therefore occur when the bending moment reaches the value that would cause first ply failure. This value can be determined by applying the failure criterion to each ply until the lowest M_{max} is found. The internal bending moment can be related to the external applied loads by the equations of static equilibrium, so that the applied loads corresponding to first ply failure can also be determined. Since the maximum stress does not necessarily occur on the outer surface, first ply failure may occur in an interior ply. One of the difficulties encountered in inspection for ply failure in laminates is that only failures on the outer surfaces can be observed with the naked eye. Interior ply failures can only be detected by methods such as ultrasonic or x-ray inspection.

In most practical cases, the applied loads on a beam would be such that not only bending moments but also transverse shear forces would be developed. These transverse shear forces cause corresponding transverse shear stresses. In laminated beams, the transverse shear stresses are often referred to as interlaminar shear stresses. Pagano [1] has also developed

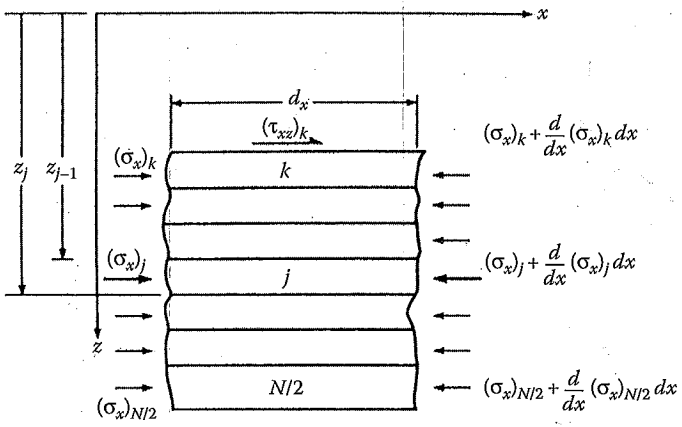

FIGURE 7.5
Differential element of a laminated beam showing interlaminar shear stress that is necessary for static equilibrium when the bending moment varies along the length.

a mechanics of materials approach for estimating these interlaminar shear stresses, as summarized here.

Recall from the mechanics of materials [2] that the bending moment, M, is related to the transverse shear force, V, by the equation

$$\frac{dM}{dx} = V \tag{7.16}$$

Thus, the presence of the shear force implies that the bending moment must change along the length of the beam (the x direction). From equation (7.13), we see that if the bending moment changes with respect to x, so, too, must the normal stress, σ_x. This means that the normal stresses acting on the two faces of the jth ply in a differential element must be different, as shown in figure 7.5. Since the element cannot be in static equilibrium under these normal stresses alone, the interlaminar shear stress, $(\tau_{xz})_k$, must act at the inner edge of the kth ply, as shown in figure 7.5. From static equilibrium of the element with respect to the forces along the x direction,

$$(\tau_{xz})_k dx + \sum_{j=k}^{N/2} \int_{z_{j-1}}^{z_j} (\sigma_x)_j dz - \sum_{j=k}^{N/2} \int_{z_{j-1}}^{z_j} \left[(\sigma_x)_j + \frac{d(\sigma_x)_j}{dx} dx \right] dz = 0 \tag{7.17}$$

or

$$(\tau_{xz})_k = \sum_{j=k}^{N/2} \int_{z_{j-1}}^{z_j} \frac{d(\sigma_x)_j}{dx} dz \tag{7.18}$$

Substituting equation (7.13) and equation (7.16) in equation (7.18) and integrating, we find that the interlaminar stress at the inner edge of the kth ply is

$$(\tau_{xz})_k = \frac{V}{E_f I_{yy}} \sum_{j=k}^{N/2} \int_{z_{j-1}}^{z_j} (E_x)_j z dz \tag{7.19}$$

for a rectangular beam having an even number of plies of uniform thickness, $z_j = jh/N$, and equation (7.19) reduces to

$$(\tau_{xz})_k = \frac{3V}{2bh} \left[\frac{S}{E_f} \right] \tag{7.20}$$

where

$$S = \frac{4}{N^2} \sum_{j=k}^{N/2} (E_x)_j (2j-1) \tag{7.21}$$

Equation (7.20) is seen to be similar to the "mechanics of materials" equation for transverse shear stress in a homogeneous isotropic beam, which is

$$\tau_{xy} = \frac{3V}{2bh} \left[1 - 4\left(\frac{z}{h}\right)^2 \right] \tag{7.22}$$

Thus, the transverse shear stress is given by

$$\tau_{xy} = \frac{3V}{2bh} \beta \tag{7.23}$$

where

$$\beta = \begin{cases} 1 - 4\left(\frac{z}{h}\right)^2 & \text{for a homogeneous isotropic beam} \\ \frac{S}{E_f} & \text{for a laminated beam} \end{cases}$$

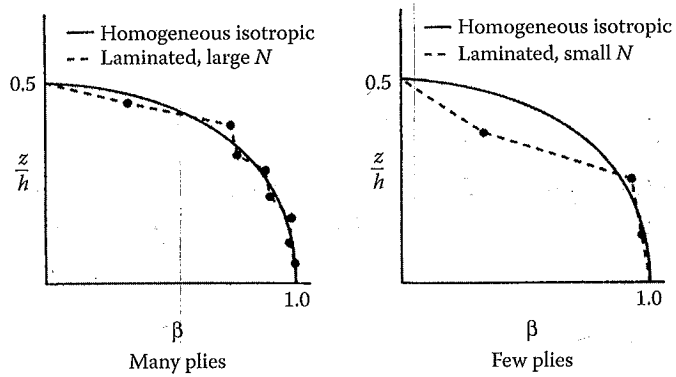

FIGURE 7.6
Variation of shear stress, as governed by the factor β, across half the beam thickness for homogeneous, isotropic beams and for laminated beams. Results are given for laminated beams with a small number of plies and a large number of plies.

The shear stress distribution, as governed by the variation of the factor β, is shown for both types of beams in figure 7.6. As the number of plies increases, the shear stress distribution for the laminated beam can be expected to approach the parabolic distribution described by equation (7.22). For a small number of plies, however, the laminated beam shear stress distribution departs significantly from the parabolic distribution.

Interlaminar stresses are responsible for an important failure mode in composites known as delamination. Recall that the failure criteria discussed in chapter 4 were based only on in-plane stresses in the lamina. Both normal and shear components of the interlaminar stresses in laminated plates along with failure criteria, which include the interlaminar stresses, will be discussed later.

EXAMPLE 7.1

Determine the flexural and Young's moduli of E-glass/epoxy laminated beams having stacking sequences of $[0/90/0]_s$ *and* $[90/0/90]_s$. *The ply moduli are* $E_1 = 5 \times 10^6$ *psi (34.48 GPa) and* $E_2 = 1.5 \times 10^6$ *psi (10.34 GPa), and the plies all have the same thickness.*

Solution. The total number of plies is $N = 6$ in each case, and only the stacking sequences are different. Since the ply thicknesses are all the same, we can use equation (7.9) for the flexural modulus in both cases. For the $[0/90/0]_s$ beam

$$E_f = \frac{8}{N^3}\sum_{j=1}^{N/2}(E_x)_j(3j^2 - 3j - 3j + 1)$$

or

$$E_f = \frac{8}{(6)^3}\{5[3(1)^2 - 3 + 1] + 1.5[3(2)^2 - 3(2) + 1] + 5[3(3)^2 - 3(3) + 1]\} \times 10^6 \text{ psi}$$

$$= 4.09 \times 10^6 \text{psi} (28.2 \text{ GPa})$$

The Young's modulus, or extensional modulus, can be estimated by using the rule of mixtures

$$E_x = E_1 \upsilon_1 + E_2 \upsilon_2$$

where υ_1 = volume fraction of longitudinal (0°) plies and υ_2 = volume fraction of transverse (90°) plies. Therefore,

$$E_x = \left[5\left(\frac{4}{6}\right) + 1.5\left(\frac{2}{6}\right)\right] \times 10^6 \text{psi} = 3.83 \times 10^6 \text{psi} \qquad (26.4 \text{GPa})$$

For the $[90/0/90]_s$ beam

$$E_f = \frac{8}{(6)^3}\{1.5(1) + 5(7) + 1.5(19)\} \times 10^6 \text{psi} = 2.4 \times 10^6 \text{psi} (16.55 \text{ GPa})$$

and

$$E_x = \left[1.5\left(\tfrac{4}{6}\right) + 5\left(\tfrac{2}{6}\right)\right] \times 10^6 \text{psi} = 2.66 \times 10^6 \text{psi} \quad (18.34 \text{ GPa})$$

Note that the flexural modulus depends on the stacking sequence and is not the same as the Young's modulus. The Young's modulus does not depend on the stacking sequence (i.e., the rule of mixtures gives the same result regardless of the ply-stacking sequence, as long as the number of longitudinal and transverse plies remains unchanged).

EXAMPLE 7.2

For the $[90/0/90]_s$, *E-glass/epoxy beam described in example 7.1, sketch the distribution of normal and shear stresses through the thickness of the beam. Assume a ply thickness of 0.01 in (0.254 mm).*

Solution. The normal stress is given by equation (7.13), but the ratio $M/E_f I_{yy}$ is constant for a given cross section, and the stress distribution across the thickness is governed by the product $(E_x)_j z$. The

be determined to within a constant $K_1 = M/E_1 I_{yy}$ by finding the corresponding variation of $(E_x)_j z$.

For the outer surface of ply number 3 (the outer transverse ply), the ply modulus is $(E_x)_3 = E_2 = 1.5 \times 10^6$ psi, $z = 0.03$ in and the stress is $\sigma_x = K_1(1.5 \times 10^6)(0.03) = 4.5 \times 10^4 K_1$.

For the inner surface of ply number 3, $z = 0.02$ in and the stress is $\sigma_x = K_1(1.5 \times 10^6)(0.02) = 3.0 \times 10^4 K_1$.

Similarly, for the outer surface of ply number 2, the stress is $\sigma_x = K_1(5 \times 10^6)(0.02) = 10 \times 10^4 K_1$.

For the inner surface of ply number 2, $\sigma_x = K_1(5 \times 10^6)(0.01) = 5 \times 10^4 K_1$.

For the outer surface of ply number 1, $\sigma_x = K_1(1.5 \times 10^6)(0.01) = 1.5 \times 10^4 K_1$.

For the inner surface of ply number 1 (on the neutral surface), $\sigma_x = 0$.

The predicted distribution of σ_x across the thickness is plotted in figure 7.7(a). It is seen that the maximum normal stress occurs not on the outer surface as in a homogeneous isotropic beam but, rather, at the outer edge of ply number 2.

The interlaminar shear stress at the inner surface of the kth ply for a beam with an even number of uniform thickness plies is given by equation (7.20) and equation (7.21). For a given cross section, however, the ratio $3V/2bhE_f$ can be set equal to a constant, K_2, and the shear stress can be written as $(\tau_{xz})_k = K_2 S$, where S is defined by equation (7.21). The shear stress distribution can then be determined to within a constant K_2 by finding the variation of S across the thickness.

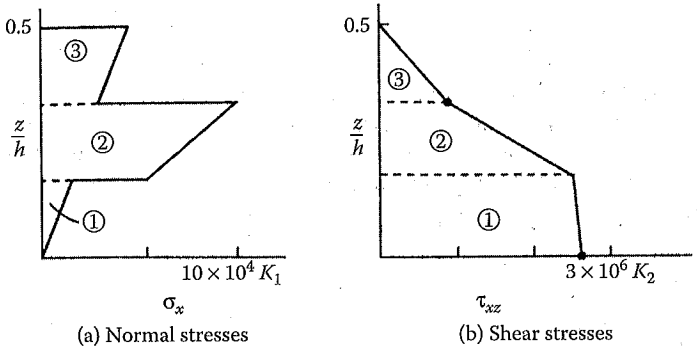

FIGURE 7.7
Stress distributions for the beam described in example 7.2.

From equation (7.20) and equation (7.21),

$$(\tau_{xz})_k = \frac{3V}{2bh}\left[\frac{S}{E_f}\right] = K_2 S$$

$$\text{where} \quad S = \frac{4}{N^2}\sum_{j=k}^{N/2}(E_x)_j(2j-1)$$

for $k = 1$

$$S = \frac{4}{(6)^2}\{1.5[2(1)-1]+5[2(2)-1]+1.5[2(3)-1]\}\times 10^6$$

$$= 2.66 \times 10^6 \text{ psi (18.34 GPa)}$$

For $k = 2$

$$S = \frac{4}{(6)^2}\{5[2(2)-1]+1.5[2(3)-1]\}\times 10^6$$

$$= 2.5 \times 10^6 \text{ psi (17.24 GPa)}$$

For $k = 3$

$$S = \frac{4}{(6)^2}\{1.5[2(3)-1]\}\times 10^6$$

$$= 0.833 \times 10^6 \text{ psi (5.74 GPa)}$$

Finally, for k = 4, equation (7.20) gives the shear stress at the inner surface of an "imaginary ply" whose inner surface is the same as the outer surface of ply number 3 or the outer surface of the laminate. Since there is no material in this "imaginary ply," S = 0 and the shear stress must be zero on the outer surface. This also satisfies the boundary condition that the outer surface must be stress-free. The predicted distribution of τ_{xz} across the thickness is plotted in figure 7.7(b). As with the shear stress in a homogeneous isotropic beam, the maximum shear stress occurs on the neutral surface and the shear stress at the outer surface is zero. The deviation from the parabolic distribution is substantial, however, because of the small number of plies.

7.3 Theory of Laminated Plates with Coupling

While the simplified theory of laminated beams in pure flexure is useful and instructive, it is restricted to symmetric laminates without coupling that are subjected to a single bending moment. In this section, we will discuss the more general CLT, which does not have these restrictions. Using this theory, we can analyze nonsymmetric laminates whose arbitrarily oriented plies may have various coupling effects that may lead to complex combinations of extensional, flexural, and torsional deformations. In addition, in-plane loading due to shear and axial forces and both bending and twisting moments are included. The most important limitation of the CLT is that each ply is assumed to be in a state of plane stress and that interlaminar stresses are neglected.

What is now referred to as the CLT has apparently evolved from work in the 1950s and 1960s by investigators such as Smith [3], Pister and Dong [4], Reissner and Stavsky [5], Stavsky [6], Lekhnitskii [7], and Stavsky and Hoff [8]. The major difference between this theory and the classical theory of homogeneous, isotropic plates [9] is in the form of the lamina stress-strain relationships. Other elements of the theory such as the deformation hypothesis, the equilibrium equations (Appendix A), and the strain–displacement relationships (Appendix B) are the same as those used in the classical plate theory [9].

Although the laminate is made up of multiple laminae, it is assumed that the individual laminae are perfectly bonded together so as to behave as a unitary, nonhomogeneous anisotropic plate. Interfacial slip is not allowed, and the interfacial bonds are not allowed to deform in shear, which means that displacements across lamina interfaces are assumed to be continuous. These assumptions mean that the deformation hypothesis from the classical homogeneous plate theory can be used for the laminated plate. The laminate force–deformation equations resulting from this deformation hypothesis are now derived following the procedure outlined by Whitney [10]. Although Whitney has presented a general analysis including the equations of motion, only the static analysis will be considered here.

Figure 7.8 defines the coordinate system to be used in developing the laminated plate analysis. The *xyz* coordinate system is assumed to have its origin on the middle surface of the plate, so that the middle surface lies in the *xy* plane. The displacements at a point in the *x*, *y*, and *z* directions are u, v, and w, respectively. The basic assumptions relevant to the present static analysis are [10]:

1. The plate consists of orthotropic laminae bonded together, with the principal material axes of the orthotropic laminae oriented along arbitrary directions with respect to the *xy* axes.

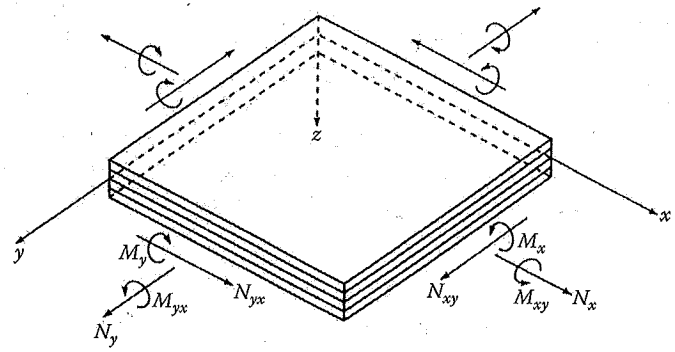

FIGURE 7.8
Coordinate system and stress resultants for laminated plate.

2. The thickness of the plate, t, is much smaller than the lengths along the plate edges, a and b.
3. The displacements u, v, and w are small compared with the plate thickness.
4. The in-plane strains ε_x, ε_y, and γ_{xy} are small compared with unity.
5. Transverse shear strains γ_{xz} and γ_{yz} are negligible.
6. Tangential displacements u and v are linear functions of the z coordinate.
7. The transverse normal strain ε_z is negligible.
8. Each ply obeys Hooke's law.
9. The plate thickness t is constant.
10. Transverse shear stresses τ_{xz} and τ_{yz} vanish on the plate surfaces defined by $z = \pm t/2$.

Assumption 5 is a result of the assumed state of plane stress in each ply, whereas assumptions 5 and 6 together define the Kirchhoff deformation hypothesis that normals to the middle surface remain straight and normal during deformation. According to assumptions 6 and 7, the displacements can be expressed as

$$\begin{aligned} u &= u^0(x,y) + zF_1(x,y) \\ v &= v^0(x,y) + zF_2(x,y) \\ w &= w^0(x,y) = w(x,y) \end{aligned} \tag{7.24}$$

where u^0 and v^0 are the tangential displacements of the middle surface along the x and y directions, respectively. Due to assumption 7, the

displacement at the middle surface, $w^0(x, y)$, is the same as the transverse displacement of any point having the same x and y coordinates, so $w^0(x, y) = w(x, y)$. At this point it is appropriate to mention that in order to account for possible warping of the cross section of the laminate and resulting transverse shear deformations, it is necessary to use a so-called higher-order lamination theory. For example, Christensen [11] describes one such theory, which is based on the assumption that the displacements are *nonlinear* functions of the z coordinate as follows:

$$\begin{aligned} u &= u^0(x,y) + z\psi_x(x,y) + z^2\zeta_x(x,y) + z^3\phi_x(x,y) \\ \upsilon &= \upsilon^0(x,y) + z\psi_y(x,y) + z^2\zeta_y(x,y) + z^3\phi_y(x,y) \\ w &= w^0(x,y) + z\psi_z(x,y) + z^2\zeta_z(x,y) \end{aligned} \tag{7.25}$$

Such a theory is beyond the scope of this book, however, and we will only develop the CLT based on equation (7.24). Substituting equations (7.24) in the strain–displacement equations (Appendix B) for the transverse shear strains and using assumption 5, we find that

$$\begin{aligned} \gamma_{xz} &= \frac{\partial u}{\partial z} + \frac{\partial w}{\partial x} = F_1(x,y) + \frac{\partial w}{\partial x} = 0 \\ \gamma_{yz} &= \frac{\partial \upsilon}{\partial z} + \frac{\partial w}{\partial y} = F_2(x,y) + \frac{\partial w}{\partial x} = 0 \end{aligned} \tag{7.26}$$

and that

$$F_1(x,y) = -\frac{\partial w}{\partial x} \qquad F_2(x,y) = -\frac{\partial w}{\partial x} \tag{7.27}$$

Substituting equations (7.24) and equations (7.27) in the strain–displacement relations for the in-plane strains (Appendix B), we find that

$$\begin{aligned} \varepsilon_x &= \frac{\partial u}{\partial x} = \varepsilon_x^0 + zk_x \\ \varepsilon_y &= \frac{\partial \upsilon}{\partial y} = \varepsilon_y^0 + zk_y \\ \gamma_{xy} &= \frac{\partial u}{\partial y} + \frac{\partial \upsilon}{\partial x} = \gamma_{xy}^0 + z\kappa_{xy} \end{aligned} \tag{7.28}$$

where the strains on the middle surface are

$$\varepsilon_x^0 = \frac{\partial u^0}{\partial x} \qquad \varepsilon_y^0 = \frac{\partial \upsilon^0}{\partial y} \qquad \gamma_{xy}^0 = \frac{\partial u^0}{\partial y} + \frac{\partial \upsilon^0}{\partial x} \tag{7.29}$$

and the curvatures of the middle surface are

$$\kappa_x = -\frac{\partial^2 w}{\partial x^2} \qquad \kappa_y = -\frac{\partial^2 w}{\partial y^2} \qquad \kappa_{xy} = -2\frac{\partial^2 w}{\partial x\,\partial y} \tag{7.30}$$

κ_x is a bending curvature associated with bending of the middle surface in the xz plane and κ_y is a bending curvature associated with bending of the middle surface in the yz plane. κ_{xy} is a twisting curvature associated with out-of-plane twisting of the middle surface, which lies in the xy plane before deformation.

Since equations (7.28) give the strains at any distance z from the middle surface, the stresses along arbitrary xy axes in the kth lamina of a laminate may be found by substituting equations (7.28) into the lamina stress–strain relationships from equations (2.35) as follows:

$$\begin{Bmatrix} \sigma_x \\ \sigma_y \\ \tau_{xy} \end{Bmatrix}_k = \begin{bmatrix} \bar{Q}_{11} & \bar{Q}_{12} & \bar{Q}_{16} \\ \bar{Q}_{12} & \bar{Q}_{22} & \bar{Q}_{26} \\ \bar{Q}_{16} & \bar{Q}_{26} & \bar{Q}_{66} \end{bmatrix}_k \begin{Bmatrix} \varepsilon_x^0 + z\kappa_x \\ \varepsilon_y^0 + z\kappa_y \\ \gamma_{xy}^0 + z\kappa_{xy} \end{Bmatrix} \tag{7.31}$$

where the subscript k refers to the kth lamina. Comparing the laminated plate stresses in equations (7.31) with the laminated beam stress given by equation (7.3), we notice several differences. The laminated beam analysis only gives the uniaxial stress, σ_x, due to the bending curvature, whereas the laminated plate analysis gives the 2-D lamina stresses σ_x, σ_y, and τ_{xy} due to bending and twisting curvatures and to the midplane biaxial extension and shear. In addition, the laminated plate analysis includes the stresses due to shear coupling, as discussed in chapter 2.

In the laminated beam analysis, equation (7.3) for lamina stress is seen to be of limited practical use because the curvature is not generally known and is difficult to measure. Thus, the lamina stress was related to the applied bending moment by using the static equilibrium relationship in equation (7.4). The result was that a more useful equation for stress, equation (7.13), was developed. The bending moment can be related to the loads on the structure by additional static equilibrium equations. Similarly, in the laminated plate analysis, the midplane strains

and curvatures in equations (7.31) must be related to applied forces and moments by static equilibrium equations in order to make these equations more useful. In the laminated plate analysis, however, it is convenient to use forces and moments per unit length rather than forces and moments. The forces and moments per unit length shown in figure 7.8 are also referred to as stress resultants.

For example, the force per unit length, N_x, is given by

$$N_x = \int_{-t/2}^{t/2} \sigma_x \, dz = \sum_{k=1}^{N} \left\{ \int_{z_{k-1}}^{z_k} (\sigma_x)_k \, dz \right\} \tag{7.32}$$

and the moment per unit length, M_x, is given by

$$M_x = \int_{-t/2}^{t/2} \sigma_x z \, dz = \sum_{k=1}^{N} \left\{ \int_{z_{k-1}}^{z_k} (\sigma_x)_k z \, dz \right\} \tag{7.33}$$

where t is the laminate thickness, $(\sigma_x)_k$ the stress in the *kth* lamina, z_{k-1}, the distance from middle surface to inner surface of the kth lamina, and z_k, the corresponding distance from middle surface to outer surface of the *kth* lamina, as shown in figure 7.9.

Substituting the lamina stress–strain relationships from equations (7.31) in equation (7.32) and equation (7.33), respectively, we find that

$$N_x = \sum_{k=1}^{N} \int_{z_{k-1}}^{z_k} \left\{ (\bar{Q}_{11})_k \left(\varepsilon_x^0 + z\kappa_x \right) + (\bar{Q}_{12})_k \left(\varepsilon_y^0 + z\kappa_y \right) + (\bar{Q}_{16})_k \left(\gamma_{xy}^0 + z\kappa_{xy} \right) \right\} dz \tag{7.34}$$

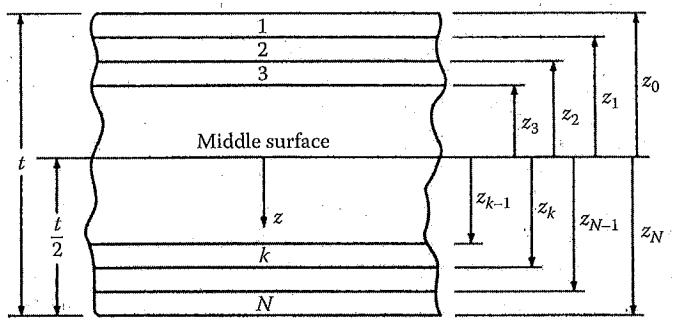

FIGURE 7.9
Laminated plate geometry and ply numbering system. *Caution:* The ply numbering system here is different from that used in figure 7.2 for the laminated beam analysis.

and

$$M_x = \sum_{k=1}^{N} \int_{z_{k-1}}^{z_k} \left\{ (\bar{Q}_{11})_k \left(\varepsilon_x^0 + z\kappa_x \right) + (\bar{Q}_{12})_k \left(\varepsilon_y^0 + z\kappa_y \right) + (\bar{Q}_{16})_k \left(\gamma_{xy}^0 + z\kappa_{xy} \right) \right\} z \, dz \tag{7.35}$$

Combining terms and rearranging equation (7.34) and equation (7.35), we find that

$$N_x = A_{11}\varepsilon_x^0 + A_{12}\varepsilon_y^0 + A_{16}y_{xy}^0 + B_{11}\kappa_x + B_{12}\kappa_y + B_{16}\kappa_{xy}y \tag{7.36}$$

and

$$M_x = B_{11}\varepsilon_x^0 + B_{12}\varepsilon_y^0 + B_{16}y_{xy}^0 + D_{11}\kappa_x + D_{12}\kappa_y + D_{16}\kappa_{xy} \tag{7.37}$$

where the laminate extensional stiffnesses are given by

$$A_{ij} = \int_{-t/2}^{t/2} (\bar{Q}_{ij})_k \, dz = \sum_{k=1}^{N} (\bar{Q}_{ij})_k (z_k - z_{k-1}) \tag{7.38}$$

The laminate-coupling stiffnesses are given by

$$B_{ij} = \int_{-t/2}^{t/2} (\bar{Q}_{ij})_k z \, dz = \frac{1}{2} \sum_{k=1}^{N} (\bar{Q}_{ij})_k \left(z_k^2 - z_{k-1}^2 \right) \tag{7.39}$$

and the laminate-bending stiffnesses are given by

$$D_{ij} = \int_{-t/2}^{t/2} (\bar{Q}_{ij})_k z^2 \, dz = \frac{1}{3} \sum_{k=1}^{N} (\bar{Q}_{ij})_k \left(z_k^3 - z_{k-1}^3 \right) \tag{7.40}$$

where the subscripts i, j = 1, 2, or 6. The other stress resultants can be written in similar form, and the complete set of equations can be expressed in matrix form as

$$\begin{Bmatrix} N_x \\ N_y \\ N_{xy} \\ M_x \\ M_y \\ M_{xy} \end{Bmatrix} = \begin{bmatrix} A_{11} & A_{12} & A_{16} & B_{11} & B_{12} & B_{16} \\ A_{12} & A_{22} & A_{26} & B_{12} & B_{22} & B_{26} \\ A_{16} & A_{26} & A_{66} & B_{16} & B_{26} & B_{66} \\ B_{11} & B_{12} & B_{16} & D_{11} & D_{12} & D_{16} \\ B_{12} & B_{22} & B_{26} & D_{12} & D_{22} & D_{26} \\ B_{16} & B_{26} & B_{66} & D_{16} & D_{26} & D_{66} \end{bmatrix} \begin{Bmatrix} \varepsilon_x^0 \\ \varepsilon_x^0 \\ \gamma_{xy}^0 \\ \kappa_x \\ \kappa_y \\ \kappa_{xy} \end{Bmatrix} \tag{7.41}$$

or in partitioned form as

$$\left\{\begin{matrix} N \\ \hline M \end{matrix}\right\} = \left[\begin{array}{c|c} A & B \\ \hline B & D \end{array}\right] \left\{\begin{matrix} \varepsilon^0 \\ \hline \kappa \end{matrix}\right\} \tag{7.42}$$

From equations (7.42), we can see that the extensional stiffness matrix $[A]$ relates the in-plane forces $\{N\}$ to the midplane strains $\{\varepsilon^0\}$, and the bending stiffness matrix $[D]$ relates the moments $\{M\}$ to the curvatures $\{k\}$. The coupling stiffness matrix $[B]$ couples the in-plane forces $\{N\}$ with the curvatures $\{\kappa\}$ and the moments $[M]$ with the midplane strains $\{\varepsilon^0\}$. A laminate having nonzero B_{ij} will bend or twist under in-plane loads. Such a laminate will also exhibit midplane stretching under bending and twisting moment loading. It can be easily shown that laminate geometric and material property symmetry with respect to the middle surface leads to the condition that all $B_{ij} = 0$ and that asymmetry about the middle surface leads to nonzero B_{ij}.

The decomposition of typical force and moment terms in equations (7.41) is illustrated in figure 7.10 and figure 7.11, respectively. Note in figure 7.10 that the corresponding force–deformation relationship for a homogeneous isotropic plate would only include the first two terms and no coupling terms of any kind, whereas in figure 7.11, the corresponding moment-curvature relationship for a homogeneous isotropic plate would only include the fourth and fifth terms and no coupling terms of any kind.

It is now clear that there may be coupling effects at both the lamina level and the laminate level, but the two types of coupling are not necessarily related. Lamina shear coupling is a result of anisotropic material behavior and the presence of 16 and 26 terms in the lamina stiffness or

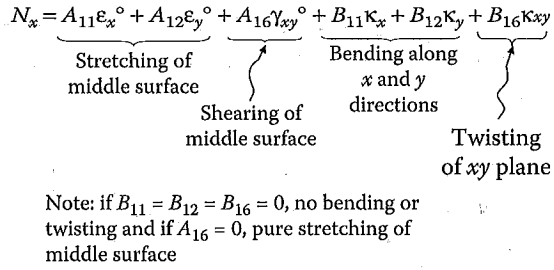

FIGURE 7.10
Illustration of decomposition of coupling effects in a general laminate loaded by a single force per unit length N_x.

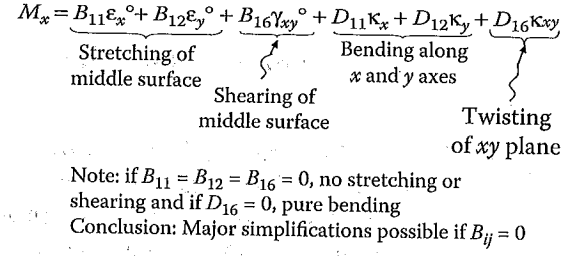

FIGURE 7.11
Illustration of decomposition of coupling effects in a general laminate loaded by a single bending moment per unit length M_x.

compliance matrices (recall section 2.6). This type of coupling at the lamina level also leads to coupling at the laminate level due to terms such as A_{16}, A_{26}, D_{16}, and D_{26}. On the other hand, the B_{ij}-type coupling at the laminate level is due to geometric and/or material property asymmetry with respect to the middle surface and is unrelated to material anisotropy. For example, it is possible for a laminate to have nonzero B_{ij} even with isotropic laminae if they are stacked in nonsymmetrical fashion, but the isotropic lamina properties lead to the condition $A_{16} = A_{26} = D_{16} = 0$. Figure 7.12 illustrates the two different types of coupling that appear in one specific laminate force–deformation equation. In the next section, the nature of the stiffness matrices for several special types of laminates will be summarized.

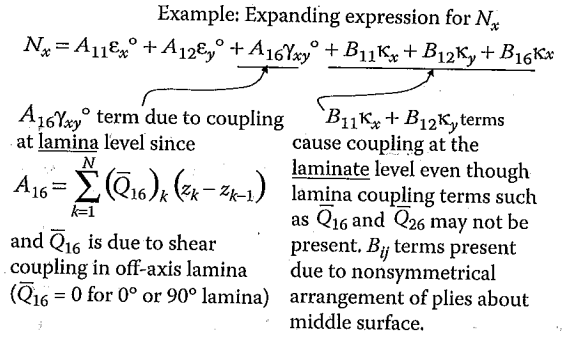

FIGURE 7.12
Illustration of the difference between lamina level coupling and laminate level coupling in a general laminate loaded by a single force per unit length N_x.

7.4 Stiffness Characteristics of Selected Laminate Configurations

As shown in the previous section, the number of nonzero terms in the laminate stiffness matrices is reduced for certain laminate configurations. Symmetry or antisymmetry of geometric and material properties about the middle surface, ply orientations, and ply-stacking sequences are all factors that govern the form of the laminate stiffness matrices. It is particularly important to be able to understand the effects of these factors on the type of coupling that may exist in the stiffness matrices of commonly used laminates.

Before beginning the discussion of special laminate configurations, it is useful to define several terms that are associated with special ply orientations. Although these ply orientations, by themselves, do not necessarily produce simplifications in the stiffness matrices, they are often used in combination with other terms to describe special laminates which do have simplified stiffness matrices. "Angle-ply" laminates have lamina orientations of either $+\theta$ or $-\theta$, where $0° \leq \theta \leq 90°$. Depending on ply-stacking sequences, angle-ply laminates may be symmetric, antisymmetric, or asymmetric with respect to the middle surface. "Cross-ply" laminates consist of plies oriented at either $\theta = 0°$ or $\theta = 90°$. A balanced cross-ply laminate has equal numbers of 0° and 90° plies. Depending on the ply arrangement, cross-ply laminates may be either symmetric or asymmetric with respect to the middle surface, but not antisymmetric. Since all plies in a cross-ply laminate behave as specially orthotropic laminae, such a laminate will always have $A_{16} = A_{26} = D_{16} = D_{26} = 0$. However, since all plies in an angle-ply laminate behave as generally orthotropic laminae, the 16 and 26 terms may not vanish.

7.4.1 Symmetric Laminates

A symmetric laminate has both geometric and material property symmetry about the middle surface. That is, the ply material, ply orientation, and ply thickness at a positive distance z from the middle surface are identical to the corresponding values at an equal negative distance z from the middle surface. Examples of symmetric angle-ply and cross-ply laminates are shown figure 7.13(a) and figure 7.13(b), respectively. Such a symmetry condition when substituted in equation (7.39) leads to the major simplification that all $B_{ij} = 0$. This means that bending–stretching coupling will not be present in such laminates. Consequently, in-plane loads will not generate bending and twisting curvatures that cause out-of-plane warping, and bending or twisting moments will not produce an extension of the middle surface. This can be particularly important in structures that

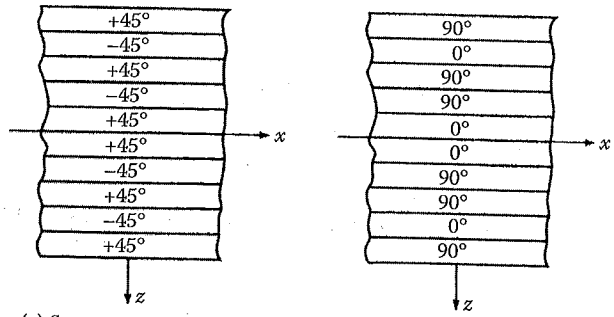

(a) Symmetric angle-ply (b) Symmetric cross-ply

FIGURE 7.13
Examples of symmetric laminates. Ply orientations and material properties are symmetric about middle surface.

are subjected to changes in environmental conditions, where the resulting hygrothermal forces would lead to undesirable warping in nonsymmetric laminates.

EXAMPLE 7.3

Determine the stiffness matrix for a [+45/–45/–45 +45] symmetric angle-ply laminate consisting of 0.25-mm thick unidirectional AS/3501 carbon/epoxy laminae. An exploded view of the laminate is shown in figure 7.14.

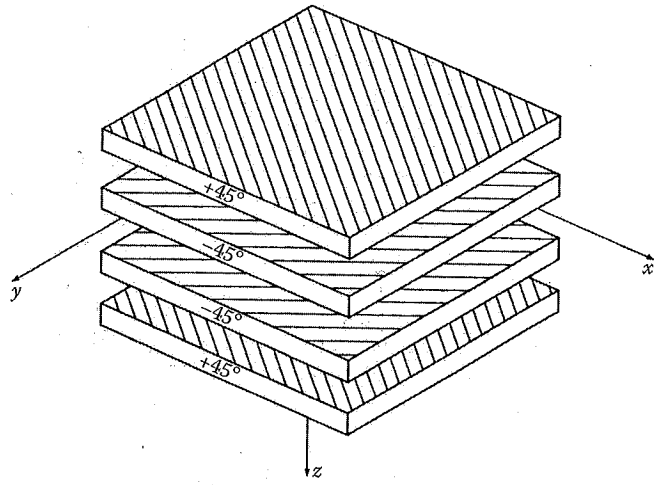

FIGURE 7.14
Exploded view of [+45/–45/–45/+45] symmetric laminate.

Solution. From table 2.2, the lamina engineering constants are

$$E_1 = 138\ \text{GPa} \quad E_2 = 9\ \text{GPa} \quad G_{12} = 6.9\ \text{GPa} \quad \nu_{12} = 0.3$$

$$\text{and} \quad \nu_{21} = \nu_{12}\frac{E_2}{E_1} = 0.3\frac{9.0}{138.0} = 0.0196$$

Substitution of the above engineering constants in equations (2.27) yields the components of the lamina stiffness matrix associated with the principal material axes:

$$[Q] = \begin{bmatrix} 138.8 & 2.72 & 0 \\ 2.72 & 9.05 & 0 \\ 0 & 0 & 6.9 \end{bmatrix} \text{GPa}$$

The transformed lamina stiffness matrices for the +45° and –45° plies are then found by substituting the above stiffnesses in equations (2.36) or equations (2.43) and equations (2.44). For the +45° plies,

$$[\bar{Q}]_{+45°} = \begin{bmatrix} 45.22 & 31.42 & 32.44 \\ 31.42 & 45.22 & 32.44 \\ 32.44 & 32.44 & 35.6 \end{bmatrix} \text{GPa}$$

For the –45° plies,

$$[\bar{Q}]_{-45°} = \begin{bmatrix} 45.22 & 31.42 & -32.44 \\ 31.42 & 45.22 & -32.44 \\ -32.44 & -32.44 & 35.6 \end{bmatrix} \text{GPa}$$

Note that the only difference between the stiffness matrices for the plies is that the shear coupling terms (i.e., the terms with subscripts 16 and 26) for the –45° ply have the opposite sign from the corresponding terms for +45° ply. Before calculating the laminate stiffnesses, we must determine distances from the middle surface on the various ply interfaces according to figure 7.9. The distances are $z_0 = -0.50$ mm, $z_1 = -0.25$ mm, $z_2 = 0$, $z_3 = 0.25$ mm, and $z_4 = 0.5$ mm. The laminate extensional stiffnesses are then found by substituting these distances along with the lamina stiffness in equations (7.38):

$$[A] = \begin{bmatrix} 45.22 & 31.42 & 0 \\ 31.42 & 45.22 & 0 \\ 0 & 0 & 35.6 \end{bmatrix} \text{GPa-mm}$$

Similarly, the laminate-coupling stiffnesses are found from equation (7.39):

$$[B] = \begin{bmatrix} 0 & 0 & 0 \\ 0 & 0 & 0 \\ 0 & 0 & 0 \end{bmatrix} \text{GPa-mm}^2$$

and the laminate-bending stiffnesses are found from equations (7.40):

$$[D] = \begin{bmatrix} 3.77 & 2.62 & 2.03 \\ 2.62 & 3.77 & 2.03 \\ 2.03 & 2.03 & 2.97 \end{bmatrix} \text{GPa-mm}^3$$

7.4.2 Antisymmetric Laminates

An antisymmetric laminate has plies of identical material and thickness at equal positive and negative distances from the middle surface, but the ply orientations are antisymmetric with respect to the middle surface. That is, the ply orientation at a positive distance z is $+\theta$, if the ply orientation at an equal negative distance z is $-\theta$. Examples of antisymmetric angle-ply laminates are shown in figure 7.15. Note that the antisymmetric definition has no meaning for a cross-ply laminate, which must be either symmetric or nonsymmetric. It can be shown that by substituting the antisymmetric condition into equations (7.38) and equations (7.40), the coupling terms $A_{16} = A_{26} = D_{16} = D_{26} = 0$. From equations (7.39), it can also be shown that $B_{11} = B_{12} = B_{22} = B_{66} = 0$ for the antisymmetric angle-ply laminate.

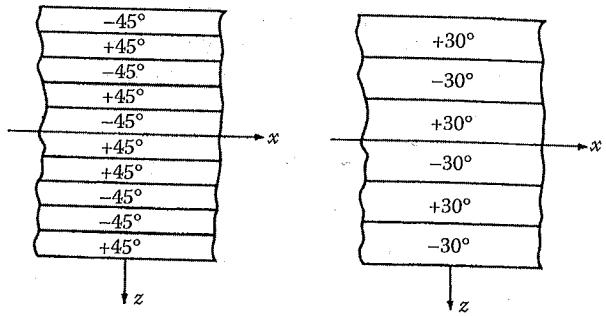

FIGURE 7.15
Examples of antisymmetric angle-ply laminates. Although ply orientations are antisymmetric about middle surface, the material distribution is symmetric.

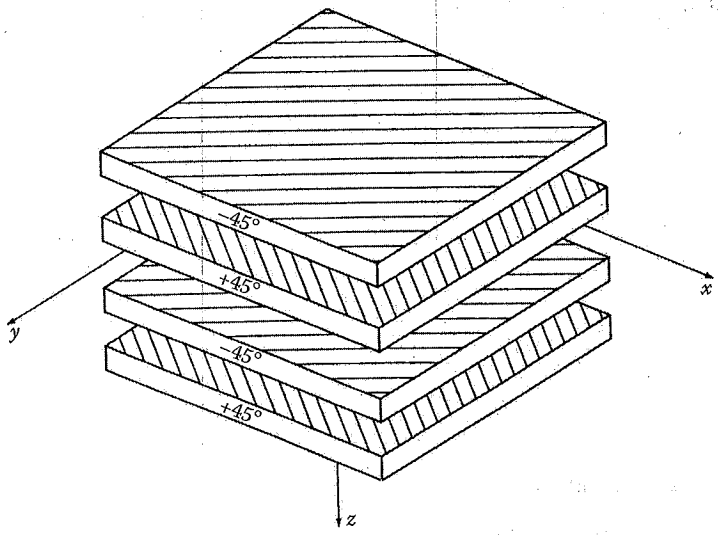

FIGURE 7.16
Exploded view of [−45/+45/−45/+45] antisymmetric laminate.

EXAMPLE 7.4

Determine the stiffness matrix for a [−45/+45/−45/+45] antisymmetric angle-ply laminate consisting of the same 0.25-mm thick unidirectional AS/3501 carbon/epoxy laminae that were used in example 7.3. An exploded view of the laminate is shown in figure 7.16.

Solution. Since the lamina orientations are still +45° and −45°, the lamina stiffnesses are the same as those calculated in example 7.3. The distances z_k are also the same as those shown in example 7.3, since the ply thicknesses and the number of plies are the same. Laminate extensional stiffnesses are then found by substituting these values, along with the antisymmetric stacking sequence, in equations (7.38):

$$[A] = \begin{bmatrix} 45.22 & 31.42 & 0 \\ 31.42 & 45.22 & 0 \\ 0 & 0 & 35.6 \end{bmatrix} \text{GPa-mm}$$

Note that these results are identical to those in example 7.3 because we still have two plies at +45° and two plies at −45°. Thus, the stacking sequence has no effect on [*A*] as long as the number of plies at a given orientation

remains the same. The laminate-coupling stiffnesses are found from equations (7.39):

$$[B] = \begin{bmatrix} 0 & 0 & 4.055 \\ 0 & 0 & 4.055 \\ 4.055 & 4.055 & 0 \end{bmatrix} \text{GPa-mm}^2$$

Note that due to the antisymmetry, $B_{11} = B_{22} = B_{12} = B_{66} = 0$ but B_{16} and B_{26} have nonzero values; this is true in general for antisymmetric angle-ply laminates. Thus, the antisymmetric laminate has extension–twisting and bending–shearing coupling, but the symmetric laminate does not. The laminate-bending stiffnesses are found from equation (7.40):

$$[D] = \begin{bmatrix} 3.77 & 2.62 & 0 \\ 2.62 & 3.77 & 0 \\ 0 & 0 & 2.97 \end{bmatrix} \text{GPa-mm}^3$$

Note that D_{11}, D_{22}, D_{12}, and D_{66} are the same as the corresponding values in example 7.3, but we now have $D_{16} = D_{26} = 0$. Thus, bending–twisting coupling is present in symmetric angle-ply laminates, but not in antisymmetric angle-ply laminates.

7.4.3 Quasi-Isotropic Laminates

Although it may seem unlikely, it is possible to use orthotropic laminae to construct a laminate that exhibits some elements of isotropic behavior. For example, if a laminate consists of three or more identical orthotropic laminae (i.e., all have the same material and geometric properties) that are oriented at the same angle relative to adjacent laminae, the extensional stiffness matrix [*A*] will be isotropic, but the other stiffness matrices [*B*] and [*D*] will not necessarily have isotropic form. Such a laminate is called a quasi-isotropic or planar isotropic laminate, and the angle between adjacent laminae must be π/N, where N is the total number of laminae. For example, [60/0/−60] and [90/45/0/−45] laminates are quasi-isotropic.

Recall that in section 6.4 it was mentioned that randomly oriented fiber composites could be modeled as planar isotropic or quasi-isotropic laminates. Now it is clear that although a randomly oriented fiber composite must theoretically have an infinite number of fiber orientations to be isotropic, the in-plane behavior of such materials can be modeled by using a quasi-isotropic laminate having only three laminae, as in the [60/0/−60] laminate.

Recall also that the stress–strain relationships for an isotropic lamina are given by equation (2.26), with the additional requirements that $Q_{11} = Q_{22}$,

$Q_{66} = (Q_{11} - Q_{12})/2$, and $Q_{16} = Q_{26} = 0$. Similarly, the extensional force–deformation relationships for the quasi-isotropic laminate are given by

$$\begin{Bmatrix} N_x \\ N_x \\ N_{xy} \end{Bmatrix} = \begin{bmatrix} A_{11} & A_{12} & 0 \\ A_{12} & A_{11} & 0 \\ 0 & 0 & (A_{11} - A_{12})/2 \end{bmatrix} \begin{Bmatrix} \varepsilon_x^0 \\ e_y^0 \\ \gamma_{xy}^0 \end{Bmatrix} \tag{7.43}$$

In general, such simplifications are not possible for the [B] and [D] matrices, as can be shown by calculating the stiffness matrices for quasi-isotropic laminates such as [60/0/–60] or [90/45/0/–45].

In section 6.4, it was shown that the invariants could be useful in the development of the stress–strain relationships and equations for the engineering constants of a planar isotropic, randomly oriented fiber composite. Similarly, the invariants can be used in the study of quasi-isotropic laminates. For example, by substituting the lamina stiffnesses in terms of invariants from equations (2.43) in equations (7.38) for the laminate extensional stiffnesses, we find that

$$\begin{aligned} A_{11} &= A_{22} = U_1 t \\ A_{12} &= U_4 t \\ A_{66} &= \frac{(U_1 - U_4)t}{2} \end{aligned} \tag{7.44}$$

Using developments similar to those in section 6.4, we can show that the effective extensional engineering constants for quasi-isotropic laminates are given by equations (6.43).

EXAMPLE 7.5

Determine the stiffness matrices and engineering constants for a quasi-isotropic [60/0/–60] laminate consisting of the same laminae that were described in example 7.3. Figure 7.17 shows an exploded view of the laminate.

Solution. The required lamina stiffnesses are the Q_{ij} in example 7.3 and the appropriate transformed stiffnesses for 60° and –60° from equations (2.36) or equations (2.43) and equations (2.44). Substituting these stiffnesses in equations (7.38), we find that the laminate extensional stiffnesses are

$$[A] = \begin{bmatrix} 44.68 & 12.80 & 0 \\ 12.80 & 44.68 & 0 \\ 0 & 0 & 15.94 \end{bmatrix} \text{GPa-mm}$$

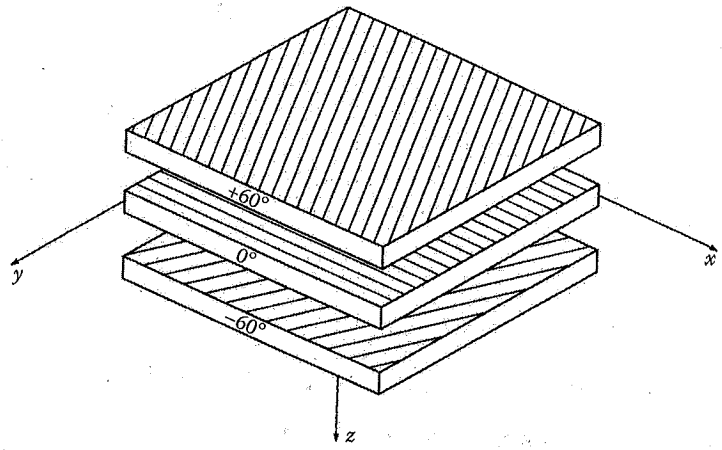

FIGURE 7.17
Exploded view of [+60/0/–60] quasi-isotropic laminate.

It is easily shown that this matrix is of the isotropic form shown in equations (7.43). The laminate-coupling stiffnesses from equations (7.39) are

$$[B] = \begin{bmatrix} 0 & 0 & -1.96 \\ 0 & 0 & -5.06 \\ -1.96 & -5.06 & 0 \end{bmatrix} \text{GPa-mm}^2$$

and the bending stiffnesses from equations (7.40) are

$$[D] = \begin{bmatrix} 0.856 & 0.824 & 0 \\ 0.824 & 2.88 & 0 \\ 0 & 0 & 0.972 \end{bmatrix} \text{GPa-mm}^3$$

It is seen that the matrices [B] and [D] do not have the isotropic form of equations (7.43). It can also be shown that by changing the lamina orientations while maintaining equal angles between adjacent laminae (e.g., [75/15/–45], [30/–30/–90], or [0/–60/–120]), the A_{ij} remain unchanged but the B_{ij} and D_{ij} do not. Thus, the laminate is isotropic with respect to in-plane behavior only.

The engineering constants for the laminate may be found by using the invariants. By substituting the Q_{ij} from example 7.3 in equation (2.44), we find that

$U_1 = 59.57$ GPa and $U_4 = 17.07$ GPa

Substituting these results in equations (6.43), we find that the engineering constants are

$$\tilde{E} = 54.68 \text{ GPa} \quad \tilde{G} = 21.25 \text{ GPa} \quad \text{and} \quad \tilde{\nu} = 0.287$$

Note that the A_{ij} can also be found by using the invariants U_1 and U_4, along with the laminate thickness, t, in equations (7.44).

7.5 Derivation and Use of Laminate Compliances

Since the applied loads are generally known rather than the deformations, it is often necessary to use the inverted form of the laminate force–deformation relationships shown in equation (7.41) and equation (7.42). The use of the inverted equations means that we must deal with the laminate compliance matrix instead of the laminate stiffness matrix. In this section, the inverted equations are derived and used to calculate the lamina stresses and strains due to known laminate loads. The inverted equations are also used in the derivation of the laminate engineering constants and in the comparison of predicted and measured laminate compliances.

7.5.1 Inversion of Laminate Force–Deformation Equations

The general laminate force–deformation equations shown in equations (7.42) can be expressed as

$$\left\{\begin{matrix} N \\ \hline M \end{matrix}\right\} = \left[\begin{matrix} A & B \\ \hline B & D \end{matrix}\right] \left\{\begin{matrix} \varepsilon^0 \\ \hline \kappa \end{matrix}\right\} = [E] \left\{\begin{matrix} \varepsilon^0 \\ \hline \kappa \end{matrix}\right\} \tag{7.45}$$

where the A_{ij}, B_{ij}, and D_{ij} make up the laminate stiffness matrix, $[E]$. The fully inverted form of this equation can be obtained directly by premultiplying both sides of the equation by the compliance matrix, which is the inverse of the stiffness matrix

$$\left\{\begin{matrix} \varepsilon^0 \\ \hline \kappa \end{matrix}\right\} = \left[\begin{matrix} A & B \\ \hline B & D \end{matrix}\right]^{-1} \left\{\begin{matrix} N \\ \hline M \end{matrix}\right\} = [E]^{-1} \left\{\begin{matrix} N \\ \hline M \end{matrix}\right\} \tag{7.46}$$

Alternatively, equations (7.46) are derived below by the inversion of subdivided smaller matrices, as shown by Halpin [12].

From equations (7.45), the in-plane forces per unit length are

$$\{N\} = [A]\{\varepsilon^0\} + [B]\{\kappa\} \tag{7.47}$$

whereas the moments per unit length are

$$\{M\} = [B]\{\varepsilon^0\} + [D]\{\kappa\} \tag{7.48}$$

The midplane strains may be obtained from equations (7.47) as

$$\{\varepsilon^0\} = [A]^{-1}\{N\} - [A]^{-1}[B]\{\kappa\} \tag{7.49}$$

Substitution of these strains in equations (7.48) gives

$$\{M\} = [B][A]^{-1}\{N\} - [B][A]^{-1}[B]\{\kappa\} + [D]\{\kappa\} \tag{7.50}$$

Equations (7.49) and equations (7.50) can be combined to give a partially inverted form of equations (7.45) as follows:

$$\left\{\begin{matrix} \varepsilon^0 \\ \hline M \end{matrix}\right\} = \left[\begin{matrix} A^* & B^* \\ \hline C^* & D^* \end{matrix}\right] \left\{\begin{matrix} N \\ \hline \kappa \end{matrix}\right\} \tag{7.51}$$

where

$$[A^*] = [A]^{-1}$$

$$[B^*] = -[A]^{-1}[B]$$

$$[C^*] = [B][A]^{-1}$$

$$[D^*] = [D] - [B][A]^{-1}[B]$$

Inverting the last set of partitioned equations (7.51) to solve for the curvatures, we find that

$$\{\kappa\} = [D^*]^{-1}\{M\} - [D^*]^{-1}[C^*]\{N\} \tag{7.52}$$

Now substituting equations (7.52) in equations (7.49), we have

$$\{\varepsilon^0\} = ([A^*] - [B^*][D^*]^{-1}[C^*])\{N\} + [B^*][D^*]^{-1}\{M\} \tag{7.53}$$

Equations (7.52) and equation (7.53) can now be combined in partitioned matrix form to give

$$\left\{\begin{array}{c}\varepsilon^0\\ \hline \kappa\end{array}\right\}=\left[\begin{array}{c|c}A' & B'\\ \hline C' & D'\end{array}\right]\left\{\begin{array}{c}N\\ \hline M\end{array}\right\} \tag{7.54}$$

where

$$[A']=[A^*]-[B^*][D^*]^{-1}[C^*]$$

$$[B']=[B^*][D^*]^{-1}$$

$$[C']=-[D^*]^{-1}[C^*]=[B']^T=[B']$$

$$[D']=[D^*]^{-1}$$

and the compliance matrix is

$$\left[\begin{array}{c|c}A' & B'\\ \hline C' & D'\end{array}\right]=[E]^{-1} \tag{7.55}$$

Since the stiffness matrix $[E]$ is symmetric, the compliance matrix must also be symmetric.

7.5.2 Determination of Lamina Stresses and Strains

Now that we have the inverted laminate force–deformation relationships in equations (7.54), the calculation of lamina stresses and strains from known laminate forces and moments is a straightforward procedure. For a laminate at constant temperature and moisture content, the stresses in the kth lamina are given by equations (7.31), which can be written in abbreviated matrix notation as

$$\{\sigma\}_k=[\bar{Q}]_k(\{\varepsilon^0\}+z\{\kappa\}) \tag{7.56}$$

where the midplane strains $\{\varepsilon^0\}$ and curvatures $\{\kappa\}$ are given in terms of laminate forces and moments by equations (7.54). The lamina stresses from equations (7.56) can then be used in conjunction with a lamina strength criterion to check each lamina against failure. The analysis of hygrothermal stresses will be discussed later in section 7.6, and laminate strength analysis will be presented in section 7.8.

EXAMPLE 7.6

The symmetric angle-ply laminate described in example 7.3 is subjected to a single uniaxial force per unit length $N_x = 50$ MPa-mm. Determine the resulting stresses associated with the x and y axes in each lamina.

Solution. Due to symmetry, $[B] = 0$ and $[A'] = [A^*] = [A]^{-1}$. Since $\{M\} = 0$ here,

$$\{\varepsilon^0\}=[A']\{N\}=[A]^{-1}\{N\}$$

Using the inverse of the $[A]$ matrix from example 7.3, we find that

$$\left\{\begin{array}{c}\varepsilon_x^0\\ \varepsilon_y^0\\ \gamma_{xy}^0\end{array}\right\}=\left[\begin{array}{ccc}0.04276 & -0.0297 & 0\\ -0.0297 & 0.04276 & 0\\ 0 & 0 & 0.02809\end{array}\right]\left\{\begin{array}{c}50\\ 0\\ 0\end{array}\right\}\times(10^{-3})=\left\{\begin{array}{c}0.002138\\ -0.001485\\ 0\end{array}\right\}$$

where $(\text{GPa-mm})^{-1} = 10^{-3}\ (\text{MPa-mm})^{-1}$. Substituting the above strains and the lamina stiffnesses from example 7.3 in equations (7.56), we find that the stresses in the +45° plies are

$$\left\{\begin{array}{c}\sigma_x\\ \sigma_x\\ \tau_{xy}\end{array}\right\}=\left[\begin{array}{ccc}45.22 & 31.42 & 32.44\\ 31.42 & 45.22 & 32.44\\ 32.44 & 32.44 & 35.6\end{array}\right]\left\{\begin{array}{c}0.002138\\ -0.001485\\ 0\end{array}\right\}\times 10^3=\left\{\begin{array}{c}50\\ 0\\ 21.2\end{array}\right\}\text{MPa}$$

where 10^3 MPa = GPa. Similarly, the stresses in the –45° plies are

$$\left\{\begin{array}{c}\sigma_x\\ \sigma_x\\ \tau_{xy}\end{array}\right\}=\left[\begin{array}{ccc}45.22 & 31.42 & -32.44\\ 31.42 & 45.22 & -32.44\\ -32.44 & -32.44 & 35.6\end{array}\right]\left\{\begin{array}{c}0.002138\\ -0.001485\\ 0\end{array}\right\}\times 10^3=\left\{\begin{array}{c}50\\ 0\\ -21.2\end{array}\right\}\text{MPa}$$

Note that since the curvatures vanish for this problem, the stresses do not depend on the distance z.

EXAMPLE 7.7

The antisymmetric angle-ply laminate described in example 7.4 is subjected to a single uniaxial force per unit length $N_x = 50$ MPa-mm. Determine the resulting stresses associated with the x and y axes in each lamina.

Solution. Since this laminate is not symmetric, we must invert the full stiffness matrix as in equation (7.46) or equation (7.54). Forming the full stiffness matrix from the [A], [B], and [D] matrices in example 7.4 and inverting, we find the resulting midplane strains and curvatures to be

$$\begin{Bmatrix} \varepsilon_x^0 \\ \varepsilon_y^0 \\ \gamma_{xy}^0 \\ \kappa_x \\ \kappa_y \\ \kappa_{xy} \end{Bmatrix} = \begin{bmatrix} 0.04386 & -0.02861 & 0 & 0 & 0 & -0.02083 \\ -0.02861 & 0.04386 & 0 & 0 & 0 & -0.02083 \\ 0 & 0 & 0.03284 & -0.02083 & -0.02083 & 0 \\ 0 & 0 & -0.02083 & 0.52625 & 0.34331 & 0 \\ 0 & 0 & -0.02083 & -0.34331 & 0.52625 & 0 \\ -0.02083 & -0.02083 & 0 & 0 & 0 & 0.39356 \end{bmatrix}$$

$$\times \begin{Bmatrix} 50 \\ 0 \\ 0 \\ 0 \\ 0 \\ 0 \end{Bmatrix} \times 10^{-3} = \begin{Bmatrix} 0.002193\,\text{mm/mm} \\ -0.001430\,\text{mm/mm} \\ 0\,\text{mm/mm} \\ 0\,\text{mm}^{-1} \\ 0\,\text{mm}^{-1} \\ -0.001042\,\text{mm}^{-1} \end{Bmatrix}$$

where again the factor of 10^{-3} has been introduced for dimensional consistency. Due to the curvatures, the total strains and stresses now depend on the distance z (unlike example 7.6). For example, at the top surface of the #1 ply (–45°), z = –0.5 mm and the resulting total strains are

$$\varepsilon_x = \varepsilon_x^0 + z\kappa_x = 0.002193 + (-0.5)(0) = 0.002193\,\text{mm/mm}$$
$$\varepsilon_y = \varepsilon_y^0 + z\kappa_y = -0.00143 + (-0.5)(0) = -0.00143\,\text{mm/mm}$$
$$\gamma_{xy} = \gamma_{xy}^0 + z\kappa_{xy} = 0 + (-0.5)(-0.001042) = 0.000521\,\text{mm/mm}$$

Similarly, at the bottom surface of the #1 ply (–45°), or at the top surface of the #2 ply (+45°), z = 0.25 mm and the strains are

$$\varepsilon_x = 0.002193 + (-0.25)(0) = 0.002193\,\text{mm/mm}$$
$$\varepsilon_y = -0.00143 + (-0.25)(0) = -0.00143\,\text{mm/mm}$$
$$\gamma_{xy} = 0 + (-0.25)(-0.001042) = 0.000261\,\text{mm/mm}$$

At the top surface of the #3 ply (–45°), or at the bottom surface of the #2 ply, z = 0 and the strains are

$$\varepsilon_x = 0.002193\,\text{mm/mm}$$
$$\varepsilon_y = -0.00143\,\text{mm/mm}$$
$$\gamma_{xy} = 0$$

At the top surface of the #4 ply (+45°), or at the bottom surface of the #3 ply (–45°), z = 0.25 mm and

$$\varepsilon_x = 0.002193\,\text{mm/mm}$$
$$\varepsilon_y = -0.00143\,\text{mm/mm}$$
$$\gamma_{xy} = -0.000261\,\text{mm/mm}$$

Finally, at the bottom of the #4 ply (+45°), z=+0.5 mm and

$$\varepsilon_x = 0.002193\,\text{mm/mm}$$
$$\varepsilon_y = -0.00143\,\text{mm/mm}$$
$$\gamma_{xy} = -0.000521\,\text{mm/mm}$$

The stresses at the top surface of the #1 ply (–45°) are then

$$\begin{Bmatrix} \sigma_x \\ \sigma_x \\ \tau_{xy} \end{Bmatrix} = \begin{bmatrix} 45.22 & 31.42 & -32.44 \\ 31.42 & 45.22 & -32.44 \\ -32.44 & -32.44 & 35.6 \end{bmatrix} \begin{Bmatrix} 0.002193 \\ -0.001430 \\ 0.000521 \end{Bmatrix} \times 10^3$$

$$= \begin{Bmatrix} 37.3 \\ -12.7 \\ -6.2 \end{Bmatrix} \text{MPa}$$

where again 10^3 Mpa = GPa. Similar calculations for the other plies yield the values shown in the following table:

Location	σ_x(MPa)	σ_y(MPa)	τ_{xy}(MPa)
#1 Top	37.3	–12.7	–6.2
#1 Bottom	45.8	–4.2	–15.5
#2 Top	62.7	12.7	34.0
#2 Bottom	54.2	4.2	24.7
#3 Top	54.2	4.2	–24.7
#3 Bottom	62.7	12.7	–34.0
#4 Top	45.8	–4.2	15.5
#4 Bottom	37.3	–12.7	6.2

Thus, the stress distribution across the thickness of the antisymmetric laminate is quite complex, even for simple uniaxial loading. This is typical for laminates which exhibit coupling.

7.5.3 Determination of Laminate Engineering Constants

It is sometimes more convenient to use effective laminate engineering constants rather than the laminate stiffnesses defined in equation (7.38), equation (7.39), and equation (7.40). These effective laminate engineering constants may be derived by using laminate compliances. For example, the force–deformation relationships for a symmetric laminate under in-plane loads only are given by

$$\begin{Bmatrix} N_x \\ N_y \\ N_{xy} \end{Bmatrix} = \begin{bmatrix} A_{11} & A_{12} & A_{16} \\ A_{12} & A_{22} & A_{26} \\ A_{16} & A_{26} & A_{66} \end{bmatrix} \begin{Bmatrix} \varepsilon_x^0 \\ \varepsilon_y^0 \\ \gamma_{xy}^0 \end{Bmatrix} \tag{7.57}$$

and the corresponding inverted force–deformation relationships are

$$\begin{Bmatrix} \varepsilon_x^0 \\ \varepsilon_y^0 \\ \gamma_{xy}^0 \end{Bmatrix} = \begin{bmatrix} A'_{11} & A'_{12} & A'_{16} \\ A'_{12} & A'_{22} & A'_{26} \\ A'_{16} & A'_{26} & A'_{66} \end{bmatrix} \begin{Bmatrix} N_x \\ N_y \\ N_{xy} \end{Bmatrix} \tag{7.58}$$

The effective longitudinal Young's modulus of the laminate, E_x, governs the response of the laminate under the single axial load per unit length N_x with $N_y = N_{xy} = 0$ (fig. 7.18[a]) and is defined as

$$E_x = \frac{\sigma_x}{\varepsilon_x^0} = \frac{N_x/t}{A'_{11}N_x} = \frac{1}{tA'_{11}} \tag{7.59}$$

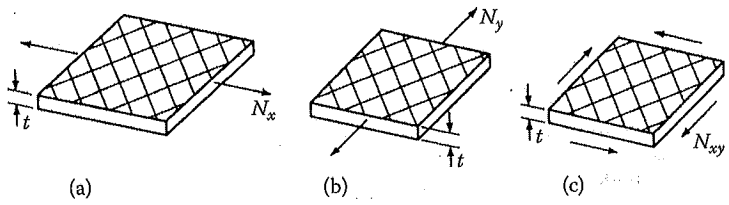

FIGURE 7.18
In-plane loading of symmetric laminate for defining the in-plane laminate engineering constants.

The effective transverse Young's modulus of the laminate, E_y, governs the response of the laminate under the single axial load per unit length N_y with $N_x = N_{xy} = 0$ (fig. 7.18[b]) and is defined as

$$E_y = \frac{\sigma_y}{\varepsilon_y^0} = \frac{N_y/t}{A'_{22}N_y} = \frac{1}{tA'_{22}} \tag{7.60}$$

The effective laminate in-plane shear modulus, G_{xy}, governs the laminate response under the pure shear load per unit length N_{xy} with $N_x = N_y = 0$ (fig. 7.18[c]) and is defined as

$$G_{xy} = \frac{\tau_{xy}}{\gamma_{xy}^0} = \frac{N_{xy}/t}{A'_{66}N_{xy}} = \frac{1}{tA'_{66}} \tag{7.61}$$

Similarly, the effective laminate longitudinal Poisson's ratio is

$$\nu_{xy} = -\frac{A'_{12}}{A'_{11}} \tag{7.62}$$

and the effective laminate shear coupling ratios analogous to those given in equation (2.40) and equation (2.41) for the orthotropic lamina are

$$\eta_{x,xy} = \frac{A'_{16}}{A'_{16}} \quad \text{and} \quad \eta_{xy,y} = \frac{A'_{26}}{A'_{66}} \tag{7.63}$$

Using similar derivations, the effective laminate flexural moduli may be expressed in terms of the flexural compliances. For the symmetric laminate subjected to bending only, the laminate moment–curvature relationships are given by

$$\begin{Bmatrix} M_x \\ M_y \\ M_{xy} \end{Bmatrix} = \begin{bmatrix} D_{11} & D_{12} & D_{16} \\ D_{12} & D_{22} & D_{26} \\ D_{16} & D_{26} & D_{66} \end{bmatrix} \begin{Bmatrix} \kappa_x \\ \kappa_y \\ \kappa_{xy} \end{Bmatrix} \tag{7.64}$$

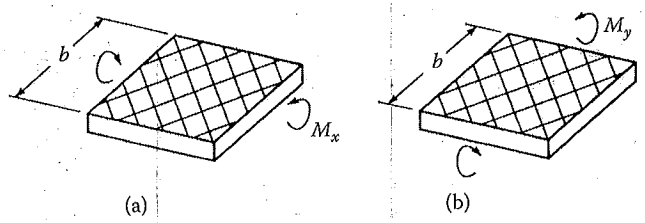

FIGURE 7.19
Bending moment leading of symmetric laminate for defining the laminate flexural moduli.

and the inverted forms are given by

$$\begin{Bmatrix} \kappa_x \\ \kappa_y \\ \kappa_{xy} \end{Bmatrix} = \begin{bmatrix} D'_{11} & D'_{12} & D'_{16} \\ D'_{12} & D'_{22} & D'_{26} \\ D'_{16} & D'_{26} & D'_{66} \end{bmatrix} \begin{Bmatrix} M_x \\ M_y \\ M_{xy} \end{Bmatrix} \tag{7.65}$$

Thus, when the laminate is subjected to a pure bending moment per unit length M_x with $M_y = M_{xy} = 0$ (fig. 7.19[a]), the resulting curvature is

$$\kappa_x = D'_{11} M_x = D'_{11} \frac{M}{b} = \frac{1}{\rho_x} \tag{7.66}$$

where M is the total bending moment, which is $M_x b$, b the laminate width, and ρ_x the radius of curvature = $1/\kappa_x$.

For an equivalent homogeneous beam, the moment–curvature relationship is

$$\frac{M}{E_{fx} I_{yy}} = \frac{1}{\rho_x} \tag{7.67}$$

where I_{yy} is the second moment of inertia of the beam about the neutral axis, which is $bt^3/12$, and E_{fx} the flexural modulus of the beam along the x direction.

Recall that the flexural modulus was also defined by equation (7.8) and equation (7.9) according to laminated beam theory. Combining equation (7.66) and equation (7.67), we find that the flexural modulus is related to the laminate compliance D'_{11}, by the equation

$$E_{fx} = \frac{12}{t^3 D'_{11}} \tag{7.68}$$

Similarly, the flexural modulus along the y direction (fig. 7.19[b]) is found to be

$$E_{fy} = \frac{12}{t^3 D'_{22}} \tag{7.69}$$

Although the laminate stiffnesses A_{ij}, B_{ij}, and D_{ij} are meaningful parameters for all laminate configurations, the engineering constants may not be. Clearly, the use of effective engineering constants must be restricted to those cases where the deformations are similar to the deformations associated with the engineering constant being used. That is, in the above examples for symmetric laminates the $B_{ij} = 0$ and warping under in-plane loads or midplane extension under bending or twisting moments will not occur, so the deformations of the laminate under load would be similar to those for the equivalent homogeneous material. However, the use of engineering constants for the antisymmetric laminate may not be appropriate because of the complex deformations due to coupling effects.

EXAMPLE 7.8

For the symmetric laminate described in example 7.3 and example 7.6, determine the effective Young's moduli, in-plane shear modulus, longitudinal Poisson's ratio, and shear-coupling ratios associated with the x *and* y *axes.*

Solution. The effective longitudinal Young's modulus is given by equation (7.59):

$$E_x = \frac{1}{t A'_{11}} = \frac{1}{(1)(0.04276)} = 23.4 \text{ GPa}$$

Note that due to the ±45° ply orientations for this laminate, $E_x = E_y$. The effective in-plane shear modulus is given by equation (7.61):

$$G_{xy} = \frac{1}{t A'_{66}} = \frac{1}{(1)(0.02809)} = 35.6 \text{ GPa}$$

The effective longitudinal Poisson's ratio is given by equation (7.62):

$$\nu_{xy} = -\frac{A'_{12}}{A'_{11}} = -\frac{-0.0297}{0.04276} = 0.694$$

Since $A_{16} = A_{26} = 0$ for this laminate, it is seen from equations (7.63) that the effective shear–coupling ratios $\eta_{x,xy} = \eta_{xy,y} = 0$. Due to the complex

coupling effects acting in the antisymmetric laminate of example 7.4 and example 7.7, the use of engineering constants for such a laminate would be questionable.

7.5.4 Comparison of Measured and Predicted Compliances

Experimental verification of the laminate theory can be done by applying known loads to laminate and by measuring resulting deformations and then comparing measured deformations with those predicted from the laminate theory. Alternatively, the compliances that are formed from ratios of strains to loads or ratios of curvature to moments for certain simple loading conditions can be experimentally determined and compared with predicted values. The latter approach has been used by Tsai [13] who reported results for cross-ply and angle-ply glass/epoxy laminates. Only the results for the angle-ply laminates will be discussed here.

In order to determine the compliances of the laminates under various loads, electrical resistance strain gage rosettes with gages oriented at 0° (x direction), 45°, and 90° (y direction) were attached on both sides of the test specimens (fig. 7.20). From equations (7.28), the measured normal strains on the upper surface (where $z = -t/2$) are related to the corresponding midplane strains and curvatures by

$$\varepsilon_x^U = \varepsilon_x^0 - \frac{t}{2}\kappa_x \tag{7.70}$$

$$\varepsilon_y^U = \varepsilon_y^0 - \frac{t}{2}k_y \tag{7.71}$$

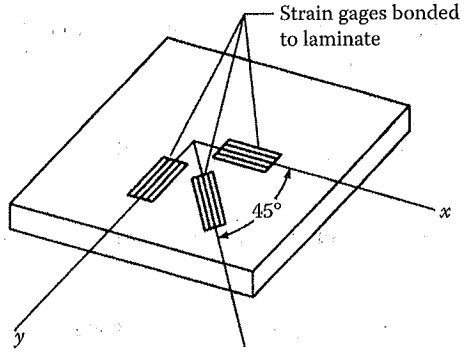

FIGURE 7.20
Strain gage rosette bonded to upper surface of laminate.

where ε_x^U is the measured normal strain along the x direction on upper surface and ε_y^U the measured normal strain along y direction on upper surface.

Similarly, the normal strains on the lower surface (where $z = t/2$) are given by

$$\varepsilon_x^L = \varepsilon_x^0 + \frac{t}{2}\kappa_x \tag{7.72}$$

$$\varepsilon_y^L = \varepsilon_y^0 + \frac{t}{2}\kappa_y \tag{7.73}$$

where ε_x^L is the measured normal strain along the x direction on the lower surface and ε_y^L the measured normal strain along the y direction on the lower surface.

Equation (7.70) and equation (7.72) can be solved simultaneously for the midplane strain, ε_x^0, and curvature, κ_x, whereas ε_y^0 and κ_y can be determined from equation (7.71) and equation (7.73). Although the surface shear strains γ_{xy}^U and γ_{xy}^L are not measured directly like the normal strains, they can be determined from the measured strains along 0°, 45°, and 90° and the strain transformation relationships similar to equations (2.33). For example, from equation (2.33), the measured normal strain along the 45° direction on the upper surface, ε_{45}^U, is related to the corresponding strains along the x and y axes by

$$\varepsilon_{45}^U = \varepsilon_x^U \cos^2\theta + \varepsilon_y^U \sin^2\theta + \gamma_{xy}^U \sin\theta\cos\theta \tag{7.74}$$

and substituting $\theta = 45°$ and solving for γ_{xy}^U, we find that

$$\gamma_{xy}^U = 2\varepsilon_{45}^U - \left(\varepsilon_x^U + \varepsilon_y^U\right) \tag{7.75}$$

Thus, the shear strain is related to the measured strains on the right-hand side of equation (7.75). Similarly, for the lower surface

$$\gamma_{xy}^L = 2\varepsilon_{45}^L - \left(\varepsilon_x^L + \varepsilon_y^L\right) \tag{7.76}$$

Now the last part of equations (7.28) is used to relate the surface shear strains to the midplane shear strains and twisting curvatures:

$$\gamma_{xy}^U = \gamma_{xy}^0 - \frac{t}{2}\kappa_{xy} \tag{7.77}$$

$$\gamma_{xy}^L = \gamma_{xy}^0 + \frac{t}{2}\kappa_{xy} \tag{7.78}$$

These equations can be solved simultaneously for γ^0_{xy} and γ_{xy}, so that all midplane strains and curvatures can be determined from the six measured surface strains. For known loading conditions, the compliances can then be found.

For a uniaxial loading-test of such a strain-gaged specimen with $N_x \neq 0$ and $N_y = N_{xy} = M_x = M_y = M_{xy} = 0$ (fig. 7.18[a]), equations (7.54) can be used to determine six compliances from known loads, midplane strains, and curvatures as follows:

$$A'_{11} = \frac{\varepsilon^0_x}{N_x} \qquad B'_{11} = \frac{\kappa_x}{N_x}$$

$$A'_{12} = \frac{\varepsilon^0_y}{N_x} \qquad B'_{12} = \frac{\kappa_y}{N_x} \tag{7.79}$$

$$A'_{16} = \frac{\gamma^0_{xy}}{N_x} \qquad B'_{16} = \frac{\kappa_{xy}}{N_x}$$

Similar data from a pure flexure test, with $M_x \neq 0$ and $N_x = N_y = N_{xy} = M_y = M_{xy} = 0$ (fig. 7.19[a]) can be used to find the six compliances:

$$B'_{11} = \frac{\varepsilon^0_x}{M_x} \qquad D'_{11} = \frac{\kappa_x}{M_x}$$

$$B'_{12} = \frac{\varepsilon^0_y}{M_x} \qquad D'_{12} = \frac{\kappa_y}{M_x} \tag{7.80}$$

$$B'_{16} = \frac{\gamma^0_{xy}}{M_x} \qquad D'_{16} = \frac{\kappa_{xy}}{M_x}$$

All compliances can be determined from such tests. In addition, some compliances can be determined from more than one test (e.g., the B_{ij} in the above tests). A comparison of measured and predicted compliances of angle-ply glass/epoxy laminates having two or three plies of various lamination angles is shown in figure 7.21 from Tsai [13]. Predicted compliances were determined by using measured lamina properties as follows [13]:

$$E_1 = 7.8 \times 10^6 \text{ psi} \quad (53.8 \text{ MPa})$$

$$E_2 = 2.6 \times 10^6 \text{ psi} \quad (17.9 \text{ MPa})$$

$$G_{12} = 1.25 \times 10^6 \text{ psi} \quad (8.6 \text{ MPa})$$

$$\nu_{12} = 0.25$$

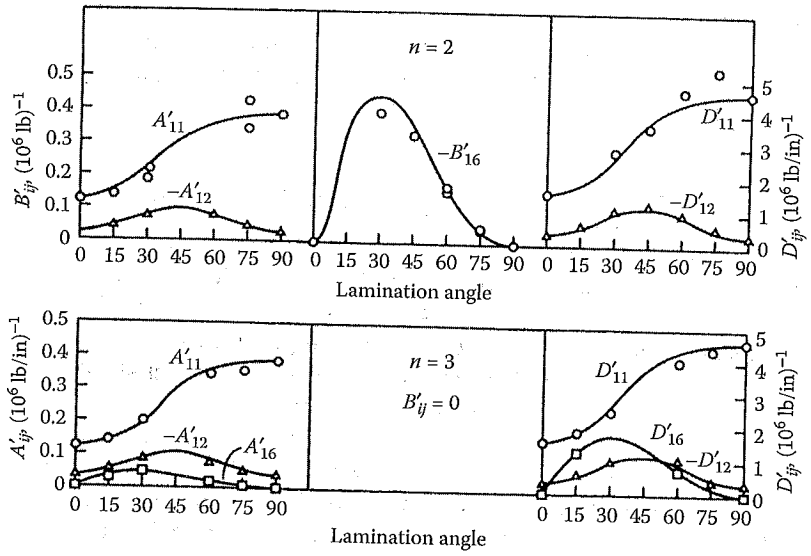

FIGURE 7.21
Measured and predicted compliances for glass/epoxy angle-ply laminates for various lamination angles. (From Tsai, S.W. 1964. *Structural Behavior of Composite Materials.* NASA CR-71.)

The agreement between measured and predicted values in figure 7.21 is quite good, which means that the laminate theory must be reasonably accurate. It is interesting to note that the predicted B_{ij}-type coupling occurs for the two ply antisymmetric laminate but not for the three ply symmetric laminate. Note also that the predicted A_{16}, A_{26}, D_{16}, and D_{26}-type coupling occurs for the three ply laminate but not for the two ply laminate.

7.6 Hygrothermal Effects in Laminates

The analysis of hygrothermal behavior of the lamina in chapter 5 can now be extended to laminates. If we again restrict the discussion to polymer matrix composites, the two main effects of changes in the hygrothermal environment on laminate behavior are degradation of properties and changes in the stress and strain distributions. In this section, the analysis of both these effects along with the prediction of laminate hygrothermal expansion coefficients will be discussed. The basic assumption in all these discussions is that of linearity. That is, we assume that mechanical and hygrothermal effects can be treated separately and then combined using superposition. Coupling between the effects is ignored, as this would lead

to nonlinear equations. Another key assumption used here is that temperature and moisture distributions in the laminate are uniform. That is, the temperature and moisture concentration are assumed to be the same for each ply in the laminate.

7.6.1 Hygrothermal Degradation of Laminates

The analysis of hygrothermal degradation in laminates involves the combination of the lamina degradation analysis in section 5.2, with the laminate analysis described earlier in this chapter. For example, given a combination of temperature and moisture, equation (5.7) can be used to estimate the degraded matrix property, which is then substituted in the appropriate micromechanics equations to estimate the degraded lamina properties such as E_1, E_2, G_{12}, and ν_{12}. The degraded lamina properties are then used in equations (7.38) to equations (7.40) to find the corresponding degraded laminate stiffnesses. Hygrothermal properties such as the coefficients of thermal expansion and hygroscopic expansion can also be degraded using empirical equations such as equation (5.34). These properties would then be used to estimate hygrothermal stresses, as shown in the next section.

7.6.2 Hygrothermal Stresses in Laminates

In section 5.3, the analysis of hygrothermal stresses in an isolated lamina due to temperature and moisture was developed. We now consider the corresponding lamina stresses due to interaction with other laminae in the laminate. Hygrothermal stresses are not only generated during the use of composite materials in various environmental conditions, but also are generated during fabrication. The hygrothermal stresses induced by fabrication are usually referred to as residual stresses. Composites are processed or cured at elevated temperatures and then cooled to room temperature. Due to differences between fiber and matrix coefficient of thermal expansions (CTEs) in the lamina and differences between lamina CTEs in the laminate, residual stresses of fabrication may occur at both the micromechanical and the macromechanical levels. One particularly important result of residual stresses is that in nonsymmetric laminates the B_{ij}-type coupling can cause residual warping of the cured laminate.

In section 7.5.2 the lamina stresses without hygrothermal effects were found by using equations (7.56). As shown in section 5.3, however, when changes in temperature and moisture concentration occur, the total strains in the kth lamina are given by

$$\{\varepsilon\}_k = [\bar{S}]_k\{\sigma\}_k + \{\alpha\}_k \Delta T + \{\beta\}_k c \tag{7.81}$$

and the resulting stresses are given by

$$\{\sigma\}_k = [\bar{Q}]_k(\{\varepsilon\}_k - \{\alpha\}_k \Delta T - \{\beta\}_k c) \tag{7.82}$$

where the subscript k refers to the kth lamina. As shown in section 5.3, if the lamina is completely restrained by adjacent laminae, the total strains $\{\varepsilon\}_k = 0$ and the resulting hygrothermal stresses are given by

$$\{\sigma\}_k = [\bar{Q}]_k(-\{a\}_k \Delta T - \{\beta\}_k c) \tag{7.83}$$

In a laminate, however, the total lamina strains generally do not vanish, but are instead given by

$$\{\varepsilon\}_k = \{\varepsilon^0\} + z\{\kappa\} \tag{7.84}$$

and the resulting stresses, including hygrothermal effects, are given by

$$\{\sigma\}_k = [\bar{Q}]_k\left(\{\varepsilon^0\} + z\{\kappa\} - \{\alpha\}_k \Delta T - \{\beta\}_k c\right) \tag{7.85}$$

Following the procedure outlined in equation (7.32) to equation (7.42), the resultant laminate forces per unit length are found by integrating equations (7.85) through the thickness of the laminate:

$$\begin{aligned}\{N\} &= \int \{\sigma\}_k dz = \int [\bar{Q}]_k\left(\{\varepsilon^0\} + z\{\kappa\} - \{\alpha\}_k \Delta T - \{\beta\}_k c\right) dz \\ &= [A]\{\varepsilon^0\} + [B]\{\kappa\} - \{N^T\} - \{N^M\}\end{aligned} \tag{7.86}$$

where the thermal forces due to temperature change are given by

$$\{N^T\} = \int [\bar{Q}]_k \{\alpha\}_k \Delta T dz = (\Delta T)\sum_{k=1}^{N} [\bar{Q}]_k \{\alpha\}_k (z_k - z_{k-1}) \tag{7.87}$$

and the hygroscopic forces due to moisture are given by

$$\{N^M\} = \int [\bar{Q}]_k \{\beta\}_k c dz = (c)\sum_{k=1}^{N} [\bar{Q}]_k \{\beta\}_k (z_k - z_{k-1}) \tag{7.88}$$

Similarly, the resultant moments per unit length are

$$\{M\} = \int \{\sigma\}_k z\,dz = \int [\bar{Q}]_k \left(\{\varepsilon^0\} + z\{\kappa\} - \{\alpha\}_k \Delta T - \{\beta\}_k c\right) z\,dz$$
$$= [B]\{\varepsilon^0\} + [D][\kappa] - \{M^T\} - \{M^M\} \tag{7.89}$$

where the thermal moments due to temperature changes are

$$\{M^T\} = \int [\bar{Q}]_k \{\alpha\}_k \Delta T z\,dz = \frac{\Delta T}{2} \sum_{k=1}^{N} [\bar{Q}]_k \{\alpha\}_k \left(z_k^2 - z_{k-1}^2\right) \tag{7.90}$$

and the hygroscopic moments due to moisture are given by

$$\{M^M\} = \int [\bar{Q}]_k \{\beta\}_k cz\,dz = \frac{c}{2} \sum_{k=1}^{N} [\bar{Q}]_k \{\beta\}_k \left(Z_k^2 - z_{k-1}^2\right) \tag{7.91}$$

Rearranging equation (7.86) and equation (7.89), we find that

$$\{N\} + \{N^T\} + \{N^M\} = [A]\{\varepsilon^0\} + [B]\{\kappa\} \tag{7.92}$$

and

$$\{M\} + \{M^T\} + \{M^M\} = [B]\{\varepsilon^0\} + [D]\{\kappa\} \tag{7.93}$$

or

$$\begin{Bmatrix} N^E \\ \hline M^E \end{Bmatrix} = \left[\begin{array}{c|c} A & B \\ \hline B & D \end{array}\right] \begin{Bmatrix} \varepsilon^0 \\ \hline \kappa \end{Bmatrix} \tag{7.94}$$

where the total effective forces (mechanical plus hygrothermal) are

$$\{N^E\} = \{N\} + \{N^T\} + \{N^M\} \tag{7.95}$$

and the total effective moments (mechanical plus hygrothermal) are

$$\{M^E\} = \{M\} + \{M^T\} + \{M^M\} \tag{7.96}$$

Alternatively, the inverted forms of equations (7.94) are given by

$$\begin{Bmatrix} \varepsilon^0 \\ \hline \kappa \end{Bmatrix} = \left[\begin{array}{c|c} A' & B' \\ \hline B' & D' \end{array}\right] \begin{Bmatrix} N^E \\ \hline M^E \end{Bmatrix} \tag{7.97}$$

Thus, the lamina stresses for combined mechanical and hygrothermal loading are determined by using a procedure similar to that outlined in section 7.5.2. That is, the midplane strains and curvatures are determined from the total effective forces and moments according to equations (7.97); then the lamina stresses are determined from equations (7.85).

EXAMPLE 7.9

The antisymmetric angle-ply laminate described in example 7.4 is heated from 20°C (68°F) to 100°C (212°F). Assuming that the lamina properties do not change over this temperature range, determine the hygrothermal stresses.

Solution. From table 5.3, the lamina CTEs associated with the principal material axes are

$$\alpha_1 = 0.88 \times 10^{-6}/°C \qquad \alpha_2 = 31.0 \times 10^{-6}/°C$$

The CTEs associated with the +45° and −45° lamina orientations are found by using the transformations in equations (5.22):

$$\begin{Bmatrix} \alpha_x \\ \alpha_y \\ \alpha_{xy}/2 \end{Bmatrix}_{+45°} = \begin{bmatrix} 0.5 & 0.5 & -1.0 \\ 0.5 & 0.5 & 1.0 \\ 0.5 & -0.5 & 0 \end{bmatrix} \begin{Bmatrix} 0.88 \\ 31.0 \\ 0 \end{Bmatrix} \times 10^{-6} = \begin{Bmatrix} 15.94 \\ 15.94 \\ -15.06 \end{Bmatrix} \times 10^{-6}/°C$$

$$\begin{Bmatrix} \alpha_x \\ \alpha_y \\ \alpha_{xy}/2 \end{Bmatrix}_{+45°} = \begin{bmatrix} 0.5 & 0.5 & 1.0 \\ 0.5 & 0.5 & -1.0 \\ -0.5 & 0.5 & 0 \end{bmatrix} \begin{Bmatrix} 0.88 \\ 31.0 \\ 0 \end{Bmatrix} \times 10^{-6} = \begin{Bmatrix} 15.94 \\ 15.94 \\ 15.06 \end{Bmatrix} \times 10^{-6}/°C$$

Next, the thermal forces due to temperature change are found by substituting the above values and the lamina stiffnesses from example 7.3 in equation (7.87). Note also that the third element in column vector $\{\alpha\}_k$ in equation (7.87) is α_{xy}, not $\alpha_{xy}/2$ as in the above transformations. Since $z_k - z_{k-1} = t/4$ for all laminae,

$$\{N^T\} = ([\bar{Q}]_{+45°}\{\alpha\}_{+45°} + [\bar{Q}]_{-45°}\{\alpha\}_{-45°})2(\Delta T)(t/4)$$

or

$$\begin{Bmatrix} N_x^T \\ N_y^T \\ N_{xy}^T \end{Bmatrix} = \begin{bmatrix} 45.22 & 31.42 & 32.44 \\ 31.42 & 45.22 & 32.44 \\ 32.44 & 32.44 & 35.6 \end{bmatrix} \begin{Bmatrix} 15.94 \\ 15.94 \\ -30.12 \end{Bmatrix} (10^{-6})(2)(80)(0.25)$$

$$+ \begin{bmatrix} 45.22 & 31.42 & -32.44 \\ 31.42 & 45.22 & -32.44 \\ -32.44 & -32.44 & 35.6 \end{bmatrix} \begin{Bmatrix} 15.94 \\ 15.94 \\ 30.12 \end{Bmatrix} (10^{-6})(2)(80)(0.25)$$

$$= \begin{Bmatrix} 1.956 \\ 1.956 \\ 0 \end{Bmatrix} \times 10^{-2}\,\text{GPa-mm}$$

Similarly, the thermal moments are found from equations (7.90) as

$$\{M^T\} = \left([\bar{Q}]_{-45^\circ} \{\alpha\}_{-45^\circ} \left(z_1^2 - z_0^2 \right) + [\bar{Q}]_{+45^\circ} \{\alpha\}_{+45^\circ} \left(z_2^2 - z_1^2 \right) \right.$$

$$\left. + [\bar{Q}]_{-45^\circ} \{\alpha\}_{-45^\circ} \left(z_3^2 - z_2^2 \right) + [\bar{Q}]_{+45^\circ} \{\alpha\}_{+45^\circ} \left(z_4^2 - z_3^2 \right) \right) \frac{\Delta T}{2}$$

or

$$\begin{Bmatrix} M_x^T \\ M_y^T \\ M_{xy}^T \end{Bmatrix} = \begin{Bmatrix} 0 \\ 0 \\ -3.81 \end{Bmatrix} \times 10^{-4}\,\text{GPa-mm}^2$$

From equation (7.95) and equation (7.96), we have $\{N^E\} = \{N^T\}$ and $\{M^E\} = \{M^T\}$. Using these results along with the compliances from example 7.7 in equation (7.97), we find that the midplane strains and curvatures are

$$\begin{Bmatrix} \varepsilon_x^0 \\ \varepsilon_y^0 \\ \gamma_{xy}^0 \\ \kappa_x \\ \kappa_y \\ \kappa_{xy} \end{Bmatrix} = \begin{Bmatrix} 3.06\,\text{mm/mm} \\ 3.06\,\text{mm/mm} \\ 0\,\text{mm/mm} \\ 0\,\text{mm}^{-1} \\ 0\,\text{mm}^{-1} \\ -9.65\,\text{mm}^{-1} \end{Bmatrix} \times 10^{-4}$$

Note that the thermal twisting moment, M_{xy}^T, causes a corresponding twisting curvature, κ_{xy}, which means that the laminate will warp under the temperature change. Stresses along the x and y axes are now found by substituting the above midplane strains and curvatures, along with the

lamina stiffnesses from example 7.3, in equation (7.85). Stresses at the top and bottom of each ply are given in the following table:

Location	σ_x (MPa)	σ_y (MPa)	τ_{xy} (MPa)
#1 Top	−11.8	−11.8	−5.7
#1 Bottom	−3.9	−3.9	−14.3
#2 Top	11.8	11.8	31.6
#2 Bottom	3.9	3.9	23.0
#3 Top	3.9	3.9	−23.0
#3 Bottom	11.8	11.8	−31.6
#4 Top	−3.9	−3.9	14.3
#4 Bottom	−11.8	−11.8	5.7

As with example 7.7, the stress distribution is quite complex because of the coupling effect.

7.6.3 Laminate Hygrothermal Expansion Coefficients

The effective hygrothermal expansion coefficients for the laminate can be calculated directly by combining the definitions of the coefficients with the appropriate laminate equations. For example, the effective CTE of a laminate along the x direction is

$$\alpha_x = \frac{\varepsilon_x^0}{\Delta T} \tag{7.98}$$

For a symmetric laminate with $B_{ij} = 0$, the midplane strain along the x direction due to a temperature change T only is given by the first of equations (7.97):

$$\varepsilon_x^0 = A'_{11} N_x^T + A'_{12} N_y^T + A'_{16} N_{xy}^T \tag{7.99}$$

The desired thermal expansion coefficient, α_x, is then found by substituting the thermal forces from equation (7.87) in equation (7.99) and then by substituting the result in equation (7.98). It is important to note that this procedure effectively relates the laminate CTE to lamina CTEs, lamina stiffnesses, laminate compliances, and laminate geometry. The temperature change, ΔT, will cancel out since it appears in both the numerator and the denominator. Similar results can be obtained for other thermal and hygroscopic expansion coefficients. As with the effective laminate engineering constants, it is appropriate to restrict the use of the effective hygrothermal expansion coefficients to those cases where the deformations are similar to the deformations associated with the particular coefficient being used.

For example, it is probably not a good practice to use such coefficients to describe the hygrothermal behavior of a laminate that exhibits significant warping due to coupling effects.

7.7 Interlaminar Stresses

One of the key limitations of the CLT is that each ply is assumed to be in plane stress in the xy plane (fig. 7.8), and that interlaminar stresses associated with the z axis are neglected. Such interlaminar stresses can cause delamination or separation of the laminae, which is a failure mode that we have not previously considered. In this section, 3-D stress analyses that yield the interlaminar stresses will be discussed, and the resulting interlaminar stresses will be used later in a laminate strength analysis.

A state of plane stress actually does exist in the laminae of a laminate in regions sufficiently far away from geometric discontinuities such as free edges. A 3-D elasticity solution by Pipes and Pagano [14] has shown, however, that even in a laminate under simple uniaxial loading (fig. 7.22), there is a "boundary layer" region along the free edges where a 3-D state of stress exists, and that the boundary layer thickness is roughly equal to the laminate thickness.

The behavior of interlaminar stresses near a free edge in a laminate will be demonstrated here by using the three stress equilibrium equations from the theory of elasticity (Appendix A):

$$\frac{\partial \sigma_x}{\partial x}+\frac{\partial \tau_{xy}}{\partial y}+\frac{\partial \tau_{xz}}{\partial z}=0 \tag{7.100}$$

$$\frac{\partial \tau_{yx}}{\partial x}+\frac{\partial \sigma_y}{\partial y}+\frac{\partial \tau_{yz}}{\partial z}=0 \tag{7.101}$$

$$\frac{\partial \tau_{zx}}{\partial x}+\frac{\partial \tau_{zy}}{\partial y}+\frac{\partial \sigma_z}{\partial z}=0 \tag{7.102}$$

For the uniaxially loaded laminate in figure 7.22, we now consider a region near the free edges, where $y = \pm b$, and assume that the stresses do not vary along the loading direction (the x axis). It follows that $\partial \sigma_x / \partial x = 0$ and from equation (7.100), the interlaminar shear stress, $\tau_{xz}(z)$, is given by

$$\tau_{xz}(z)=-\int_{-t/2}^{z}\frac{\partial \tau_{xy}}{\partial y}\,dz \tag{7.103}$$

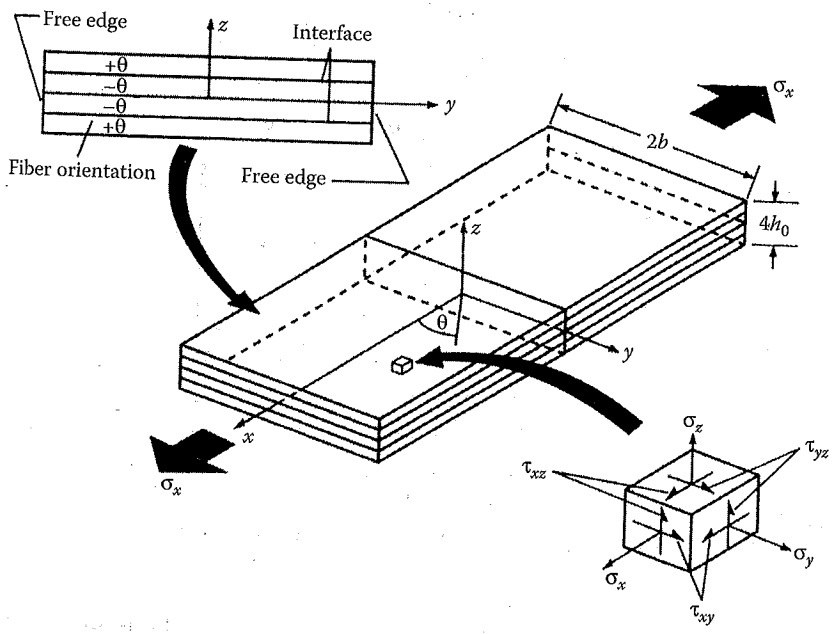

FIGURE 7.22
Pipes and Pagano model for analysis of interlaminar stresses in a laminate under uniaxial extension. (From Pipes, R.B. and Pagano, N.J. 1970. *Journal of Composite Materials*, 4, 538–548. With permission.)

We now assume that the in-plane shear stress, τ_{xy}, has a constant value given by the CLT in the interior regions of the laminae. As we move along the y direction toward a free edge, however, τ_{xy} must decrease to zero at the stress-free surfaces where $y = \pm b$. Thus, as $y \to \pm b$, $|\partial \tau_{xy}/\partial y|$ must increase. It follows from equation (7.103) that τ_{xz} must increase from zero in the interior region to a very large value as $y \to \pm b$, as shown in figure 7.23. The region where these rapid changes take place is referred to as the interlaminar stress boundary layer region, as shown in figure 7.23. From equation (7.101) and equation (7.102), respectively, the other interlaminar stresses as

$$\tau_{yz}(z)=-\int_{-t/2}^{z}\frac{\partial \sigma_y}{\partial y}\,dz \tag{7.104}$$

$$\sigma_z(z)=-\int_{-t/2}^{z}\frac{\partial \tau_{yz}}{\partial y}\,dz \tag{7.105}$$

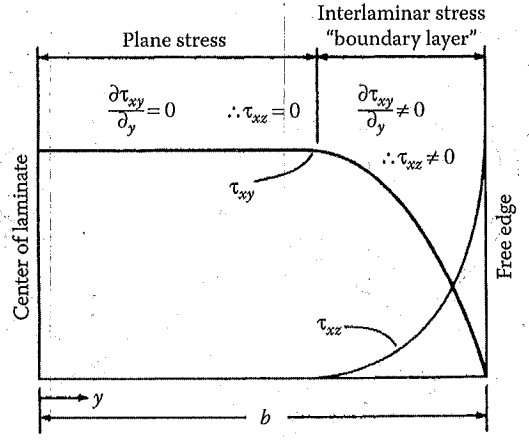

FIGURE 7.23
Schematic representation of in-plane shear stress and interlaminar shear stress distributions at ply interface.

Pipes and Pagano [14] used a finite difference numerical scheme to solve the three governing field equations that are generated by combining the three-dimensional versions of the stress equilibrium equations (Appendix A), the lamina stress–strain relationships (Equation 7.22), and the strain–displacement relations (Appendix B). The equations were solved subject to stress-free boundary conditions along the free edges of a four layer ±45° graphite/epoxy laminate under uniform axial strain, ε_x. Figure 7.24 shows the complete stress results obtained by Pipes and Pagano [14]. It is important to note that the in-plane stresses σ_x and τ_{xy} from the 3-D analysis agree with those predicted by the CLT in the central portion of the laminate, but both stresses drop in the boundary layer region near the free edge. On the other hand, the interlaminar stresses σ_z, τ_{xz}, and τ_{yz} are all equal to zero in the central portion of the laminate but change rapidly near the free edge. The shear stress τ_{xz} is the largest of the interlaminar stresses, as it appeared to grow without bound at $y/b = 1.0$. Pipes and Pagano suspected that a singularity for this stress component exists at the free edge, but it was not possible to prove the existence of such a singularity with the approximate finite difference solution. Analytical proof of the existence of these singularities was published later by Wang and Choi [15,16].

The numerical results of Pipes and Pagano [14] for a variety of laminate cross-sectional aspect ratios led to the conclusion that the boundary layer region of 3-D stresses extends inward approximately one laminate thickness from the free edge. This conclusion was later verified experimentally by Pipes and Daniel [17] who used a Moiré technique to measure displacements along the x direction on the surface of the laminate. The

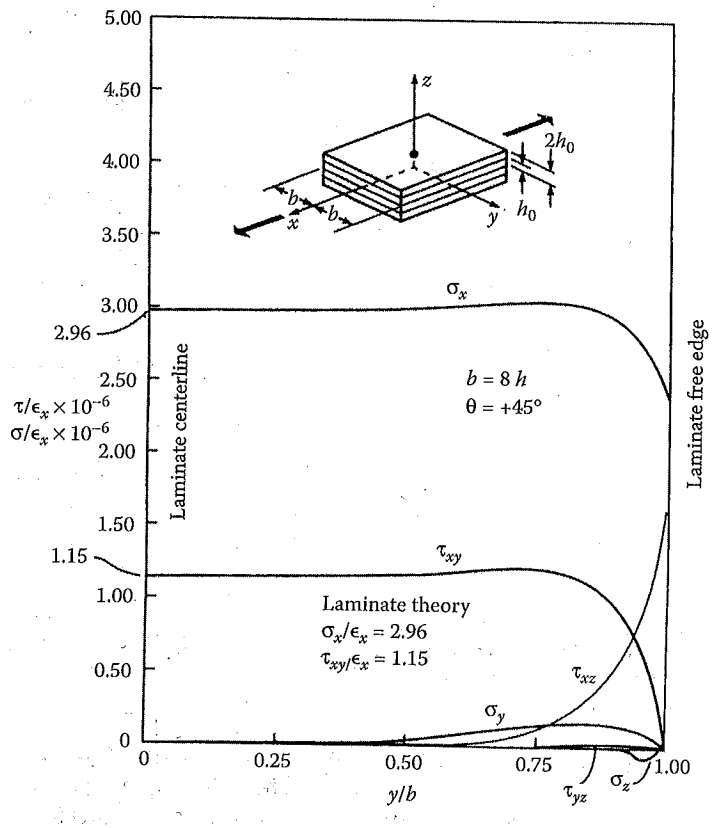

FIGURE 7.24
Distribution of all stresses from Pipes and Pagano analysis. (From Pipes, R.B. and Pagano, N.J. 1970. *Journal of Composite Materials*, 4, 538–548. With permission.)

measured surface displacement profiles, which also clearly indicated the presence of the boundary layer, agreed closely with those predicted by the Pipes and Pagano analysis.

It has been shown both analytically and experimentally that the lamina-stacking sequence influences interlaminar stresses and, consequently, delamination in laminates. Pipes and Pagano [18] used an approximate elasticity solution to study the effect of the stacking sequence on the interlaminar shear stress in ±45° laminates, as shown in figure 7.25. It is clear from figure 7.25 that when layers having the same orientation are stacked together (which increases the apparent layer thickness), the interlaminar shear stress, τ_{xz}, is higher than for the case where layers of opposite orientation are stacked together. In a separate paper, Pagano and Pipes [19] showed that a change in the stacking sequence can actually cause the

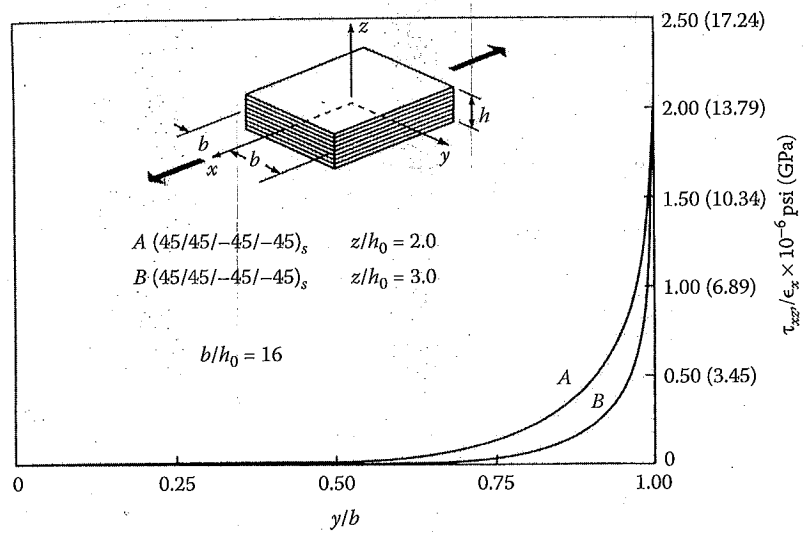

FIGURE 7.25
Effect of stacking sequence on interlaminar shear stress. (From Pipes, R.B. and Pagano, N.J. 1974. *Journal of Applied Mechanics*, 41, Series E (3), 668–672. Reprinted by permission of The American Society of Mechanical Engineers.)

interlaminar normal stress, σ_z, to change from tensile to compressive. Since tensile interlaminar normal stresses would tend to cause separation of the plies, while compressive interlaminar normal stresses would tend to keep the plies together, stacking sequences that produce the former stress state should have lower strengths than those producing the latter stress state. Experimental results such as those by Whitney and Browning [20] and Whitney and Kim [21] seem to support this conclusion. Ply orientation also has a strong effect on interlaminar stresses, as shown by Pipes and Pagano [14].

Since the publication of the Pipes and Pagano solution, a number of investigators have used other methods to study the "free-edge" interlaminar stress phenomenon. Rybicki [22], Wang and Crossman [23], Herakovich [24], and Hwang and Gibson [25] all used 3-D finite element analyses to investigate interlaminar stresses. The quarter-domain finite element model used by Hwang and Gibson [25] for the analysis of the original Pipes and Pagano [14] laminate is shown in figure 7.26. Finite element stress distributions near the free edge from Wang and Crossman [23] and Hwang and Gibson [25] are compared with those from an empirical solution derived from the theory of elasticity by Hwang [26] in figure 7.27. The empirical elasticity solution by Hwang [26] is based on a similar solution by Whitney [27], which, in turn, is an attempt to fit the

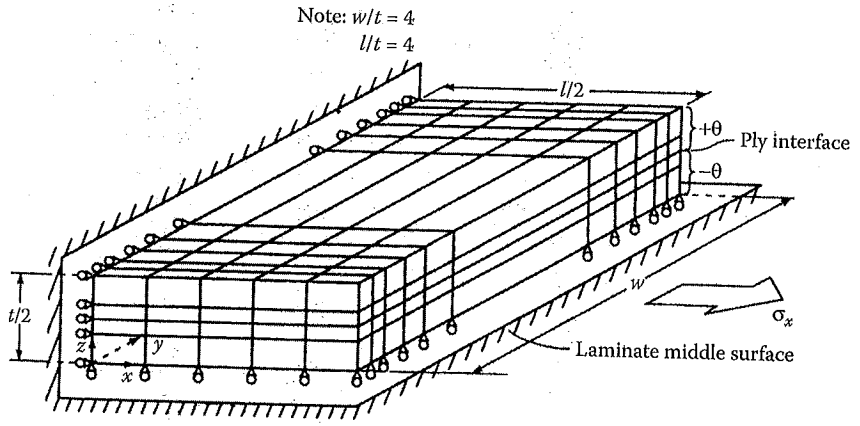

FIGURE 7.26
Quarter domain finite element model of laminate used by Hwang and Gibson to analyze the Pipes–Pagano problem. (From Hwang, S.J. and Gibson, R.F. 1992. *Composite Structures*, 20, 29–35. Reprinted by permission of Elsevier Publishers, Ltd.)

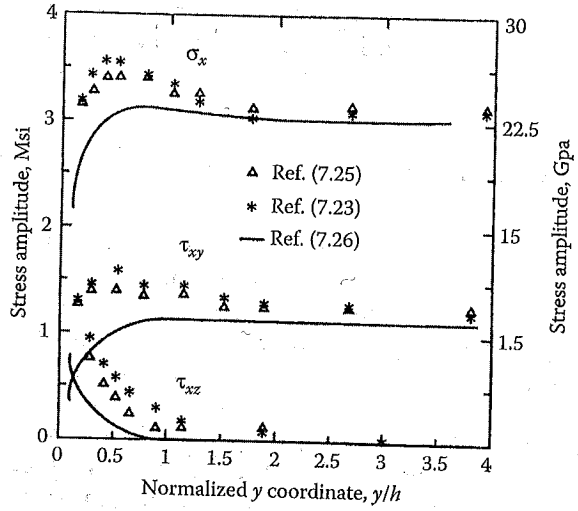

FIGURE 7.27
Comparison of stress distributions near the free edge. (From Hwang, S.J. and Gibson, R.F. 1992. *Composite Structures*, 20, 29–35. Reprinted by permission of Elsevier Publishers, Ltd.)

finite difference results of Pipes and Pagano [14] with relatively simple empirical equations that satisfy the stress equilibrium equations (equation [7.100] to equation [7.102]) and the free-edge boundary conditions. Thus, the empirical results shown by the solid curve in figure 7.27 should be very close to the original Pipes and Pagano results. Although the stress distributions from the two finite element models show good agreement with each other, both sets of stresses are seen to be greater than those from the empirical solution near the free edge. Improved approximate polynomial solutions have been proposed by Conti and De Paulis [28].

7.8 Laminate Strength Analysis

Recall that in section 4.2, we discussed several multiaxial strength criteria for estimating the strength of individual laminae under in-plane stresses. Such strength criteria can also be used on a ply-by-ply basis for a laminate to determine which ply fails first under in-plane loads. In section 7.7, however, we have seen that interlaminar stresses in laminates also have to be taken into account because they may lead to a different mode of failure known as delamination. This section deals with the analysis of both first ply failure due to in-plane stresses and delamination due to interlaminar stresses. The mechanical behavior of the laminate after first ply failure and subsequent ply failures is also discussed.

7.8.1 First Ply Failure and Subsequent Ply Failures Due to In-Plane Stresses

The prediction of first ply failure due to in-plane stresses is a straightforward application of the appropriate multiaxial lamina strength criterion in combination with the lamina stress analysis from the CLT. The loads corresponding to first ply failure are not necessarily the laminate failure loads, however, since a laminate generally has plies at several orientations. That is, there will usually be a sequence of ply failures at different loads culminating in ultimate laminate failure when all plies have failed. Thus, the ultimate load-carrying capacity of the laminate may be significantly higher than the first ply failure load, and prediction of laminate failure based on first ply failure may be too conservative.

In the analysis of first ply failure and subsequent ply failures, the stiffness matrices for the failed plies and the corresponding laminate stiffness matrix must be modified after each ply failure to reflect the effects of those failures. Figure 7.28 shows an idealized piecewise linear laminate load–deformation curve with several "knees" due to ply failures. The total

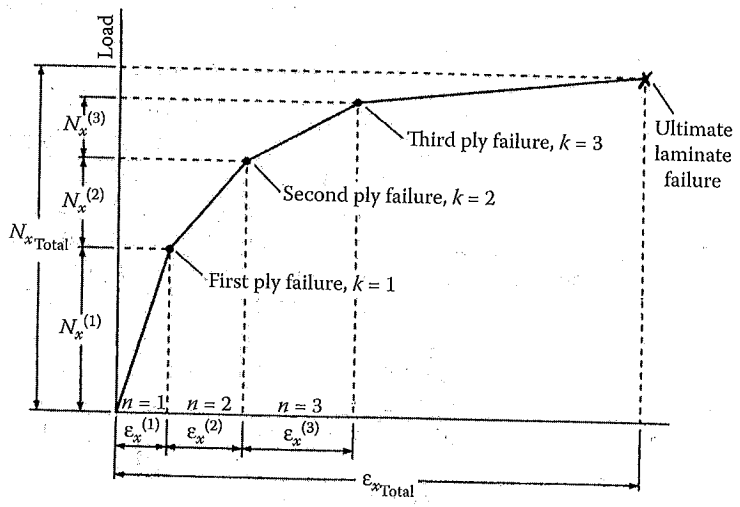

FIGURE 7.28
Idealized load–strain curve for uniaxially loaded laminate showing multiple ply failures leading up to ultimate laminate failure.

forces and moments at the kth knee in the curve are related to the corresponding forces and moments for the nth section of such a curve (where $n \leq k$) by the summation

$$\begin{Bmatrix} N \\ M \end{Bmatrix}_{\text{Total}} = \sum_{n=1}^{k} \begin{Bmatrix} N^{(n)} \\ M^{(n)} \end{Bmatrix} \tag{7.106}$$

where the superscript (n) on a parameter denotes the particular value of that parameter associated with the nth section. The corresponding midplane strains and curvatures are given by

$$\begin{Bmatrix} \varepsilon^0 \\ \kappa \end{Bmatrix}_{\text{Total}} = \sum_{n=1}^{k} \begin{Bmatrix} \varepsilon^{0(n)} \\ \kappa^{(n)} \end{Bmatrix} \tag{7.107}$$

Using the piecewise linear assumption, the load–deformation relationship for the nth section can be approximated by modifying equations (7.42) as

$$\left\{\begin{array}{c} N^{(n)} \\ \hline M^{(n)} \end{array}\right\} = \left[\begin{array}{c|c} A^{(n)} & B^{(n)} \\ \hline B^{(n)} & D^{(n)} \end{array}\right] \left\{\begin{array}{c} \varepsilon^{0(n)} \\ \hline \kappa^{(n)} \end{array}\right\} \tag{7.108}$$

where the $[A^{(n)}]$, $[B^{(n)}]$, and $[D^{(n)}]$ are the modified stiffness matrices after the $(n-1)$th ply failure. But the calculation of these modified laminate stiffnesses requires that we know the modified ply stiffnesses, $[Q^{(n)}]$, and before we can modify the ply stiffness matrices, we must know the type of failure. That is, if the ply failure is caused by the in-plane shear stress exceeding the shear strength, the shear modulus and the transverse modulus of that ply may be severely degraded by longitudinal cracks, but the longitudinal modulus may not be affected significantly by these cracks. Alternatively, all the ply stiffnesses for the failed ply could be equated to zero or some very small number in the calculation of the degraded laminate stiffnesses.

Halpin [12] has used a procedure similar to the one outlined above to analyze the uniaxial stress–strain response of a $[0/\pm45/90]_s$ glass/epoxy laminate. The Maximum Strain Criterion was used to predict ply failure, and the ply stiffnesses of the failed plies were set equal to zero. The predicted stress–strain curve shows good agreement with the corresponding experimental data, as shown in figure 7.29. Notice that the curve has two "knees" — the first one at the strain corresponding to failure of the 90° plies and the second one at the strain corresponding to failure of the ±45° plies. The knee for the ±45° ply failure is more distinct than the one for the 90° ply failure, because the laminate has twice as many ±45° plies as it does 90° plies. Ultimate laminate failure occurs at the longitudinal failure strain for the 0° plies. It is also interesting to note that the experimental data do

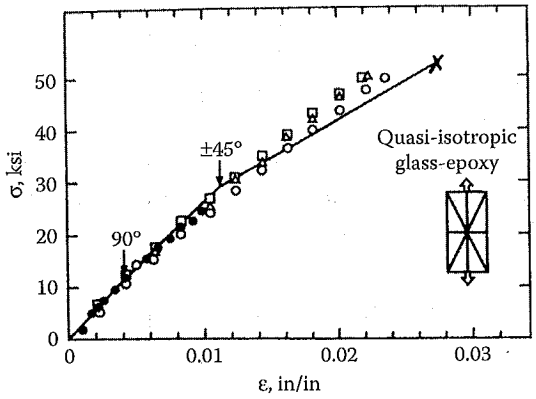

FIGURE 7.29
Comparison of predicted and measured stress–strain response of $[0/\pm45/90]_s$ glass/epoxy laminate. (From Halpin, J.C. 1984. *Primer on Composite Materials: Analysis.* Technomic Publishing Co., Lancaster, PA. With permission.)

not show as much of a change in slope at the knees as the theoretical curve does. This may be due to the fact that actual ply failure occurs gradually over a finite strain range, whereas instantaneous ply failure at a single strain level is assumed in the analysis. The same reasoning may explain the absence of jumps in the stress–strain curve after ply failure [29]. A horizontal jump would be predicted if the test data were taken under load-control, whereas a vertical jump would be predicted for a displacement-control test. Hahn and Tsai [29] have observed that the knee in the stress–strain curve for cross-ply laminates is quite obvious if the 90° plies are all stacked adjacent to each other, but the knee is not so obvious if the 0° and 90° plies are arranged in an alternating 0°/90° sequence. Restraint of the failed 90° plies by the remaining 0° plies was thought to be more effective in the alternating 0°/90° sequence, making the failure of the 90° plies more gradual.

The in-plane strength of ±θ angle-ply laminates may also be analyzed using a multiaxial lamina strength criterion and the CLT, but the piecewise linear approximation of the stress–strain curve may not be needed. This is because if the lamina tensile and compressive strengths are equal, all plies fail simultaneously in the angle-ply laminate, and the stress–strain curve does not have the characteristic knees shown in figure 7.28 and figure 7.29. Tsai [30] has used the Tsai–Hill Criterion to predict the strength of glass/epoxy angle-ply laminates as a function of the lamination angle θ, and the predictions are seen to agree well with experimental data in figure 7.30. The predicted laminate stiffness A_{11} also shows good agreement with the prediction from the CLT in figure 7.30.

EXAMPLE 7.10

A $[90/0/90]_s$ laminate consisting of the AS/3501 laminae described in example 7.3 is subjected to tensile uniaxial loading along the x direction. Using the Maximum Strain Criterion, find the loads corresponding to first ply failure and subsequent ply failures; then plot the load–strain curve up to failure.

Solution. The failure strains are found by substituting the data from table 2.2 and table 4.1 in equation (4.1):

$$e_L^{(+)} = \frac{s_L^{(+)}}{E_1} = \frac{1448}{138\times10^3} = 0.0105$$

$$e_T^{(+)} = \frac{s_T^{(+)}}{E_2} = \frac{48.3}{9\times10^3} = 0.0054$$

Using these results in the Maximum Strain Criterion, we see that first ply failure occurs at a strain $\varepsilon_x = e_T^{(+)} = 0.0054$. To find the corresponding load

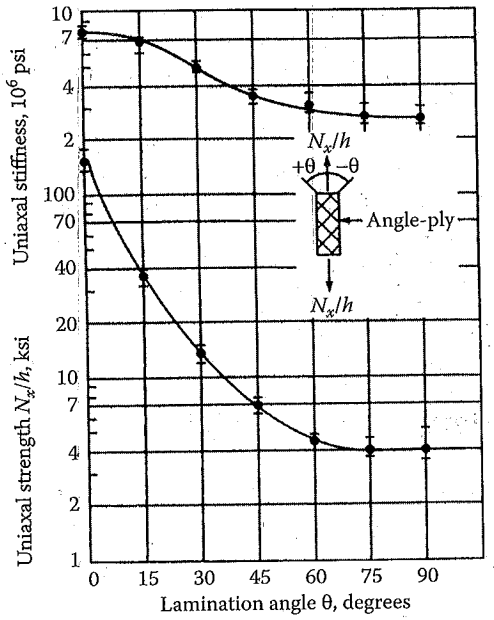

FIGURE 7.30
Comparison of predicted and measured uniaxial strength and stiffness of glass/epoxy angle-ply laminates. (From Tsai, S.W. 1965. *Strength Characteristics of Composite Materials*, NASA CR-224.)

N_x at first ply failure, it is necessary to find the initial laminate stiffness matrix $[A^{(1)}]$. From example 7.3, the lamina stiffness matrix for the 0° plies is given by

$$[\bar{Q}]_{0^\circ} = [Q] = \begin{bmatrix} 138.8 & 2.72 & 0 \\ 2.72 & 9.05 & 0 \\ 0 & 0 & 6.9 \end{bmatrix} \text{ GPa}$$

The stiffness matrix for the 90° plies is formed by simply interchanging the 11 and 22 terms in the stiffness matrix for the 0° plies:

$$[\bar{Q}]_{90^\circ} = \begin{bmatrix} 9.05 & 2.72 & 0 \\ 2.72 & 138.8 & 0 \\ 0 & 0 & 6.9 \end{bmatrix} \text{ GPa}$$

For the first section of the load–strain curve, the laminate stiffness matrix is therefore

$$[A^{(1)}] = [\bar{Q}]_{0^\circ}(2)(0.25) + [\bar{Q}]_{90^\circ}(4)(0.25) = 0.5[\bar{Q}]_{0^\circ} + [\bar{Q}]_{90^\circ}$$

$$\text{or} \quad [A^{(1)}] = \begin{bmatrix} 78.45 & 4.08 & 0 \\ 4.08 & 143.3 & 0 \\ 0 & 0 & 10.35 \end{bmatrix} \text{ GPa-mm}$$

At first ply failure, the laminate load–deformation equations can be written as

$$\begin{Bmatrix} N_x^{(1)} \\ 0 \\ 0 \end{Bmatrix} = \begin{bmatrix} 78.45 & 4.08 & 0 \\ 4.08 & 143.3 & 0 \\ 0 & 0 & 10.35 \end{bmatrix} \begin{Bmatrix} 0.0054 \\ \varepsilon_y^{(1)} \\ \gamma_{xy}^{(1)} \end{Bmatrix}$$

These equations can be solved simultaneously to get the following values of loads and strains at first ply failure:

$$N_x^{(1)} = 0.423 \text{ GPa-mm}; \qquad \varepsilon_y^{(1)} = -0.000154; \qquad \gamma_{xy}^{(1)} = 0$$

We will now demonstrate two different approaches for modifying the laminate stiffness matrix after first ply failure.

(a) In the first approach, we simply set all ply stiffnesses equal to zero for the failed 90° plies. The adjusted laminate stiffness matrix is then

$$[A^{(2)}] = 0.5[\bar{Q}]_{0^\circ} = \begin{bmatrix} 69.4 & 1.36 & 0 \\ 1.36 & 4.52 & 0 \\ 0 & 0 & 3.45 \end{bmatrix} \text{ GPa-mm}$$

Now the 0° ply failure and the ultimate laminate failure occurs at a strain level $\varepsilon_x = e_L^{(+)} = 0.0105$, which means that the strain increment for the second section of the load–strain curve is

$$\varepsilon_x^{(2)} = e_L^{(+)} - \varepsilon_x^{(1)} = 0.0105 - 0.0054 = 0.0051$$

The load–deformation equations describing the second section of the load–strain curve are

$$\begin{Bmatrix} N_x^{(2)} \\ 0 \\ 0 \end{Bmatrix} = \begin{bmatrix} 69.4 & 1.36 & 0 \\ 1.36 & 4.52 & 0 \\ 0 & 0 & 3.45 \end{bmatrix} \begin{Bmatrix} 0.0051 \\ \varepsilon_y^{(2)} \\ \gamma_{xy}^{(2)} \end{Bmatrix}$$

and the simultaneous solution of these equations yields the results

$$N_x^{(2)} = 0.352 \text{ GPa-mm}; \qquad \varepsilon_y^{(2)} = -0.00153; \qquad \gamma_{xy}^{(2)} = 0$$

The total laminate failure load is then

$$N_{x\text{Total}} = N_x^{(1)} + N_x^{(2)} = 0.423 + 0.352 = 0.775 \text{ GPa-mm}$$

and the load–strain curve is shown as curve (a) in figure 7.31.

(b) In the second approach, we set only $E_2 = G_{12} = \nu_{21} = 0$ for the failed 90° plies, but we assume that E_1, for the 90° plies is not affected by the transverse failure. According to these assumptions,

$$[\bar{Q}_{22}]_{90^\circ} = E_1 = 138 \text{ GPa}; \qquad [\bar{Q}_{11}]_{90^\circ} = [\bar{Q}_{12}]_{90^\circ} = [\bar{Q}_{66}]_{90^\circ} = 0$$

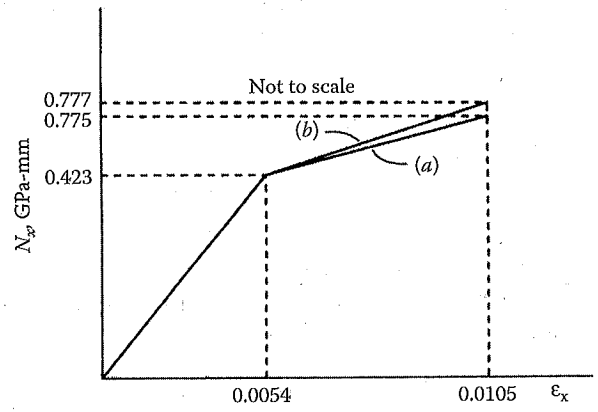

FIGURE 7.31
Predicted load–strain curves for example 7.10.

and the adjusted laminate stiffness matrix is

$$[A^{(2)}] = \begin{bmatrix} 69.4 & 1.36 & 0 \\ 1.36 & 143.3 & 0 \\ 0 & 0 & 3.45 \end{bmatrix} \text{ GPa-mm}$$

The laminate load–deformation equations for the second section are

$$\begin{Bmatrix} N_x^{(2)} \\ 0 \\ 0 \end{Bmatrix} = \begin{bmatrix} 69.4 & 1.36 & 0 \\ 1.36 & 143.3 & 0 \\ 0 & 0 & 3.45 \end{bmatrix} \begin{Bmatrix} 0.0051 \\ \in_y^{(2)} \\ \gamma_{xy}^{(2)} \end{Bmatrix}$$

and the resulting loads and strains for the second section are

$$N_x^{(2)} = 0.354 \text{ GPa-mm}; \qquad \varepsilon_y^{(2)} = -0.000048; \qquad \gamma_{xy}^{(2)} = 0$$

The total load at laminate failure is

$$N_{x\text{Total}} = 0.423 + 0.354 = 0.777 \text{ GPa-mm}$$

and the load–strain curve is shown as curve (b) in figure 7.31. It is interesting to note that although the assumptions regarding degradation of the failed plies are quite different for curves (a) and (b), the predicted load–strain curves for the two approaches are virtually the same. In general, differences in predictions from the two approaches would depend on ply properties and stacking sequences. It is also interesting to note that we might intuitively expect approach (a) to be more conservative than approach (b) and this turns out to be the case.

EXAMPLE 7.11

Repeat example 7.10 using the Maximum Stress Criterion.

Solution. From example 7.10, the load–strain relationship for the first increment is

$$\begin{Bmatrix} N_x^{(1)} \\ 0 \\ 0 \end{Bmatrix} = [A^{(1)}] \begin{Bmatrix} \varepsilon_x^{(1)} \\ \varepsilon_y^{(1)} \\ \gamma_{xy}^{(1)} \end{Bmatrix} = \begin{bmatrix} 78.45 & 4.08 & 0 \\ 4.08 & 143.3 & 0 \\ 0 & 0 & 10.35 \end{bmatrix} \begin{Bmatrix} \varepsilon_x^{(1)} \\ \varepsilon_y^{(1)} \\ \gamma_{xy}^{(1)} \end{Bmatrix} \text{GPa-mm}$$

Note that, unlike example 7.10 where, according to the Maximum Strain Criterion, the first ply failure strain along the x direction was known to be the transverse tensile failure strain in the 90° plies, we do not know the corresponding strains here, and we must find them using the Maximum Stress Criterion. Expanding the above equation,

$$N_x^{(1)} = 78.45\varepsilon_x^{(1)} + 4.08\varepsilon_y^{(1)}$$
$$0 = 4.08\varepsilon_x^{(1)} + 143.3\varepsilon_y^{(1)}$$
$$0 = 10.35\gamma_{xy}^{(1)}$$

Solving these equations simultaneously,

$$\varepsilon_y^{(1)} = -0.0285\varepsilon_x^{(1)}$$
$$\gamma_{xy}^{(1)} = 0$$
$$N_x^{(1)} = 78.33\varepsilon_x^{(1)}$$

So for the first ply failure of the 90° plies, the stresses along the x and y axes are

$$\begin{Bmatrix}\sigma_x^{(1)}\\ \sigma_y^{(1)}\\ \tau_{xy}^{(1)}\end{Bmatrix}_{90^\circ} = [\bar{Q}]_{90^\circ}\begin{Bmatrix}\varepsilon_x^{(1)}\\ -0.0285\varepsilon_x^{(1)}\\ 0\end{Bmatrix} = \begin{bmatrix}9.05 & 2.72 & 0\\ 2.72 & 138.8 & 0\\ 0 & 0 & 6.9\end{bmatrix}\begin{Bmatrix}\varepsilon_x^{(1)}\\ -0.0285\varepsilon_x^{(1)}\\ 0\end{Bmatrix}$$
$$= \begin{Bmatrix}8.972\varepsilon_x^{(1)}\\ -1.2358\varepsilon_x^{(1)}\\ 0\end{Bmatrix}\text{GPa}$$

The corresponding stresses in the 90° plies along the principal material axes are

$$\begin{Bmatrix}\sigma_1^{(1)}\\ \sigma_2^{(1)}\\ \tau_{12}^{(1)}\end{Bmatrix}_{90^\circ} = [T]_{90^\circ}\begin{Bmatrix}8.972\varepsilon_x^{(1)}\\ -1.2358\varepsilon_x^{(1)}\\ 0\end{Bmatrix} = \begin{bmatrix}0 & 1 & 0\\ 1 & 0 & 0\\ 0 & 0 & -1\end{bmatrix}\begin{Bmatrix}8.972\varepsilon_x^{(1)}\\ -1.2358\varepsilon_x^{(1)}\\ 0\end{Bmatrix} = \begin{Bmatrix}-1.2358\varepsilon_x^{(1)}\\ 8.972\varepsilon_x^{(1)}\\ 0\end{Bmatrix}\text{GPa}$$

Applying the Maximum Stress Criterion for the 90° plies, we find that

$$\sigma_1^{(1)} = -1.2358\varepsilon_x^{(1)} = S_L^{(+)} = 1448 \text{ MPa} = 1.448 \text{ GPa or } \varepsilon_x^{(1)} = -1.17$$
$$\sigma_2^{(1)} = 8.972\varepsilon_x^{(1)} = S_T^{(+)} = 48.3 \text{ MPa} = 0.0483 \text{ GPa or } \varepsilon_x^{(1)} = 0.00538$$

Choosing the smallest of these failure strains, we find that for first ply failure, we have

$$\varepsilon_x^{(1)} = 0.00538$$
$$\varepsilon_y^{(1)} = -0.0285\varepsilon_x^{(1)} = -0.0285(0.00538) = -0.000153$$
$$N_x^{(1)} = 78.33\varepsilon_x^{(1)} = 78.33(0.00538) = 0.4216 \text{ GPa-mm}$$

The corresponding stresses in the 0° plies at first ply failure are

$$\begin{Bmatrix}\sigma_x^{(1)}\\ \sigma_y^{(1)}\\ \tau_{xy}^{(1)}\end{Bmatrix}_{0^\circ} = [\bar{Q}]_{0^\circ}\begin{Bmatrix}\varepsilon_x^{(1)}\\ \varepsilon_y^{(1)}\\ \gamma_{xy}^{(1)}\end{Bmatrix} = \begin{bmatrix}138.8 & 2.72 & 0\\ 2.72 & 9.05 & 0\\ 0 & 0 & 6.9\end{bmatrix}\begin{Bmatrix}0.00538\\ -0.0001533\\ 0\end{Bmatrix} = \begin{Bmatrix}0.746\\ 0.0132\\ 0\end{Bmatrix}\text{GPa}$$
$$= \begin{Bmatrix}\sigma_1^{(1)}\\ \sigma_2^{(1)}\\ \tau_{12}^{(1)}\end{Bmatrix}_{0^\circ}$$

For the second increment after first ply failure, setting all of the ply stiffnesses equal to zero for the failed 90° plies and using the corresponding degraded laminate stiffness matrix from example 7.10, we find that

$$\begin{Bmatrix}N_x^{(2)}\\ 0\\ 0\end{Bmatrix} = [A^{(2)}]\begin{Bmatrix}\varepsilon_x^{(2)}\\ \varepsilon_y^{(2)}\\ \gamma_{xy}^{(2)}\end{Bmatrix} = \begin{bmatrix}69.4 & 1.36 & 0\\ 1.36 & 4.52 & 0\\ 0 & 0 & 3.45\end{bmatrix}\begin{Bmatrix}\varepsilon_x^{(2)}\\ \varepsilon_y^{(2)}\\ \gamma_{xy}^{(2)}\end{Bmatrix}\text{GPa-mm}$$

Solving these equations simultaneously,

$$\varepsilon_y^{(2)} = -0.3\varepsilon_x^{(2)}$$
$$N_x^{(2)} = 68.992\varepsilon_x^{(2)}$$
$$\gamma_{xy}^{(2)} = 0$$

The incremental stresses for the 0° plies are then

$$\begin{Bmatrix}\sigma_x^{(2)}\\ \sigma_y^{(2)}\\ \tau_{xy}^{(2)}\end{Bmatrix}_{0^\circ} = [\bar{Q}]_{0^\circ}\begin{Bmatrix}\varepsilon_x^{(2)}\\ \varepsilon_y^{(2)}\\ \gamma_{xy}^{(2)}\end{Bmatrix} = \begin{bmatrix}138.8 & 2.72 & 0\\ 2.72 & 9.05 & 0\\ 0 & 0 & 6.9\end{bmatrix}\begin{Bmatrix}\varepsilon_x^{(2)}\\ -0.3\varepsilon_x^{(2)}\\ 0\end{Bmatrix} = \begin{Bmatrix}137.98\varepsilon_x^{(2)}\\ 0.005\varepsilon_x^{(2)}\\ 0\end{Bmatrix}\text{GPa}$$

$$= \begin{Bmatrix}\sigma_1^{(2)}\\ \sigma_2^{(2)}\\ \tau_{12}^{(2)}\end{Bmatrix}_{0^\circ}$$

Substituting the total stresses in the 0° plies at the end of the second increment in the Maximum Stress Criterion,

$$(\sigma_1)_{\text{total}} = \sigma_1^{(1)} + \sigma_1^{(2)} = 0.746 + 137.98\varepsilon_x^{(2)} = S_L^{(+)} = 1.448\ \text{GPa} \quad \text{or} \quad \varepsilon_x^{(2)} = 0.00508$$

$$(\sigma_2)_{\text{total}} = \sigma_2^{(1)} + \sigma_2^{(2)} = 0.0132 + 0.005\varepsilon_x^{(2)} = S_T^{(+)} = 0.0483\ \text{GPa} \quad \text{or} \quad \varepsilon_x^{(2)} = 7.02$$

Choosing the smallest of the incremental strains to cause failure of the 0° plies,

$$\varepsilon_x^{(2)} = 0.00508$$

$$N_x^{(2)} = 68.992(0.00508) = 0.3505\ \text{GPa-mm}$$

The total loads and strains at final failure are then

$$(N_x)_{\text{total}} = N_x^{(1)} + N_x^{(2)} = 0.4216 + 0.3505 = 0.7721\ \text{GPa-mm}$$
$$(\varepsilon_x)_{\text{total}} = \varepsilon_x^{(1)} + \varepsilon_x^{(2)} = 0.00538 + 0.00508 = 0.01046$$

The resulting load strain plot in figure 7.32 is seen to be quite similar to the corresponding plots for the Maximum Strain Criterion in figure 7.31, but this is not necessarily the case in general.

EXAMPLE 7.12

The composite power transmission shaft shown in figure 7.33 has mean radius R = 50 mm and wall thickness t = 1 mm. The material is filament wound AS/3501 carbon/epoxy, and the wall of the shaft has a symmetric angle-ply [+45/–45/–45/ +45] lay-up sequence (same as material in example 7.3) for maximum torsional stiffness. Determine the largest torque T that can be transmitted by the shaft without failure according to the Maximum Stress Criterion.

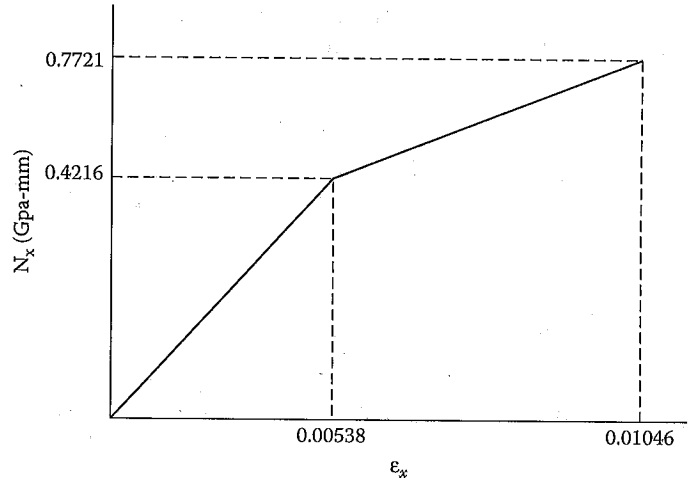

FIGURE 7.32
Predicted load–strain curve for example 7.11.

Solution. From mechanics of materials, the torsional shear stress in a thin-walled tube is approximately

$$\tau_{xy} = \frac{T}{2\pi R^2 t}$$

where T = torque in N-m, R = mean wall radius in m, and t = wall thickness in m. For the laminate analysis, the loads per unit length acting on an element of the tube wall are therefore

$$N_{xy} = \tau_{xy}t = \frac{T}{2\pi R^2} = \frac{T}{2\pi(0.05)^2} = 63.66\ T\frac{N}{m} = 63.66(10^{-6})\ T\ \text{GPa-mm}$$

$$N_x = N_y = M_x = M_y = M_{xy} = 0$$

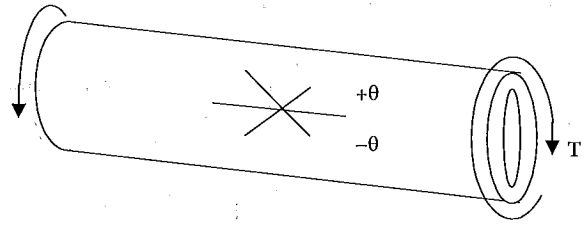

FIGURE 7.33
Composite shaft for example 7.12.

As in example 7.6, we can take advantage of the symmetry of the laminate and invert the [A] matrix to solve for the strains in term of the loads as

$$\begin{Bmatrix} \varepsilon_x^o \\ \varepsilon_y^o \\ \gamma_{xy}^o \end{Bmatrix} = [A'] \begin{Bmatrix} 0 \\ 0 \\ N_{xy} \end{Bmatrix} = \begin{bmatrix} 0.04276 & -0.0297 & 0 \\ -0.0297 & 0.04276 & 0 \\ 0 & 0 & 0.02809 \end{bmatrix} \begin{Bmatrix} 0 \\ 0 \\ 63.66(10^{-6})T \end{Bmatrix}$$

$$= \begin{Bmatrix} 0 \\ 0 \\ 1.788(10^{-6})T \end{Bmatrix}$$

Using the lamina stiffness matrices from example 7.3, the corresponding stresses in the +45° plies along the x and y axes are

$$\begin{Bmatrix} \sigma_x \\ \sigma_y \\ \tau_{xy} \end{Bmatrix}_{+45^o} = [\bar{Q}]_{+45^o} \begin{Bmatrix} \varepsilon_x^o \\ \varepsilon_y^o \\ \gamma_{xy}^o \end{Bmatrix} = \begin{bmatrix} 45.22 & 31.42 & 32.44 \\ 31.42 & 45.22 & 32.44 \\ 32.44 & 32.44 & 35.6 \end{bmatrix} \begin{Bmatrix} 0 \\ 0 \\ 1.788(10^{-6})T \end{Bmatrix}$$

$$= \begin{Bmatrix} 58.0T \\ 58.0T \\ 63.65T \end{Bmatrix} (10^{-6}) \text{ GPa} = \begin{Bmatrix} 0.058T \\ 0.058T \\ 0.06365T \end{Bmatrix} \text{MPa}$$

Similarly, for the –45° plies,

$$\begin{Bmatrix} \sigma_x \\ \sigma_y \\ \tau_{xy} \end{Bmatrix}_{-45^o} = [\bar{Q}]_{-45^o} \begin{Bmatrix} \varepsilon_x^o \\ \varepsilon_y^o \\ \gamma_{xy}^o \end{Bmatrix} = \begin{bmatrix} 45.22 & 31.42 & -32.44 \\ 31.42 & 45.22 & -32.44 \\ -32.44 & -32.44 & 35.6 \end{bmatrix} \begin{Bmatrix} 0 \\ 0 \\ 1.788(10^{-6})T \end{Bmatrix}$$

$$= \begin{Bmatrix} -58.0T \\ -58.0T \\ 63.65T \end{Bmatrix} (10^{-6}) \text{ GPa} = \begin{Bmatrix} -0.058T \\ -0.058T \\ 0.06365T \end{Bmatrix} \text{MPa}$$

In order to use the Maximum Stress Criterion, the stresses must be transformed to the principal material axes. Accordingly, for the +45° plies,

$$\begin{Bmatrix} \sigma_1 \\ \sigma_2 \\ \tau_{12} \end{Bmatrix}_{+45^o} = [T]_{+45^o} \begin{Bmatrix} \sigma_x \\ \sigma_y \\ \tau_{xy} \end{Bmatrix} = \begin{bmatrix} 0.5 & 0.5 & 1.0 \\ 0.5 & 0.5 & -1.0 \\ -0.5 & 0.5 & 0 \end{bmatrix} \begin{Bmatrix} 0.058T \\ 0.058T \\ 0.06365T \end{Bmatrix} = \begin{Bmatrix} 0.12165T \\ -0.00565T \\ (0)T \end{Bmatrix} \text{MPa}$$

Similarly, for the –45° plies,

$$\begin{Bmatrix} \sigma_1 \\ \sigma_2 \\ \tau_{12} \end{Bmatrix}_{-45^o} = [T]_{-45^o} \begin{Bmatrix} \sigma_x \\ \sigma_y \\ \tau_{xy} \end{Bmatrix} = \begin{bmatrix} 0.5 & 0.5 & -1.0 \\ 0.5 & 0.5 & 1.0 \\ 0.5 & -0.5 & 0 \end{bmatrix} \begin{Bmatrix} -0.058T \\ -0.058T \\ 0.06365T \end{Bmatrix} = \begin{Bmatrix} -0.12165T \\ 0.00565T \\ (0)T \end{Bmatrix} \text{MPa}$$

Applying the Maximum Stress Criterion for the +45° plies and using the strength data for AS/3501 from table 4.1,

$$\sigma_1 = 0.12165T = S_L^{(+)} = 1448 \text{ MPa} \quad \text{and} \quad T = 11{,}903 \ N-m$$

$$\sigma_2 = -0.00565T = -S_T^{(-)} = -248 \ MPa \quad \text{and} \quad T = 43{,}894 \ N-m$$

$$\tau_{12} = 0(T) = S_{LT} = 62.1 \text{MPa} \quad \text{and} \quad T = \infty$$

Similarly, for the –45° plies,

$$\sigma_1 = -0.12165T = -S_L^{(-)} - 1172 \text{MPa} \quad \text{and} \quad T = 9{,}634 N-m$$

$$\sigma_2 = 0.00565T = S_T^{(+)} = 48.3 \text{MPa} \quad \text{and} \quad T = 8{,}549 N-m$$

$$\tau_{12} = 0(T) = S_{LT} = 62.1 \text{MPa} \quad \text{and} \quad T = \infty$$

Note that, since the shear stress is zero along the 1,2 axes and the resulting torque needed to cause shear failure is infinite; failure due to shear is not possible. Of the remaining values, it is seen that the value of T = 8549 N-m for transverse tensile failure in the –45° plies is the smallest, so this would be the largest torque that could be transmitted without failure. It is also important to note that, if the strengths were the same in tension and compression, all plies would fail simultaneously, but since the strengths are different in tension and compression, this is not the case here.

7.8.2 Delamination Due to Interlaminar Stresses

Delamination due to interlaminar stresses can reduce the failure stress of the laminate below that predicted by the in-plane failure criteria discussed in the previous section. Failure by delamination is not necessarily the same as the initiation of delamination, however. The initiation of delamination is generally followed by stable delamination growth, which eventually leads to unstable growth and ultimate failure. The onset of delamination can be predicted by using either mechanics of materials approaches or fracture mechanics approaches. Fracture mechanics is also the preferred analytical treatment for delamination growth and failure. In this section, we will discuss mechanics of materials approaches to the prediction of delamination initiation, and fracture mechanics will be covered in chapter 9.

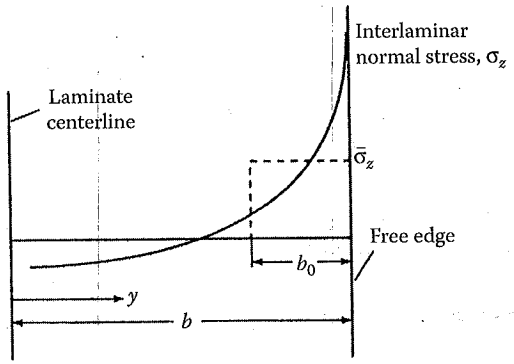

FIGURE 7.34
Graphical interpretation of average interlaminar normal stress near free edge according to the Kim–Soni Criterion.

The average stress criterion of Kim and Soni [31] was one of the first mechanics of materials approaches to the prediction of the onset of delamination. This criterion is based on the premise that delamination will begin once the average value of the interlaminar tensile normal stress, $\bar{\sigma}_z$, near the free edge reaches the interlaminar tensile strength, $s_Z^{(+)}$. A similar criterion for failure of notched laminates had been proposed previously by Whitney and Nuismer [32]. In the Kim–Soni Criterion, the averaging is done over a critical length, b_0, as shown in equation (7.109) and figure 7.34:

$$\bar{\sigma}_z = \frac{1}{b_0}\int_{b-b_0}^{b} \sigma_z(y,0)\mathrm{d}y = s_Z^{(+)} \tag{7.109}$$

The distance b was the half-width of the laminate, as shown in figure 7.22, and the critical length b_0 is assumed to be equal to one ply thickness. Due to the difficulty of measuring $s_z^{(+)}$, Kim and Soni assumed that $s_Z^{(+)} = s_T^{(+)}$. Although this criterion provided reasonably accurate predictions of the onset of delamination in composites where the tensile normal stress, σ_z, was the dominant interlaminar stress, a more general criterion was needed for cases where delamination may be affected by interlaminar shear stresses as well.

The need for a more general criterion for predicting the onset of delamination was recognized by Brewer and Lagace [33], who proposed the Quadratic Delamination Criterion:

$$\left(\frac{\bar{\sigma}_{xz}}{s_{XZ}}\right)^2 + \left(\frac{\bar{\sigma}_{yz}}{s_{YZ}}\right)^2 + \left(\frac{\bar{\sigma}_z^t}{s_z^{(+)}}\right)^2 + \left(\frac{\bar{\sigma}_z^c}{s_z^{(-)}}\right)^2 = 1 \tag{7.110}$$

where $\bar{\sigma}_{xz}$ and $\bar{\sigma}_{yz}$ are the average interlaminar shear stresses, $\bar{\sigma}_z^t$ and $\bar{\sigma}_z^c$ the average interlaminar tensile and compressive normal stresses, respectively, s_{xz} and s_{yz} the interlaminar shear strengths, and $s_Z^{(+)}$ and $s_Z^{(-)}$ the interlaminar tensile and compressive strengths, respectively.

Each of the average stress components in this case is defined as

$$\bar{\sigma}_{ij} = \frac{1}{\lambda_{avg}}\int_0^{\lambda_{avg}} \sigma_{ij}\,\mathrm{d}\lambda \tag{7.111}$$

where λ is the distance from some reference point (in this case the free edge), λ_{avg} the averaging dimension, σ_{ij} the stress component σ_{xz}, σ_{yz}, σ_z^t or σ_z^c and the overbar denotes its average value.

Brewer and Lagace found that for the $[\pm 15_n]_s$, $[\pm 15_n/0_n]_s$, and $[0_n/\pm 15_n]_s$, AS1/3501-6 carbon/epoxy laminates tested the second and fourth terms in equation (7.110) were negligible, so that the Quadratic Delamination Criterion took on the simplified form

$$\left(\frac{\bar{\sigma}_{xz}}{s_{XZ}}\right)^2 + \left(\frac{\bar{\sigma}_z^t}{s_z^{(+)}}\right)^2 = 1 \tag{7.112}$$

Transverse isotropy was assumed, so that $s_z^{(+)} = s_T^{(+)} = 53.9$ MPa. The parameters λ_{avg} and s_{xz} were used as curve-fitting parameters to obtain the best agreement with experimental data. In the corresponding experiments, laminate specimens were tested under displacement-control, and an instantaneous drop in the tensile load at delamination onset was observed. The "best-fit" parameters for all laminate configurations tested were $\lambda_{avg} = 0.178$ mm and $s_{xz} = 105$ MPa. Further support for the validity of the Quadratic Delamination Criterion and the assumption of transverse isotropy was discovered with the observation that the best-fit value of s_{xz} was the same as s_{LT}, the in-plane shear strength of this material. Although the value of λ_{avg} was not assumed to be equal to the ply thickness as in the Kim–Soni analysis, the best-fit value of 0.178 mm was of the same order as the ply thickness. A comparison of the measured and predicted delamination onset stresses for various normalized ply thicknesses, n, are shown for the $[\pm 15_n]_s$ laminate in figure 7.35. Specimens were made by stacking single plies of the same orientation together to form a ply with greater effective thickness, and the value of n is this effective ply thickness divided by the single ply thickness. Also shown in figure 7.35 are the predictions from a fracture mechanics approach, which will be discussed later.

Catastrophic failure of laminated structures is not the only undesirable result of delamination. The reduction in stiffness of a laminate during

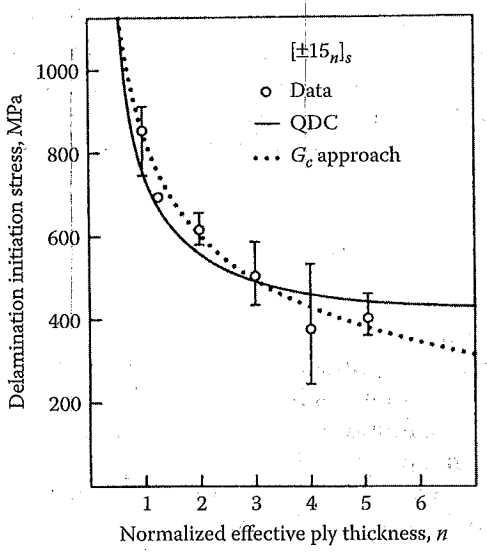

FIGURE 7.35
Predicted and measured delamination initiation stresses for $[+15_n]_s$ laminates. (From Brewer, J.C. and Lagace, P.A. 1988. *Journal of Composite Materials*, 22, 1141–1155. With permission.)

delamination growth may make the structure unsafe even if fracture does not occur. Conversely, stiffness loss can be used to characterize the growth of delamination. Thus, analytical models are needed for estimating this stiffness loss during delamination.

O'Brien [34] has developed an analysis of stiffness reduction in symmetric laminates during delamination based on a simple "rule of mixtures" and the CLT. Recall from equation (7.59) that the effective longitudinal Young's modulus of a symmetric laminate is given by

$$E_x = \frac{1}{tA'_{11}} \tag{7.113}$$

This equation was used by O'Brien to model the stiffness of the laminate without delaminations, as shown in figure 7.36(*a*). The corresponding stiffness of a laminate, which has been totally delaminated along one or more interfaces (fig. 7.36[b]), but whose sublaminates must still have the same longitudinal strain, is given by the rule of mixtures formula

$$E_{td} = \frac{\sum_{i=1}^{m} E_{xi} t_i}{t} \tag{7.114}$$

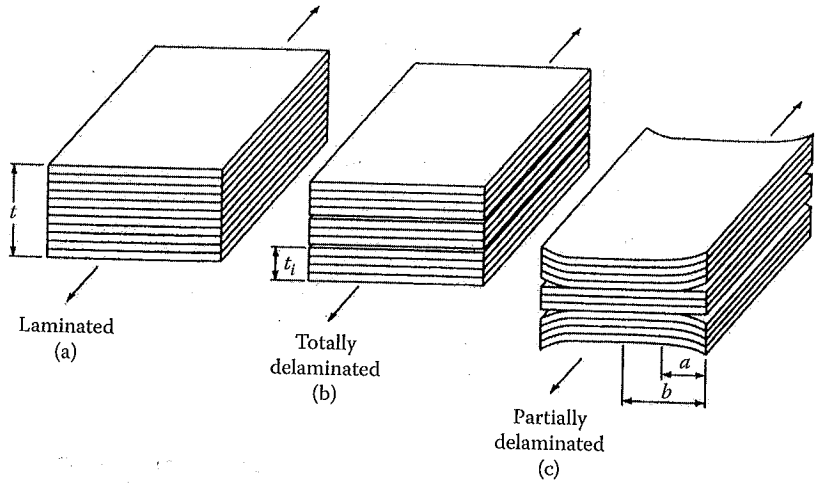

FIGURE 7.36
Rule of mixtures analysis of stiffness loss due to delamination. (From O'Brien, T.K. 1982. In: Reifsnider, K.L. ed., *Damage in Composite Materials*. ASTM STP 775, pp. 140–167. American Society for Testing and Materials, Philadelphia, PA. Copyright ASTM. With permission.)

where E_{td} is the longitudinal Young's modulus of a laminate totally delaminated along one or more interfaces, E_{xi} the longitudinal Young's modulus of ith sublaminate formed by the delamination, t_i the thickness of the ith sublaminate, and m the number of sublaminates formed by the delamination.

The longitudinal Young's modulus of a laminate that has been partially delaminated along the same interfaces (fig. 7.36[c]) is given by the rule of mixtures formula

$$E = (E_{td} - E_x)\frac{a}{b} + E_x \tag{7.115}$$

where E is the longitudinal Young's modulus of a laminate partially delaminated along one or more interfaces, a the distance that delamination extends in from the free edge, and b the half-width of the laminate.

A more general form of equation (7.115) is given by equation (7.116):

$$E = (E_{td} - E_x)\frac{A_d}{A_t} + E_x \tag{7.116}$$

where A_d is the delaminated area and A_t total interfacial area.

The predicted values of E normalized to the initial modulus, E_0, are compared with measured values of E/E_0 for various delamination sizes in $[\pm 30/\pm 30/90/90]_s$ graphite/epoxy laminates in figure 7.37, and the

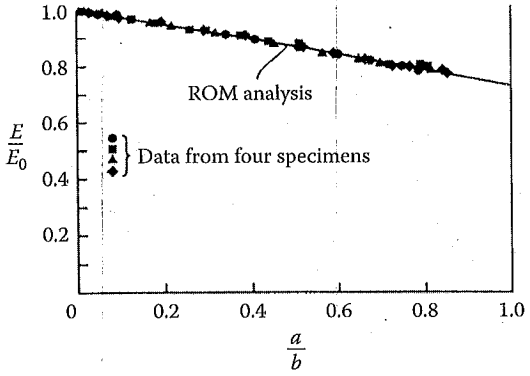

FIGURE 7.37
Predicted and measured laminate stiffness as a function of delamination size. (From O'Brien, T.K. 1982. In: Reifsnider, K.L. ed., *Damage in Composite Materials*. ASTM STP 775, pp. 140–167. American Society for Testing and Materials, Philadelphia, PA. Copyright ASTM. Reprinted with permission.)

delamination of this laminate would result in a 25.8% reduction in the laminate stiffness. Such a loss of stiffness would lead to an undesirable increase in the deflection of the structure under load.

In this section we have only been concerned with delamination near free edges in laminates, but interlaminar stresses and delamination may occur at other discontinuities such as holes, ply drops, and joints (see figure 7.38 from ref. [35]). Low-velocity impact (e.g., dropping a wrench) on a composite structure may cause internal delaminations that may

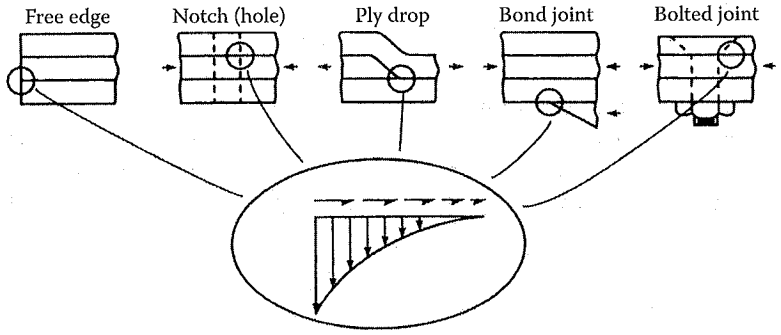

FIGURE 7.38
Interlaminar stresses occur at a variety of discontinuities in composite structures. (From Newaz, G.M. ed. 1991. *Delamination in Advanced Composites*. Technomic Publishing, Co., Lancaster, PA. With permission.)

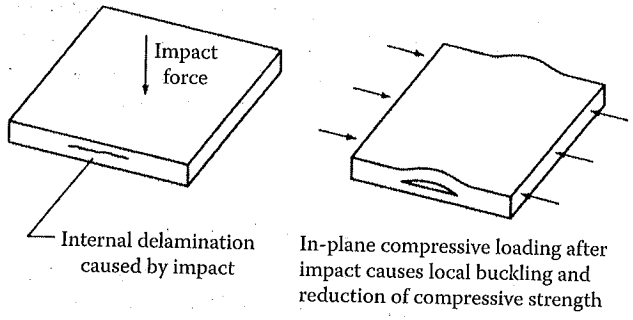

FIGURE 7.39
Reduction of in-plane compressive strength of laminate after transverse impact.

reduce the in-plane compressive strength (fig. 7.39). The so-called "compression after impact" (CAI) problem is of considerable interest, and CAI testing will be discussed later in Chapter 10. The analysis of delamination under such complex states of stress generally requires the use of fracture mechanics and finite element numerical approaches, some of which are discussed in chapter 9. The reader is also encouraged to refer to numerous analytical and experimental studies in several recent books [35–37].

There is obviously a lot of interest in the improvement of delamination resistance in laminates, and a number of such approaches will be discussed later in chapter 9.

7.9 Deflection and Buckling of Laminates

This section is concerned with the analysis of transverse deflections of laminates under transverse loading and the prediction of laminate buckling forces. Transverse deflections of laminates due to bending are generally much larger than in-plane deflections, because flexural stiffnesses are lower than extensional stiffnesses. Thus, transverse deflections are an important design consideration, and developments of analytical models for predicting such deflections are of interest. Buckling of laminates is an instability that is characterized by excessive transverse deflections under in-plane compressive or shear forces. The general equilibrium equations governing transverse deflections involve both in-plane and out-of-plane forces, but the coupling between in-plane forces and transverse deflections is usually taken into account only for the buckling analysis or for large deflection analysis. In the analysis of small transverse deflections alone, the out-of-plane forces are the most important because the

normally designed in such a way that the in-plane forces are less than the corresponding buckling loads. Only a brief introduction to deflection and buckling is given here. For more detailed coverage of these subjects, the reader is referred to the works of Whitney [10], Lekhnitskii [7], Vinson and Sierakowski [38], and Liessa [39].

7.9.1 Analysis of Small Transverse Deflections

The analysis of transverse deflections of laminated plates has its basis in the CLT, which was outlined in section 7.3 and in the differential equations of equilibrium. In order to develop the differential equations governing plate deflections, it is convenient to use an infinitesimal element, as shown in figure 7.40(a), (b), and (c) from Halpin [12]. The in-plane stress resultants and moment resultants are shown in figure 7.40(a), the moment resultants are shown in figure 7.40(b), and the transverse shear stress resultants are shown in figure 7.40(c). Transverse shear stress resultants were not considered in section 7.3, but they must be considered here in the transverse deflection analysis. In these diagrams, it is assumed that the transverse deflections are small, so that the out-of-plane components of the in-plane resultants

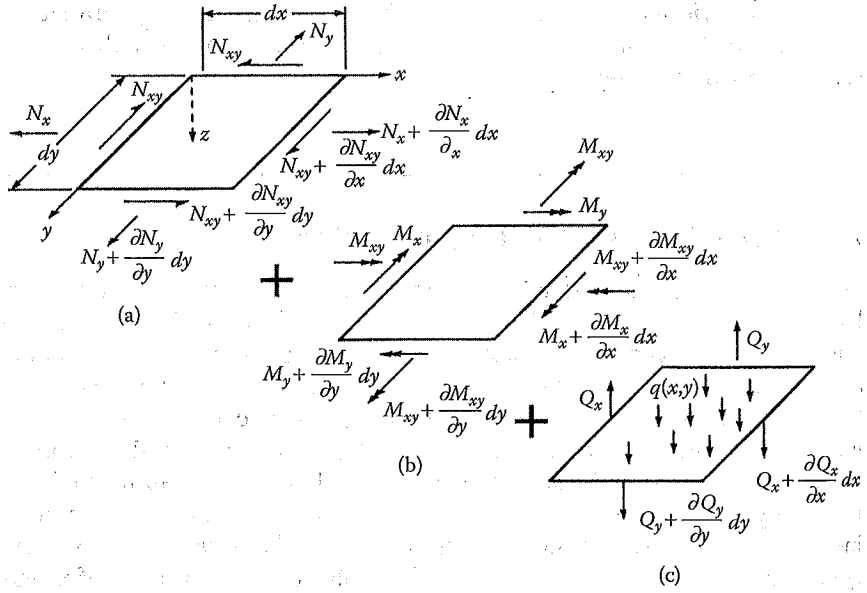

FIGURE 7.40
Stress resultants and external loads acting on laminate. (From Halpin, J.C. 1984. *Primer on Composite Materials: Analysis.* Technomic Publishing Co., Lancaster, PA. With permission.)

N_x, N_y, and N_{xy} are negligible. However, these out-of-plane components will be considered in the next section on buckling analysis. Along with the stress and moment resultants such as those defined previously in figure 7.8 and in equation 7.32 to equation 7.33, the transverse shear stress resultants Q_x and Q_y are similarly defined as

$$Q_x = \int_{-t/2}^{t/2} \tau_{xz}\, dz \tag{7.117}$$

and

$$Q_y = \int_{-t/2}^{t/2} \tau_{yz}\, dz \tag{7.118}$$

Also included in figure 7.40 is a distributed transverse load $q(x, y)$. Following the derivation by Halpin [12] for static equilibrium according to Newton's second law, the summation of forces along the x direction must be

$$N_x\, dy + \frac{\partial N_x}{\partial x} dx\, dy + N_{xy}\, dx + \frac{\partial N_{xy}}{\partial y} dx\, dy - N_x\, dy - N_{xy}\, dx = 0 \tag{7.119}$$

Equation (7.119) may be simplified as

$$\frac{\partial N_x}{\partial x} + \frac{\partial N_{xy}}{\partial y} = 0 \tag{7.120}$$

The summation of forces along the y direction yields

$$N_y\, dx + \frac{\partial N_x}{\partial y} dx\, dy + N_{xy} dy + \frac{\partial N_{xy}}{\partial x} dx\, dy - N_y\, dx - N_{xy} dy = 0 \tag{7.121}$$

or

$$\frac{\partial N_y}{\partial y} + \frac{\partial N_{xy}}{\partial x} = 0 \tag{7.122}$$

The summation of forces along the z direction gives

$$Q_x dy + \frac{\partial Q_x}{\partial x} dx\, dy + Q_y dx + \frac{\partial Q_y}{\partial y} dy\, dx - Q_x dy - Q_y dx + q(x,y) = 0 \tag{7.123}$$

or

$$\frac{\partial Q_x}{\partial x}+\frac{\partial Q_y}{\partial y}+q(x,y)=0 \tag{7.124}$$

The summation of moments about the x-axis yields

$$-M_y dx-\frac{\partial M_y}{\partial y}dy\,dx-M_{xy}dy-\frac{\partial M_{xy}}{\partial x}dx\,dy+Q_y\,dx\,dy$$
$$+\frac{\partial Q_y}{\partial y}dy\,dx\,dy+q(x,y)dx\,dy\,dy/2+Q_x dy\,dy/2 \tag{7.125}$$
$$+\frac{\partial Q_x}{\partial x}dx\,dy\,dy/2+M_y dx+M_{xy}dy-Q_x dy\,dy/2=0$$

Simplifying and neglecting products of differentials, we get

$$\frac{\partial M_y}{\partial y}+-\frac{\partial M_{xy}}{\partial x}=Q_y \tag{7.126}$$

A similar summation of moments about the y-axis gives

$$\frac{\partial M_x}{\partial x}+\frac{\partial M_{xy}}{\partial y}=Q \tag{7.127}$$

Substitution of equation (7.126) and equation (7.127) in equation (7.124) yields

$$\frac{\partial^2 M_x}{\partial x^2}+2\frac{\partial^2 M_{xy}}{\partial x\,\partial y}+\frac{\partial^2 M_y}{\partial y^2}+q(x,y)=0 \tag{7.128}$$

Equation (7.120), equation (7.122), and equation (7.128) are the differential equations of equilibrium of the plate in terms of stress and moment resultants. The corresponding equilibrium equations in terms of displacements can be derived by substituting the laminate force–deformation equation (7.41), the strain–displacement relations (7.29), and the curvature-displacement equations (7.30) in equation (7.120), equation

(7.122), and equation (7.128). The resulting set of coupled partial differential equations in the displacements u^0, v^0, and w are

$$A_{11}\frac{\partial^2 u^0}{\partial x^2}+2A_{16}\frac{\partial^2 u^0}{\partial x\,\partial y}+A_{66}\frac{\partial^2 u^0}{\partial y^2}+A_{16}\frac{\partial^2 v^0}{\partial x^2}+(A_{12}+A_{66})\frac{\partial^2 v^0}{\partial x\,\partial y}$$
$$+A_{26}\frac{\partial^2 v^0}{\partial y^2}-B_{11}\frac{\partial^3 w}{\partial x^3}-3B_{16}\frac{\partial^3 w}{\partial x^2\,\partial y} \tag{7.129}$$
$$-(B_{12}+2B_{66})\frac{\partial^3 w}{\partial x\,\partial y^2}-B_{26}\frac{\partial^3 w}{\partial y^3}=0$$

$$A_{16}\frac{\partial^2 u^0}{\partial x^2}+(A_{12}+A_{66})\frac{\partial^2 u^0}{\partial x\,\partial y}+A_{26}\frac{\partial^2 u^0}{\partial y^2}+A_{66}\frac{\partial^2 v^0}{\partial x^2}$$
$$+2A_{26}\frac{\partial^2 v^0}{\partial x\,\partial y}+A_{22}\frac{\partial^2 v^0}{\partial y^2}-B_{16}\frac{\partial^3 w}{\partial x^3}-(B_{12}+2B_{66})\frac{\partial^3 w}{\partial x^2\,\partial y} \tag{7.130}$$
$$-3B_{26}\frac{\partial^3 w}{\partial x\,\partial y^2}-B_{22}\frac{\partial^3 w}{\partial y^3}=0$$

$$D_{11}\frac{\partial^4 w}{\partial x^4}+4D_{16}\frac{\partial^4 w}{\partial x^3\,\partial y}+2(D_{12}+2D_{66})\frac{\partial^4 w}{\partial x^2\,\partial y^2}+4D_{26}\frac{\partial^4 w}{\partial x\,\partial y^3}$$
$$+D_{22}\frac{\partial^4 w}{\partial y^4}-B_{11}\frac{\partial^3 u^0}{\partial x^3}-3B_{16}\frac{\partial^3 u^0}{\partial x^2\,\partial y}-(B_{12}+2B_{66})\frac{\partial^3 u^0}{\partial x\,\partial y^2} \tag{7.131}$$
$$-B_{26}\frac{\partial^3 u^0}{\partial y^3}-B_{16}\frac{\partial^3 v^0}{\partial x^3}-(B_{12}+2B_{66})\frac{\partial^3 v^0}{\partial x^2\,\partial y}-3B_{26}\frac{\partial^3 v^0}{\partial x\,\partial y^2}$$
$$-B_{22}\frac{\partial^3 v^0}{\partial y^3}=q(x,y)$$

Note that the in-plane displacements u^0 and v^0 are coupled with the transverse displacements, w, when the coupling stiffnesses, B_{ij}, are present. For symmetric laminates with $B_{ij}=0$, equation (7.131) alone becomes the governing equation for transverse displacements. These governing partial differential equations must be solved subject to the appropriate boundary conditions. In the general case, when the in-plane displacements are coupled with the transverse displacements, the boundary conditions must be a combination of boundary conditions for a planar

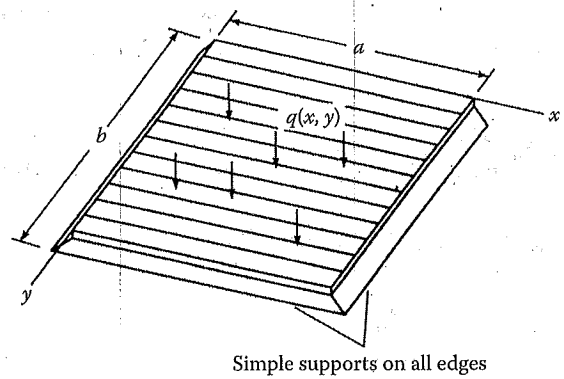

FIGURE 7.41
Simply supported, specially orthotropic plate with distributed loading.

theory of elasticity problem and boundary conditions for a plate-bending problem [10]. In this section, however, we will restrict the discussion to bending of symmetric laminated plates. That is, we will only consider transverse displacements according to equation (7.131) with all $B_{ij} = 0$.

Let us now consider the case of transverse deflection of the rectangular, specially orthotropic plate, which is simply supported on all edges and loaded with a distributed load, $q(x, y)$, as shown in figure 7.41. For a specially orthotropic plate all $B_{ij} = 0$, $A_{16} = A_{26} = D_{16} = D_{26} = 0$ and equation (7.131) becomes

$$D_{11}\frac{\partial^4 w}{\partial x^4} + 2(D_{12} + 2D_{66})\frac{\partial^4 w}{\partial x^2 \partial y^2} + D_{22}\frac{\partial^4 w}{\partial y^4} = q(x, y) \tag{7.132}$$

For the simply supported boundary condition, the transverse displacements and bending moments must vanish at the edges. In order to use the bending moment boundary conditions to solve the differential equation for displacements, however, the bending moments must be expressed in terms of displacements. Such expressions can be obtained from equation (7.30) and equation (7.41) for the specially orthotropic plate as follows:

$$M_x = D_{11}\kappa_x + D_{12}\kappa_y = -D_{11}\frac{\partial^2 w}{\partial x^2} - D_{12}\frac{\partial^2 w}{\partial y^2} \tag{7.133}$$

and

$$M_y = D_{12}\kappa_x + D_{22}\kappa_y = -D_{12}\frac{\partial^2 w}{\partial x^2} - D_{22}\frac{\partial^2 w}{\partial y^2} \tag{7.134}$$

Thus, along $x = 0$ and $x = a$,

$$w = 0$$

and

$$M_x = -D_{11}\frac{\partial^2 w}{\partial x^2} - D_{12}\frac{\partial^2 w}{\partial y^2} = 0 \tag{7.135}$$

and along $y = 0$ and $y = b$

$$w = 0$$

and

$$M_y = -D_{12}\frac{\partial^2 w}{\partial x^2} - D_{22}\frac{\partial^2 w}{\partial y^2} = 0 \tag{7.136}$$

Several approaches to the solution of such problems have been proposed [10,38]. This simplest method involves the use of double Fourier sine series to represent both the load $q(x, y)$ and the displacements $w(x, y)$. If the load can be represented as

$$q(x, y) = \sum_{m=1}^{\infty}\sum_{n=1}^{\infty} q_{mn} \sin\frac{m\pi x}{a}\sin\frac{n\pi y}{b} \tag{7.137}$$

then it can be shown that the differential equation and the boundary conditions are satisfied by solutions of the form

$$w(x, y) = \sum_{m=1}^{\infty}\sum_{n=1}^{\infty} w_{mn} \sin\frac{m\pi x}{a}\sin\frac{n\pi y}{b} \tag{7.138}$$

Substitution of equation (7.138) and equation (7.137) in equation (7.132) yields the displacement coefficients

$$w_{mn} = \frac{a^4 q_{mn}}{\pi^4\left[D_{11}m^4 + 2(D_{12} + 2D_{66})(mnR)^2 + D_{22}(nR)^4\right]} \tag{7.139}$$

where the plate aspect ratio $R = a/b$ [10]. The Fourier coefficients q_{mn} can be found for the particular assumed load distribution [9,10]. For the uniform load $q(x, y) = q_0$, a constant, it can be shown that the Fourier coefficients are

$$q_{mn} = \frac{16q_0}{\pi^2 mn} \quad \text{for} \quad m, n = 1,3,5,\ldots$$
$$\text{and} \quad q_{mn} = 0 \quad \text{for} \quad m, n = 2,4,6,\ldots \tag{7.140}$$

Displacements $w(x, y)$ for the uniformly loaded, simply supported plate may now be found by substituting equation (7.139) and equation (7.140) in equation (7.138). Moment resultants may be found by substituting these equations in equation (7.30) and then substituting the result in equation (7.41). Finally, lamina stresses may be found by combining equation (7.30), equation (7.31), equation (7.138), equation (7.139), and equation (7.140).

For boundary conditions such as clamped edges or free edges, exact series solutions similar to equation (7.138) are generally not possible. For such cases, approximate solutions must be derived using approaches such as the Rayleigh–Ritz method or the Galerkin method. For a detailed discussion of these methods and other boundary conditions, the reader is referred to the book by Whitney [10].

7.9.2 Buckling Analysis

In the derivations of equation (7.120), equation (7.122), and equation (7.124), the coupling between the in-plane forces N_x, N_y, and N_{xy} and the out-of-plane deflections, w, was ignored because of the assumption of small displacements. In order to develop the equations to predict buckling under in-plane loads, however, this coupling must be considered. Such equations can be derived by assuming the differential element of figure 7.40(a) to be oriented in a general out-of-plane position, as shown in figure 7.42. Using

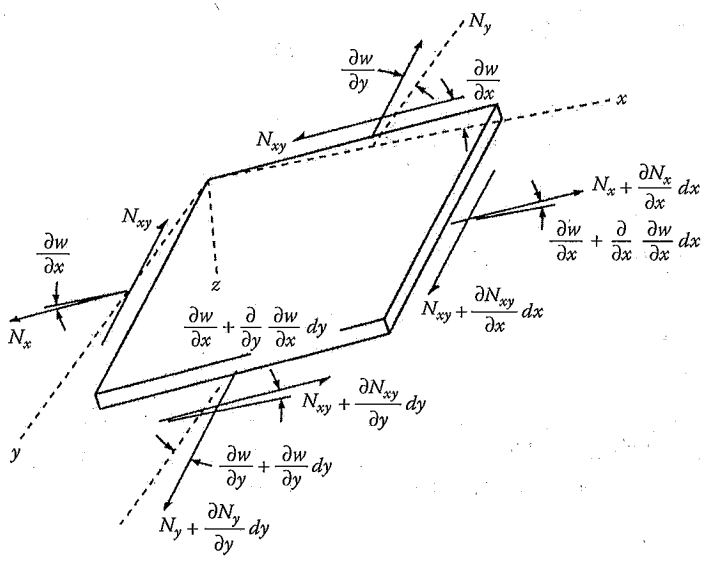

FIGURE 7.42
Differential element of laminate in out-of-plane position for buckling analysis.

figure 7.42, and taking into account the vertical components of the in-plane forces, the summation of forces in the z direction now becomes

$$\frac{\partial Q_x}{\partial x} + \frac{\partial Q_y}{\partial y} + q(x,y) + N_x \frac{\partial^2 w}{\partial x^2} + 2N_{xy} \frac{\partial^2 w}{\partial x\, \partial y} + N_y \frac{\partial^2 w}{\partial y^2} = 0 \qquad (7.141)$$

Note that equation (7.141) consists of the terms from equation (7.124) plus the terms involving the in-plane forces. Combining equation (7.141), equation (7.126), and equation (7.127), we find that

$$\frac{\partial^2 M_x}{\partial x^2} + 2\frac{\partial^2 M_{xy}}{\partial x\, \partial y} + \frac{\partial^2 M_y}{\partial y^2} + N_x \frac{\partial^2 w}{\partial x^2} + 2N_{xy} \frac{\partial^2 w}{\partial x\, \partial y} + N_y \frac{\partial^2 w}{\partial y^2} + q(x,y) = 0 \qquad (7.142)$$

Equation (7.142) consists of all the terms in equation (7.128) plus the terms involving the in-plane forces. Substitution of equation (7.141), equation (7.29), and equation (7.30) in equation (7.142) yields the equation

$$\begin{aligned} &D_{11}\frac{\partial^4 w}{\partial x^4} + 4D_{16}\frac{\partial^4 w}{\partial x^3\, \partial y} + 2(D_{12} + 2D_{66})\frac{\partial^4 w}{\partial x^2\, \partial y^2} + 4D_{26}\frac{\partial^4 w}{\partial x\, \partial y^3} \\ &+ D_{22}\frac{\partial^4 w}{\partial y^4} - B_{11}\frac{\partial^3 u^0}{\partial x^3} - 3B_{16}\frac{\partial^3 u^0}{\partial x^2\, \partial y} - (B_{12} + 2B_{66})\frac{\partial^3 u^0}{\partial x\, \partial y^2} \\ &- B_{26}\frac{\partial^3 u^0}{\partial y^3} - B_{16}\frac{\partial^3 v^0}{\partial x^3} - (B_{12} + 2B_{66})\frac{\partial^3 v^0}{\partial x^2 \partial y} - 3B_{26}\frac{\partial^3 v^0}{\partial x\, \partial y^2} \\ &- B_{22}\frac{\partial^3 v^0}{\partial y^3} = q(x,y) + N_x \frac{\partial^2 w}{\partial x^2} + 2N_{xy}\frac{\partial^2 w}{\partial x\, \partial y} + N_y \frac{\partial^2 w}{\partial y^2} \end{aligned} \qquad (7.143)$$

Note that equation (7.143) consists of the terms in equation (7.131) and the additional terms due to the in-plane forces.

We now consider the case of buckling of a rectangular, simply supported, specially orthotropic plate under a single compressive axial load, $N_x = -N$, as shown in figure 7.43. In this case, the loads $N_y = N_{xy} = q(x, y) = 0$, all $B_{ij} = 0$, the stiffnesses $A_{16} = A_{26} = D_{16} = D_{26} = 0$ and equation (7.143) becomes

$$D_{11}\frac{\partial^4 w}{\partial x^4} + 2(D_{12} + 2D_{66})\frac{\partial^4 w}{\partial x^2\, \partial y^2} + D_{22}\frac{\partial^4 w}{\partial y^4} = -N\frac{\partial^2 w}{\partial x^2} \qquad (7.144)$$

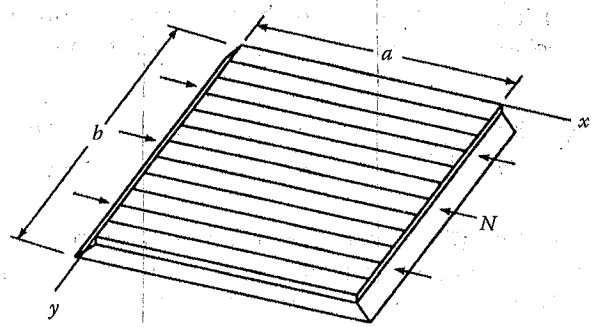

FIGURE 7.43
Simply supported, specially orthotropic plate under compressive uniaxial in-plane loading.

For the simply supported boundary condition described previously by equations (7.135) and equations (7.136), we may assume a solution of the form

$$w(x,y) = w_{mn} \sin\frac{m\pi x}{a} \sin\frac{n\pi y}{b} \tag{7.145}$$

The mode shape for a particular buckling mode is described by the subscripts m and n, since m is the number of half-sine waves along the x direction and n is the number of half-sine waves along the y direction. Substitution of this solution in the governing differential equation (7.144) leads to the equation

$$w_{mn}\pi^2\left[\left(D_{11}m^4 + 2(D_{12}+2D_{66})(mnR)^2 + D_{22}(nR)^4\right)\right] = w_{mn}Na^2m^2 \tag{7.146}$$

where again $R = a/b$. This equation has the trivial solution $w_{mn} = 0$, which is of no interest. For nontrivial solutions, the critical buckling load must be

$$N_{cr} = \frac{\pi^2}{a^2m^2}\left[\left(D_{11}m^4 + 2(D_{12}+2D_{66})(mnR)^2 + D_{22}(nR)^4\right)\right] \tag{7.147}$$

where the smallest buckling load occurs for $n = 1$, and the lowest value of the load corresponding to a particular value of m can only be determined if the D_{ij} and the plate dimensions a and b are known. As shown in figure 7.44, Hatcher and Tuttle [40] have compared experimentally determined buckling loads for simply supported, specially orthotropic graphite/epoxy panels with predicted buckling loads from equation (7.147). The value $n = 1$ is used for all predicted curves, and the curves for $m = 1$ and $m = 2$ are shown. Measurement of critical buckling loads is shown schematically in figure 7.45 and figure 7.46, where the compressive axial load

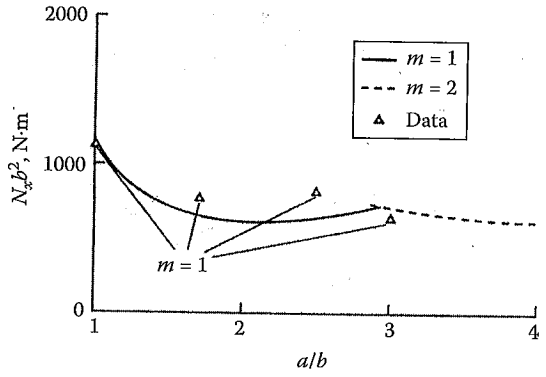

FIGURE 7.44
Comparison of predicted and measured normalized buckling load, $N_x b^2$, vs. plate aspect ratio, a/b, for $[0_{12}]$ graphite/epoxy laminates. (From Hatcher, D. and Tuttle, M. 1991. *Recent Advances in Structural Mechanics*, PVP-Vol. 225/NE-Vol. 7, pp. 21–26. American Society of Mechanical Engineers, New York. Reprinted by permission of The American Society of Mechanical Engineers.)

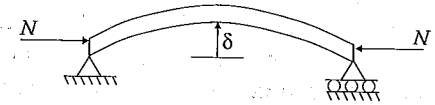

FIGURE 7.45
Measurement of critical axial buckling load for laminate.

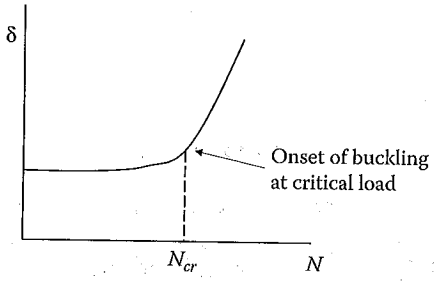

FIGURE 7.46
Variation of lateral deflection with in-plane axial load during buckling test.

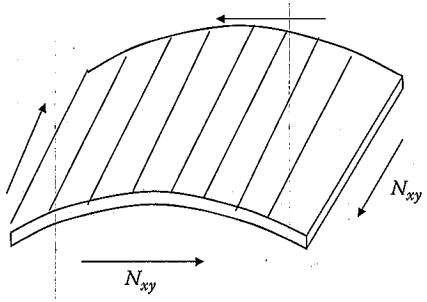

FIGURE 7.47
Buckling due to in-plane shear loads.

on the laminate is increased until the lateral deflection starts to increase dramatically and the instability known as buckling soon follows. Although the predictions are reasonably accurate for this case, it was found that the agreement for some other laminate configurations was not quite as good. Difficulties in simulating the simply supported boundary conditions and in measuring the critical buckling loads, along with other problems such as the existence of imperfections in the test panels, were cited as possible reasons for the disagreement.

Other types of buckling can occur in laminates in addition to buckling under in-plane axial loads. For example, if the critical in-plane shear load is exceeded, shear buckling can occur as shown in figure 7.47.

For laminates other than specially orthotropic and boundary conditions other than simply supported, closed-form solutions similar to equation (7.147) are generally not possible, and approximate methods such as Rayleigh–Ritz or Galerkin must be used. Exceptions include the antisymmetric cross-ply and antisymmetric angle-ply laminates, which do admit closed-form solutions [41].

7.10 Selection of Laminate Designs

When designing with conventional isotropic materials, the problem of material selection is usually solved by simply looking up the appropriate properties of candidate materials in a handbook. The selection of a composite laminate design can be a formidable task, however, due to the large number of available fiber and matrix materials and the endless variety of laminate configurations. The major differences between the analysis of laminates and the design of laminates are best explained by giving examples.

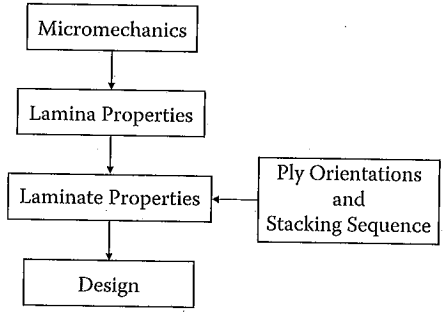

FIGURE 7.48
Flow chart for laminate analysis.

A typical analysis problem would be given a composite laminate and allowable ply stresses, determine the loads that it will support, or given the laminate, loads, and properties, determine the resulting stresses and strains. Either way, the analysis problem has a unique solution. A typical design problem would be, given a set of loads and other design constraints, select the materials and laminate configuration to withstand the loads. As opposed to the analysis problem, the design problem may have an infinite number of solutions. Depending on the number of constraints, it may be possible to reduce the number of feasible designs or to even optimize the design. A general flow chart showing the laminate design sequence is shown in figure 7.48. Depending on the degree of design flexibility desired and the availability of measured lamina level properties, the laminate design may begin either with micromechanics modeling at the fiber/matrix level or directly from measured lamina properties.

Obviously, the nature of the applied loads must be known in order to start the design process. Uniaxial loading on a unidirectional laminate is clearly the simplest case to deal with, but, unfortunately, most practical loading situations are multiaxial, and this requires the design of a multidirectional laminate. For example, if the loading is biaxial as shown in figure 7.49(a), only a crossply [0/90] laminate may be needed. However, if shear loads are present as in figure 7.49(b), some angle plies will be required as well. In the beginning stages of a design, it may be helpful to establish some practical bounds on the laminate properties based on knowledge of the mechanical behavior of certain special types of laminates. For example, figure 7.50 shows the variation of the in-plane laminate stiffness, $\bar{A}_{11}$, with ϕ, the orientation of the laminate with respect to the loading direction, for both unidirectional and quasi-isotropic laminates. The unidirectional laminate stiffness for $\phi = 0$ may be considered to represent the practical upper bound on laminate stiffness, and the

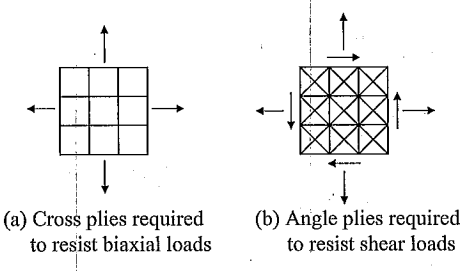

FIGURE 7.49
Lamina orientations to resist different loading conditions.

quasi-isotropic laminate may be considered to represent the practical lower bound on laminate extensional stiffness.

An essential component of any design problem is the identification all of the possible failure modes. Whether intentional or not, if a particular failure mode is overlooked in the design process, that failure mode is the one that will most likely come back to haunt the designer. A list of the major design criteria for composite laminates and the associated failure modes are provided in table 7.1. It is beyond the scope of this book to cover the analytical tools needed for all of these design criteria, and the focus here is on strength, stiffness, stability, hygrothermal effects, and creep.

In order to use the laminate analysis equations that were derived and discussed earlier in this chapter, extensive matrix algebra is obviously required. In addition, proper evaluation of laminate designs requires numerous repetitive calculations resulting from changes in loading conditions, material properties, and laminate geometry. These computational requirements are ideally suited for solutions by digital computers, and a

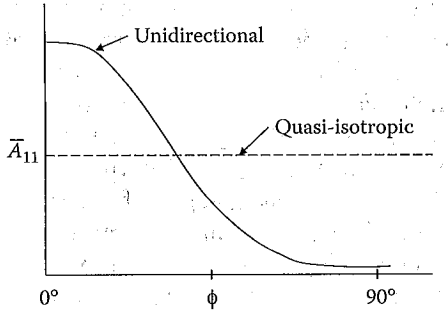

FIGURE 7.50
Variation of laminate extensional stiffness with laminate orientation for unidirectional and quasi-isotropic laminates.

TABLE 7.1

Design Criteria for Composite Laminates and the Associated Failure Modes

Design Criteria	Associated Failure Modes
Strength	Fracture (either partial or complete)
Stiffness	Excessive deformation
Stability	Buckling
Hygrothermal effects	Property degradation, expansion and contraction, residual stresses
Life or durability	Fatigue, creep
Weight	Heavier than conventional design
Cost	Not affordable
Manufacturability	Impractical to build, warping due to residual stresses

variety of software packages for laminate analysis now exist. A list of some of the available software packages is given in table 7.2. Most of these programs have been developed for use on microcomputers, and many of them will do both micromechanical analysis of laminae and laminate analysis according to the CLT. The two basic approaches used in many of these programs are (1) stress and strain analysis for prescribed loads and (2) first ply failure analysis and ultimate laminate failure analysis according

TABLE 7.2

Composite Analysis Software

Software	Company	Address
CompositePro	Peak Composites, Inc.	13299 West 84th Place, Arvada, CO 80005, web address: http:// www.compositepro.com
MICMAC, GENLAM, LAMRANK	Think Composites	101 Alma Street, #703, Palo Alto, CA 94301, web address: http:// www.thinkcomposites.com/
FiberSim	Vistagy, Inc.	200 Fifth Avenue, 5th Floor, Waltham, MA 02451, web address: http:// www.vistagy.com
HyperSizer	Collier Research	45 Diamond Hill Road, Hampton, VA 23666, web address: http:// www.hypersizer.com
Lamona	AdTech Systems Research, Inc.	1342 N. Fairfield Road, Beavercreek, OH 45432-2698, web address: http:// www.adtechsystems.com/
LAP	Anaglyph Ltd.	Suite 33, 10 Barley Mow Passage, London W4 4PH, United Kingdom, web address: http://www.anaglyph.co.uk/
The Laminator		http:// www.thelaminator.net/

to one of the multiaxial lamina strength criteria that were discussed in chapter 4. In addition, some of the programs will do specialized tasks such as deflection and buckling analyses, interlaminar stress calculations, effective property calculations, and hygrothermal and transport property calculations. Such programs are indispensable in design and analysis because hand calculations are not only too time consuming, but the possibilities for errors in such hand calculations are endless.

For composite structures having complex geometries the preferred analytical tool is the finite element method. The use of the finite element method in micromechanical analysis has already been discussed in chapter 3. Macromechanical finite element analysis of laminated structures is also widely used, and most of the popular finite element codes have special elements such as orthotropic 3-D solid elements, orthotropic 2- and 3-D shell elements, and orthotropic axisymmetric solid elements [42].

Although computer software gives the designer great flexibility in the selection of materials and laminate geometries, graphical representations that show the range of properties that can be attained with different laminate configurations are also helpful. One type of graphical representation, known as a carpet plot, is particularly useful. For example, if the ply orientations in a laminate are restricted to certain angles such as 0°, ±45°, and 90°, then a carpet plot can be generated, which shows how a given laminate property depends on the percentages of the plies at the various orientations. The carpet plots in figure 7.51 from ref. [43] show how E_x, G_{xy}, v_{xy}, and α_x for $[0_i/\pm45_j/90_k]$ Kevlar®/epoxy laminates vary with the percentages of the plies at the three angles. In this case, i is the number of 0° plies, j is the number of ±45° plies, and k is the number of 90° plies. Therefore, the percentage of 0° plies is $i/(i+j+k)$, the percentage of ±45° plies is $j/(i+j+k)$, and the percentage of 90° plies is $k/(i+j+k)$.

For example, the various ply combinations that will give a certain value of longitudinal modulus, E_x, can be determined by drawing a horizontal line in figure 7.51(a) at the value of E_x and then reading off the percentage of the plies at the three angles corresponding to a particular point on the line. Obviously, there are many possible combinations that will give the same value of E_x, and the design flexibility inherent in composite construction is again demonstrated. Carpet plots for laminate strength are also widely used. Since there would normally be more than one design constraint, an iterative approach involving the repeated use of carpet plots for several different properties may be needed for the selection of the required ply combinations. Carpet plots can be quickly generated using the output of laminate analysis software.

While composite analysis software packages and carpet plots are very convenient and efficient design tools for dealing with micromechanics analysis and laminate analysis using CLT, they generally do not include consideration of interlaminar stresses or other "secondary stresses." Indeed,

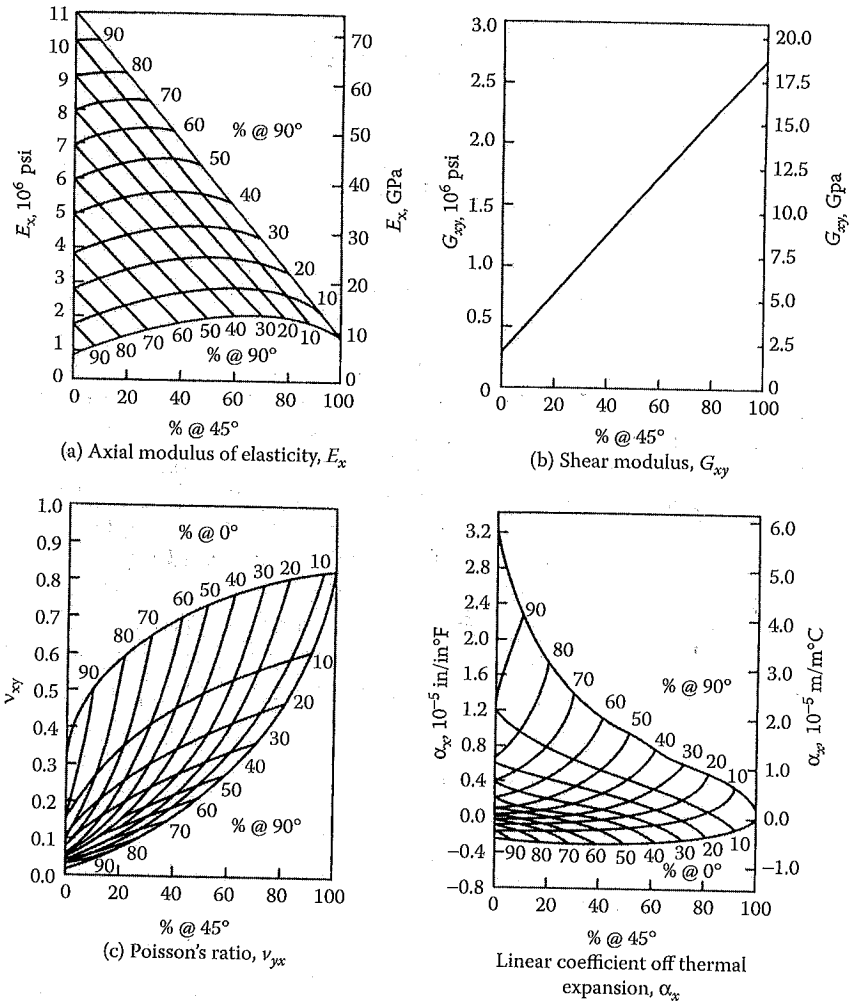

FIGURE 7.51
Carpet plots for $[0_i/\pm45_j/90_k]$ Kevlar®/epoxy laminates. (From Peters, S.T., Humphrey, W.D., and Foral, R.F. 1991. *Filament Winding Composite Structure Fabrication*, pp. 5–45. Society for Advancement of Materials and Process Engineering, Covina, CA. Reprinted by permission of The Society for the Advancement of Material and Process Engineering.)

the secondary stresses are often neglected in the design process, which tends to focus on the "primary" in-plane stresses that are directly associated with the loading. As seen in section 7.7, the interlaminar stresses often develop near free edges such as bolt holes or other discontinuities. An example of this is shown in figure 7.52, where the transverse interlaminar

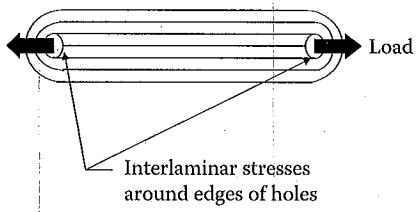

FIGURE 7.52
Interlaminar stresses in axially loaded composite link.

around the bolt holes in the composite link may lead to failure before the primary axial stresses do. Thus, the maximum applied axial load on the link may be limited by the secondary stresses more than by the primary axial stresses. There are other secondary stresses besides interlaminar stresses that may limit the applied loading on the composite more than the primary stresses do. For example, in the filament wound, composite cylindrical pressure vessel shown in figure 7.53, axial bending stresses in the composite cylinder may be generated due to rotational deformation of the lip of the metal end cap as the cylinder is internally pressurized. Since the fibers in such a filament wound vessel are oriented primarily in the circumferential or "hoop" direction, the axial direction in the cylinder

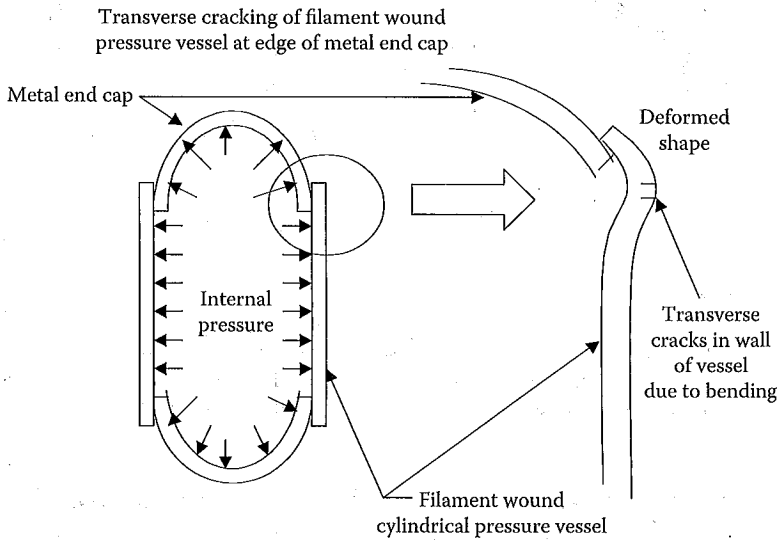

FIGURE 7.53
Axial bending stresses in filament wound composite cylinder caused by metal end cap.

corresponds to the transverse direction in the composite. As shown in chapter 4, the transverse tensile strength is generally the lowest of all the composite strengths, so the secondary bending stresses rather than the hoop stresses may limit the internal pressure that the cylinder can withstand.

A number of available handbooks and design guides are useful in the design of composite laminates and structures. These books contain not only the necessary analytical tools, but also the material property data that is required for the use of the tools. Among the recent composites handbooks are those edited by Kelly and Zweben [44], Mallick [45], Harper [46], and Donaldson and Miracle [47]. Of particular note is the five volume series *Handbook of Composites, MIL-HDBK-17* [48], which is sponsored by the U.S. Department of Defense, and is available on-line.

EXAMPLE 7.13

The reader should be able to use figure 7.51(a) to verify that a Kevlar®/epoxy laminate with a longitudinal modulus of E_x = 30 GPa can be obtained with the following ply combinations; (1) 35% at 0°, 0% at ±45°, and 65% at 90°; (2) 30% at 0°, 30% at ±45°, and 40% at 90°; and (3) 30% at 0°, 60% at ±45°, and 10% at 90°. These are only three of many possible combinations that will give the same result. Additional design constraints may also be taken into account with other carpet plots. For example, if a shear modulus, G_{xy}, of at least 5.0 GPa is needed, figure 7.51(b) indicates that the laminate should have at least 20% of its plies at ±45°. Thus, laminates (2) and (3) above both satisfy the constraints on E_x and G_{xy}, but laminate (1) does not.

EXAMPLE 7.14

An existing power transmission shaft consists of a hollow composite tube as shown in figure 7.33, and the tube wall is a filament wound quasi-isotropic $[60/0/-60]_s$ laminate of thickness t. A new shaft of the same wall thickness t is to be designed from the same lamina material, but the new laminate is to have a shear stiffness greater than that of the existing shaft. Over what range of angles θ will a $[+\theta/-\theta/-\theta]_s$ angle-ply laminate achieve this design objective?

Solution. The shear stiffness of the new angle-ply laminate is

$$(A_{66})_{ap} = \int_{-t/2}^{t/2} \bar{Q}_{66} dz = (\bar{Q}_{66})_{+\theta} \frac{t}{3} + (\bar{Q}_{66})_{-\theta} \frac{2t}{3}$$

Recalling that the lamina stiffnesses can be expressed in terms of invariants as

$$\bar{Q}_{66} = \frac{U_1 - U_4}{2} - U_3 \cos 4\theta$$

and that $\cos 4\theta = \cos(-4\theta)$, the new laminate stiffness can be written as

$$(A_{66})_{ap} = \left[\frac{U_1 - U_4}{2} - U_3 \cos 4\theta\right]\frac{t}{3} + \left[\frac{U_1 - U_4}{2} - U_3 \cos(-4\theta)\right]\frac{2t}{3}$$

$$= \frac{U_1 - U_4}{2}t - U_3 t \cos 4\theta$$

The shear stiffness of a quasi-isotropic laminate is

$$(A_{66})_{QI} = \frac{U_1 - U_4}{2}t$$

Therefore the shear stiffness of the new laminate can be expressed as

$$(A_{66})_{ap} = (A_{66})_{QI} - U_3 t \cos 4\theta$$

The variations of $(A_{66})_{ap}$ and $(A_{66})_{QI}$ with θ are shown in figure 7.54, where it can be seen that

$$(A_{66})_{ap} > (A_{66})_{QI} \quad \text{for angles } \theta \text{ in the range} \quad 22.5° \le \theta \le 67.5°.$$

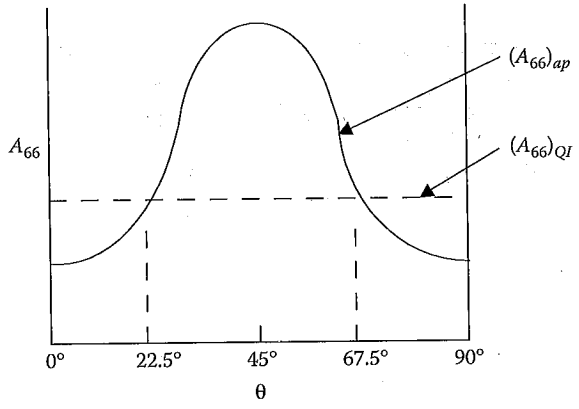

FIGURE 7.54
Variation of laminate shear stiffness with ply orientation for angle ply and quasi-isotropic laminates.

7.11 Application of Laminate Analysis to Composite Structures

Composite structures often consist of components in the form of beams, plates, shells, sandwich panels, and grids, and for detailed coverage of the mechanics of composite structures, the reader is referred to books by Vinson and Sierakowski [49], Kollar and Springer [50], and Sun [51]. The purpose of this section is to show how the previously described CLT can be applied to composite structures that are not usually thought of as being laminates. More specifically, the application of CLT to composite sandwich structures and composite grid structures will be discussed briefly. Detailed discussion of these structures is beyond the scope of this book, as both types of structures have been the subject of numerous books and journal articles, some of which are referred to here.

7.11.1 Composite Sandwich Structures

Composite sandwich structures such as the one shown in figure 1.5 are widely used in aerospace and marine applications due to the extremely high flexural stiffness-to-weight ratios and flexural strength-to-weight ratios that can be achieved with such structures. The mechanical behavior of composite sandwich structures has been described in detail by Vinson [52]. As shown in figure 1.5, composite sandwich structures consist of two composite facings adhesively bonded on both sides of a lightweight foam or honeycomb core. The equivalent laminate stiffnesses of composite sandwich panels can be found directly from CLT. As shown in figure 1.5 and figure 7.55, such structures are typically symmetric with respect to

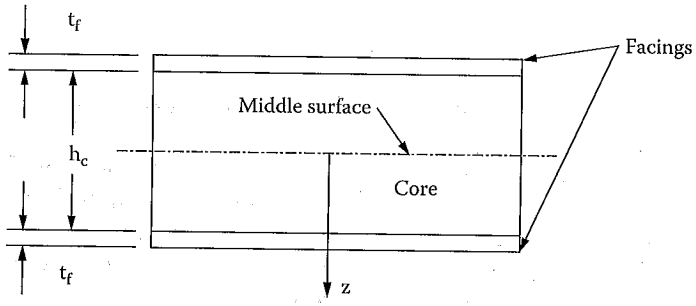

FIGURE 7.55
Geometry of composite sandwich structure for laminate analysis.

the middle surface, so the corresponding coupling stiffnesses $B_{ij} = 0$. The equivalent laminate extensional stiffnesses for the symmetric sandwich structure geometry in figure 7.55 are given by substitution in equation (7.38), as shown by Vinson [52]:

$$A_{ij} = \sum_{k=1}^{3} [\bar{Q}_{ij}]_k (z_k - z_{k-1})$$

$$= [\bar{Q}_{ij}]_f \left(-\frac{h_c}{2} - \left(\frac{h_c}{2} - t_f \right) \right) + [\bar{Q}_{ij}]_c \left(\frac{h_c}{2} - \left(-\frac{h_c}{2} \right) \right) + [\bar{Q}_{ij}]_f \left(\left(\frac{h_c}{2} + t_f \right) - \frac{h_c}{2} \right)$$

$$= [\bar{Q}_{ij}]_f (2t_f) + [\bar{Q}_{ij}]_c h_c \tag{7.148}$$

where facing properties are denoted by the subscript f and core properties are denoted by the subscript c. Similarly, equation (7.39) lead to $B_{ij} = 0$, and equation (7.40) give the following equivalent laminate flexural stiffnesses, as shown by Vinson [52]:

$$D_{ij} = \frac{1}{3} \sum_{k=1}^{3} [\bar{Q}_{ij}]_k \left(z_k^3 - z_{k-1}^3 \right)$$

$$= \frac{1}{3} [\bar{Q}_{ij}]_f \left(\left(-\frac{h_c}{2} \right)^3 - \left(-\frac{h_c}{2} - t_f \right)^3 \right) + \frac{1}{3} [\bar{Q}_{ij}]_c \left(\left(\frac{h_c}{2} \right)^3 - \left(-\frac{h_c}{2} \right)^3 \right) \tag{7.149}$$

$$+ \frac{1}{3} [\bar{Q}_{ij}]_f \left(\left(\frac{h_c}{2} + t_f \right)^3 - \left(\frac{h_c}{2} \right)^3 \right)$$

Once the equivalent laminate stiffnesses are known, the stresses and deformations can be predicted using the approaches outlined earlier in this chapter. However, there are some corrections to laminate analysis that may be required for use on sandwich structures. For example, one of the assumptions of CLT was that the transverse shear strains γ_{xz} and γ_{yz} are negligible. This may not be the case in sandwich structures, because the core is often made of foam or honeycomb material that has a low shear modulus. If the transverse shear strains are to be considered, the transverse shear stress resultants Q_x and Q_y in figure 7.40 would be related to the transverse shear strains γ_{xz} and γ_{yz} by a transverse shear stiffness

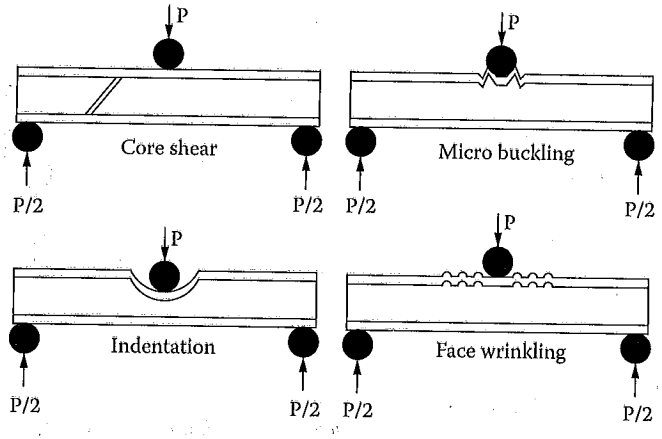

FIGURE 7.56
Failure modes of a sandwich beam in three-point bending. (From Steeves, C.A. and Fleck, N.A. 2004. *International Journal of Mechanical Sciences*, 46, 585–608. With permission.)

matrix, there will be additional strain–displacement equations to supplement equation (7.29), and the governing partial differential equations (equation [7.129] to equation [7.131]) will include additional transverse shear terms [50,52].

The application of laminate analysis in the prediction of strength in composite sandwich structures is significantly limited by the existence of important failure modes in sandwich structures that are not present in composite laminates. Laminate failure modes would only be relevant for the facings in the sandwich, but other possible failure modes are due to the core or core/facing interactions. For example, Steeves and Fleck [53] have investigated the failure modes in foam-cored composite sandwich beams under three-point bending, and the observed failure modes are summarized in figure 7.56. The failure load, P, can be estimated from simple mechanics of materials formulas for each of the failure modes once the beam parameters and dimensions are known. The lowest of the predicted failure loads would govern the design of the sandwich structure. In figure 7.57, the midpoint of the beam deflects by a transverse displacement u due to the applied load P of the mid-roller. L is the beam length between the supports, H is the overhang at each end, b is the width of the beam, c is the core thickness, and t_f is the face thickness. The relevant mechanical properties of the isotropic core are the Young's modulus E_c, shear modulus G_c, compressive strength σ_c, and shear strength τ_c. For the face sheets, the relevant properties are the axial compressive strength σ_f and Young's modulus E_f, and the dimension $d = c + t_f$.

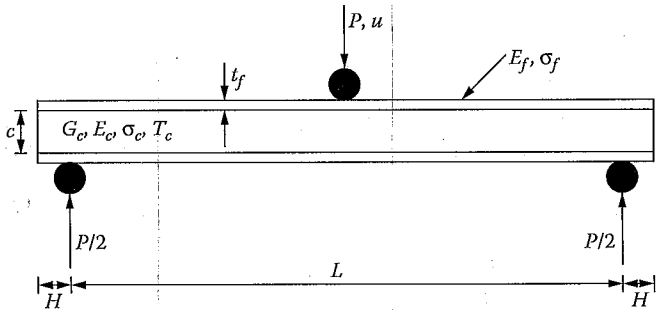

FIGURE 7.57
Geometry of a sandwich beam in three-point bending. (From Steeves, C.A. and Fleck, N.A. 2004. *International Journal of Mechanical Sciences*, 46, 585–608. With permission.)

According to Zenkert [54], the predicted collapse load for face yielding or microbuckling is given as:

$$P = \frac{4\sigma_f b t_f d}{L} \tag{7.150}$$

whereas the corresponding critical load for core shear failure can be estimated as

$$P = 2\tau_c b d \tag{7.151}$$

and the load required to produce face wrinkling is

$$P = \frac{2bt_f d}{L}\sqrt[3]{E_f E_c G_c} \tag{7.152}$$

Steeves and Fleck [55] have suggested that the load required for indentation failure is

$$P = bt_f\left(\frac{\pi^2\sigma_c^2 E_f d}{3L}\right)^{1/3} \tag{7.153}$$

There are many other aspects of composite sandwich structures that are not necessarily relevant to laminate analysis. For more detailed studies of composite sandwich structures, the reader is encouraged to explore the publications referred to earlier in this section.

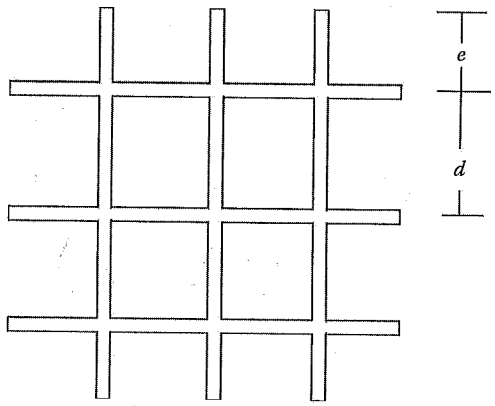

FIGURE 7.58
Orthogrid structure.

7.11.2 Composite Grid Structures

Grid stiffened geodesic structural configurations date back to the 1920s [56] when they were first used in aircraft construction with a metal grid and fabric skin. The structures of these aircraft were known for their excellent tolerance to battle damage. Along with the maturation of composite technology, there has been increasing interest in composite grid structures for the last several decades. The most common grid structures are the orthogrid, with the ribs oriented at 0 or 90° (fig. 7.58) and the isogrid, with the ribs oriented at 0 and ±60° (fig. 7.59). Composite grid structures are a promising concept for applications in plate or shell-like components of systems such as spacecraft, aircraft, automobile, containers, bridges, ships, and propellers. These structures have several advantages over traditional construction methods that use panels, sandwich cores, or expensive framework. As the ribs of the grids are made of unidirectional continuous fiber-reinforced composites, they are strong, tough, damage tolerant, and do not delaminate. As grids are open structures, they are easy to inspect and repair. With such processes as automated fiber placement and pultrusion, the potential also exists for completely automating the grid fabrication process and reducing the processing cost.

The use of laminate analysis in modeling mechanical behavior of grid structures is based on the concept of replacing the grid with a laminated plate having equivalent stiffnesses, as described by Chen and Tsai [57] and

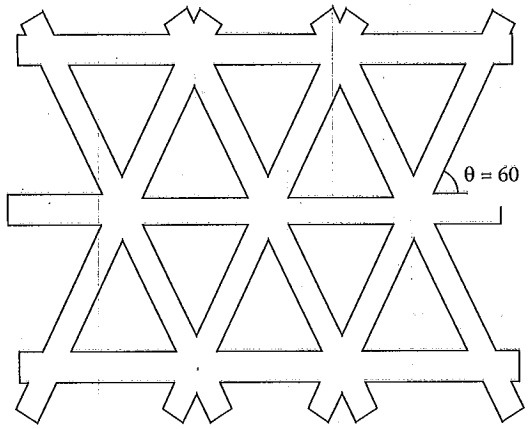

FIGURE 7.59
Isogrid structure.

Huybrechts and Tsai [58]. The grid structure can be considered as a combination of sets of parallel ribs. The equivalent axial, flexural and torsional stiffnesses of each family of parallel ribs can be calculated separately, and then the overall stiffnesses of the grid structure are obtained by the principle of superposition. Following the analysis by Chen and Tsai [57], consider the family of N parallel ribs in figure 7.60, each of which has center-to-center spacing d (figure 7.58), cross-sectional area A, and longitudinal modulus E_x.

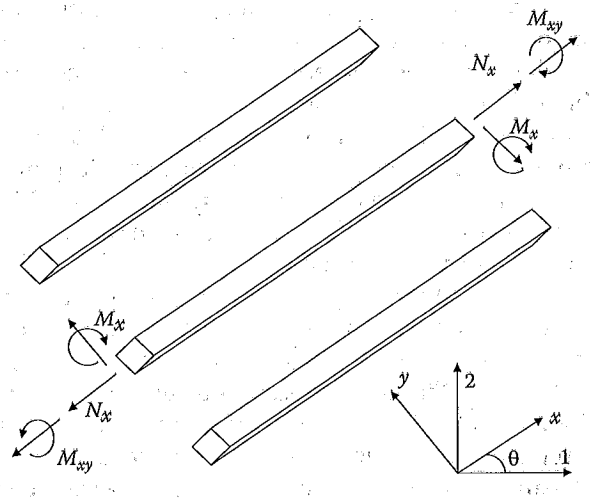

FIGURE 7.60
Family of parallel ribs for modeling of grid structure.

The direction of the local (x,y,z) coordinate axes are along and perpendicular to the ribs. Let θ be the angle between the local and global axes (1,2,3). It should be noted that the normal strain along the y direction, ε_y, the shear strains Υ_{xy} and Υ_{yz}, and the curvature κ_y in the ribs were not considered. If all N ribs are identical, static equilibrium and geometric compatibility requirements lead to the following equation relating the force per unit length along the x direction to the corresponding strain ε_x [57],

$$N_x = \frac{AE_x\varepsilon_x}{d} \tag{7.154}$$

In this case, the force per unit length is based on the effective width $(N-1)d + 2e$ for the parallel family of ribs, where the distance e in figure 7.58 approaches $d/2$. Thus, the corresponding effective width becomes approximately Nd. Transforming both the force per unit length and the strain to the global coordinates and factoring out the resulting extensional stiffnesses A_{ij} for an equivalent flat laminated plate,

$$[A] = \frac{E_xA}{d}\begin{bmatrix} m^4 & m^2n^2 & m^3n \\ m^2n^2 & n^4 & mn^3 \\ m^3n & mn^3 & m^2n^2 \end{bmatrix} = \begin{bmatrix} A_{11} & A_{12} & A_{16} \\ A_{21} & A_{22} & A_{26} \\ A_{16} & A_{26} & A_{66} \end{bmatrix} \tag{7.155}$$

where $m = \cos\theta$ and $n = \sin\theta$. Applying a similar approach for bending of the parallel family of ribs, the flexural stiffness matrix for an equivalent flat laminated plate is found to be

$$[D] = \frac{1}{d}\begin{bmatrix} E_xIm^4 + GJm^2n^2 & E_xIm^2n^2 + GJm^2n^2 & E_xIm^3n - \dfrac{GJmn(m^2-n^2)}{2} \\ E_x\,\mathrm{I}m^2n^2 - GJm^2n^2 & E_xIn^4 + GJm^2n^2 & E_xIm^3n + \dfrac{GJmn(m^2-n^2)}{2} \\ E_x\,\mathrm{I}m^3n - GJm^3n & E_x\,\mathrm{I}m^3n + GJm^3n & E_xIm^2n^2 + \dfrac{GJm^2(m^2-n^2)}{2} \\ E_x\,\mathrm{I}m^3n + GJmn^3 & E_x\,\mathrm{I}m^3n - GJmn^3 & E_xIm^2n^2 - \dfrac{GJn^2(m^2-n^2)}{2} \end{bmatrix}$$

$$= \begin{bmatrix} D_{11} & D_{12} & D_{16} \\ D_{21} & D_{22} & D_{26} \\ D_{16} & D_{26} & D_{66} \end{bmatrix} \tag{7.156}$$

where

$$J=\frac{hw^3}{16}\left[\frac{16}{3}-3.36\frac{w}{h}\left(1-\frac{w^4}{12h^4}\right)\right] \tag{7.157}$$

and E_x and G are longitudinal and shear modulus of the rib, respectively; h is rib height, and I and J are the moment of inertia with respect to the midplane and the torsional constant of the rib cross section, respectively.

For the orthogrid case, the $[D]$ matrix becomes a 3×3 symmetric matrix with D_{16}, and D_{26} equal to zero. The A_{66} term for the orthogrid must be taken into account because the bending and shear effects of ribs tangential to the midplane cannot be neglected and it becomes as [57].

$$A_{66}=1/a_{66} \tag{7.158}$$

where

$$a_{66}=\frac{1}{12}\frac{d_{90}^2 d_0}{E_x I_0^t}+\frac{1}{12}\frac{d_{90}d_0^2}{E_x I_{90}^t}+\frac{d_0}{\kappa G A_0}+\frac{d_{90}}{\kappa G A_{90}} \tag{7.159}$$

G is the shear modulus of the ribs, d_0 and d_{90} are horizontal and vertical spacing of ribs, and κ is the shear correction factor, which is taken as 5/6.

The total stiffnesses for the grid can be obtained from superposition by summing up the stiffnesses of each parallel family of ribs taking into account the orientation of each family of ribs. For example, the $[A]$ and $[D]$ matrices for the orthogrid with two families of identical ribs at $\theta=0°$ and 90° are

$$[A]_{\text{orthogrid}}=\begin{bmatrix}\frac{E_xA}{d} & 0 & 0\\ 0 & \frac{E_xA}{d} & 0\\ 0 & 0 & A_{66}\end{bmatrix} \tag{7.160}$$

$$[D]_{\text{orthogrid}}=\frac{1}{d}\begin{bmatrix}E_xI & 0 & 0\\ 0 & E_xI & 0\\ 0 & 0 & \frac{GJ}{2}\end{bmatrix} \tag{7.161}$$

Similarly, for the isogrid with three parallel families of identical ribs at $\theta=0°$, 60°, and −60°,

$$[A]_{\text{isogrid}}=\frac{\sqrt{3}E_xA}{4d}\begin{bmatrix}3 & 1 & 0\\ 1 & 3 & 0\\ 0 & 0 & 1\end{bmatrix} \tag{7.162}$$

$$[D]_{\text{isogrid}}=\frac{\sqrt{3}E_xI}{4d}\begin{bmatrix}3+\tau & 1+\tau & 0\\ 1+\tau & 3+\tau & 0\\ 0 & 0 & 1+\tau\end{bmatrix} \tag{7.163}$$

where

$$\tau=\frac{GJ}{E_xI}$$

$$I=\tfrac{1}{12}wh^3$$

and

$$J=\frac{hw^3}{16}\left[\frac{16}{3}-3.36\frac{w}{h}\left(1-\frac{w^4}{12h^4}\right)\right] \tag{7.164}$$

and h is rib height, d is the length of each side of the equilateral triangles in the isogrid, and I and J are the moment of inertia with respect to the midplane and torsional constant of the rib cross section, respectively. All of the above equations apply to the case of the grid alone, but the method can also be applied to the case where the ribs are attached to a composite laminate skin on one or both sides [57].

7.12 Problems

1. A laminated $[0/90/0/90]_s$ carbon/epoxy beam is 1 mm thick, is 20 mm wide, and has 0.125-mm thick plies. The lamina properties are

E_1 = 180 Gpa $s_L^{(+)}$ = 1700 Mpa
E_2 = 10 Gpa $s_L^{(-)}$ = 1400 MPa

$G_{12} = 7$ Gpa $\quad s_T^{(+)} = 40$ Mpa
$\nu_{12} = 0.28 \quad s_T^{(-)} = 230$ MPa

(*a*) Determine the flexural modulus for the beam.

(*b*) How could the flexural modulus be improved without changing the ply materials, the number of plies, or the ply orientations?

(*c*) Using the Maximum Stress Criterion for each ply, determine the magnitude of the maximum allowable bending moment that the beam can withstand. Which ply fails first?

(*d*) What type of analysis would be required if the ply orientations are $[+45/90/-45/0]_s$?

2. The laminated beam shown in figure 7.61 is made up of two outer plies of material "A" having Young's modulus E_A, two inner plies of material "B" having Young's modulus E_B, and a honeycomb core of negligible stiffness. Materials A and B are isotropic, but they have different thicknesses. The laminate is symmetric about the middle surface. Find the expression for the flexural modulus in terms of the given properties and the dimensions shown in figure 7.61.

3. A thin-walled composite tube having an outside diameter of 48 mm is made by securely bonding an aluminum tube inside a steel tube, as shown in figure 7.62. Determine the maximum allowable bending moment, M, that the composite tube can

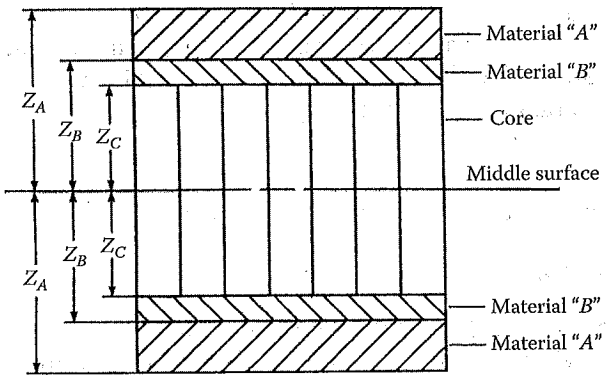

FIGURE 7.61
Laminated beam for problem 2.

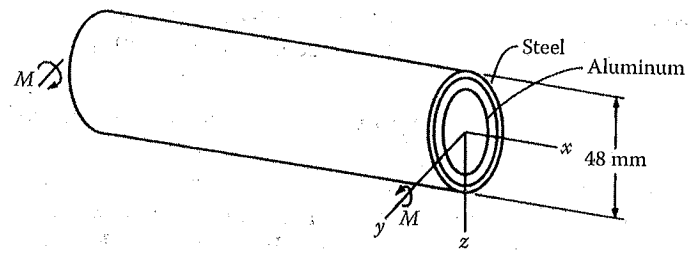

FIGURE 7.62
Composite tube for problem 3.

withstand without exceeding the yield stress of either the steel or the aluminum. The tube properties are:

	Steel	Aluminum
Young's modulus, GPa	200	78
Yield stress, MPa	259	98
Wall thickness, mm	3	6

4. Determine the stiffness matrix for a $[+45/-45]$ antisymmetric laminate consisting of 0.25-mm thick unidirectional AS/3501 carbon/epoxy plies.

5. Show that for symmetric laminates the coupling stiffnesses, B_{ij}, must all be equal to zero.

6. By expanding the $[A]$ matrix in terms of ply stiffnesses show that a "balanced" cross-ply laminate having equal numbers of 0 and 90° plies is not necessarily quasi-isotropic.

7. A $[-60/0/60]$ laminate and a $[0/45/90]$ laminate both consist of 1.0-mm thick plies having the following properties: $E_1 = 181$ GPa, $E_2 = 10.3$ GPa, $G_{12} = 7.17$ GPa, $\upsilon_{12} = 0.28$. Plot the A_{ij}, for both laminates as a function of the orientation in order to determine which, if any, of the laminates is quasi-isotropic.

8. The $[+45/-45]$ laminate described in problem 4 is subjected to a uniaxial force per unit length $N_x = 30$ MPa-mm. Find the resulting stresses and strains in each ply along the x and y directions.

9. A $[0/90]_s$ laminate is subjected to a single bending moment per unit length, M_x. If the laminate is unconstrained, so that bending along both the x and the y directions occurs freely, determine the ply stresses, $(\sigma_x)_k$, in terms of the moment, M_x, the bending stiffnesses, D_{ij} the ply stiffnesses, Q_{ij}, and the distance from the middle

surface, z. Determine the ply stresses $(\sigma_x)_k$ in terms of M_x, z, and a numerical coefficient if the properties are $E_1 = 129$ GPa, $E_2 = 12.8$ GPa, $G_{12} = 4.6$ GPa, $v_{12} = 0.313$, and $t = 1$ mm.

10. The laminate described in problem 9 is subjected to a single bending moment per unit length, M_x, and the two edges on which M_x acts are fixed so that bending along the x direction occurs freely but bending along the y direction is prevented. That is, the longitudinal curvature is unconstrained (i.e., $\kappa_x \neq 0$), but the transverse curvature is constrained (i.e., $\kappa_y = 0$). Determine the ply stresses $(\sigma_x)_k$ as in problem 9 (give equations and numerical results) and compare with the results of problem 9.
11. A $[90/0/90]_s$ laminate is fabricated from laminate consisting of isotropic fibers ($E_f = 220$ GPa, $v_f = 0.25$) embedded in an isotropic matrix ($E_m = 3.6$ GPa, $v_m = 0.4$). Each lamina is 0.25-mm thick, and the 0.01-mm diameter fibers have been precoated with a 0.00125-mm thick sizing, which is the same as the matrix material. The precoated fibers are arranged in the closest possible packing array in the matrix. Using both micromechanics and laminate analysis, find the laminate engineering constants E_x, E_y, G_{xy}, and v_{xy}. The laminate *x-axis* is parallel to the 0° lamina orientation.
12. An antisymmetric angle-ply $[+\theta/-\theta]$ laminate is to be made of carbon/epoxy and designed to have a laminate CTE, α_x, as close to zero as possible. Determine the ply orientation θ needed to meet this requirement. The lamina properties are as follows:

$$E_1 = 138 \text{ Gpa, laminate thickness} = 0.125 \text{ mm}$$
$$E_2 = 8.96 \text{ Gpa} \quad \alpha_1 = -0.3 \times 10^{-6} \text{ m/m/K}$$
$$G_{12} = 7.1 \text{ Gpa} \quad \alpha_2 = 28.1 \times 10^{-6} \text{ m/m/K}$$
$$v_{12} = 0.3$$

This problem requires extensive calculations, and the use of a computer is recommended.

13. Repeat problem 12 for a Kevlar®/epoxy composite having lamina properties as follows:

$$E_1 = 76 \text{ Gpa} \quad \text{lamina thickness} = 0.125 \text{ mm}$$
$$E_2 = 5.5 \text{ Gpa} \quad \alpha_1 = -4.0 \times 10^{-6} \text{ m/m/K}$$
$$G_{12} = 2.3 \text{ Gpa} \quad \alpha_2 = 79.0 \times 10^{-6} \text{ m/m/K}$$
$$v_{12} = 0.34$$

14. The distribution of the in-plane shear stress, τ_{xy}, along the y direction at a particular distance z from the middle surface of a uniaxially

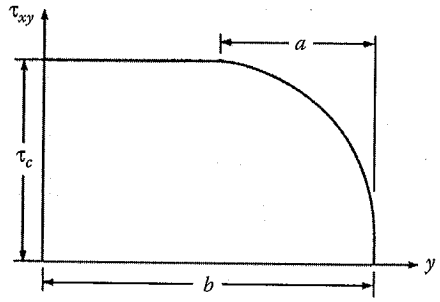

FIGURE 7.63
In-plane shear stress distribution for problem 14.

loaded laminate is idealized, as shown in figure 7.63. The interlaminar stress boundary layer region is assumed to extend inward from the free edge at $y = b$ by a distance "a," the in-plane shear stress $\tau_{xy} = \tau_c$ in the region $0 \leq y \leq (b - a)$ is assumed to be the shear stress from the CLT, and the in-plane shear stress in the boundary layer region $(b - a) \leq y \leq b$ is assumed to be of the form

$$\tau_{xy} = \frac{\tau_c}{a^2}(y - b)(b - 2a - y)$$

For the same location, determine the distribution of the interlaminar shear stress, τ_{xz}, along the y direction.

15. A filament-wound composite drive shaft for a helicopter transmits a torque T that generates shear loading of the shaft material, as shown in figure 7.64. The shaft is to be designed as a hollow tube with a two-ply $[+\theta/-\theta]$ laminated wall. If the outside diameter, the length, and the material density are fixed, use invariants

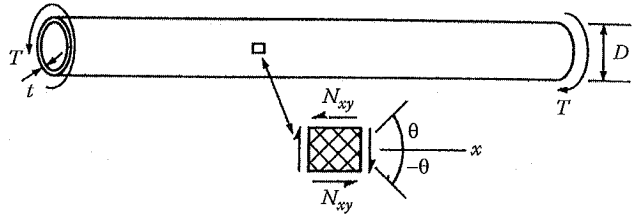

FIGURE 7.64
Filament wound shaft for problem 15.

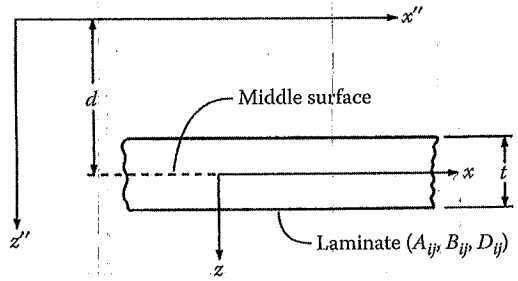

FIGURE 7.65
Laminate with parallel axes for problem 16.

to determine the angle θ, which should be used to maximize the shear stiffness-to-weight ratio, A_{66}/W, where A_{66} is the laminate shear stiffness and W *is* the shaft weight. It may be assumed that the shaft diameter, D, is much greater than the wall thickness, t.

16. Develop a "parallel axis theorem" for the effective laminate stiffnesses A_{ij}'', B_{ij}'', and D_{ij}'' associated with the (x'',z'') axes, which are parallel to the original (x,z) axes, as shown in figure 7.65. Express the new A_{ij}'', B_{ij}'', and D_{ij}'' in terms of the original A_{ij}, B_{ij}, and D_{ij}, for the (x,z) axes and the distance d between the parallel axes, where $z'' = z + d$.
17. A $[0/90/0]_s$ laminate consisting of AS/3501 carbon/epoxy laminae is subjected to uniaxial loading along the x direction. Use the Maximum Strain Criterion to find the loads corresponding to first ply failure and ultimate laminate failure; then plot the load–strain curve up to failure. Compare these results with those of example 7.10 and discuss any differences.
18. Prove that for the specially orthotropic plate shown in figure 7.41 under the loading described by equation (7.137), the solution given by equation (7.138) satisfies the differential equation (7.132) and the boundary conditions in equation (7.135) and equation (7.136).
19. Find expressions for the moments M_x, M_y, and M_{xy} and the stresses $(\sigma_x)_k$, $(\sigma_y)_k$, and $(\tau_{xy})_k$ in the kth ply of the uniformly loaded, specially orthotropic laminate with simply supported edges shown in figure 7.41.
20. Derive the differential equation and the boundary conditions governing the small transverse deflections of a simply supported, rectangular, symmetric angle-ply laminate that is subjected to distributed loading. If the loading is described by equation (7.137), does a solution of the form given in equation (7.138) satisfy this differential equation and boundary conditions? Why?

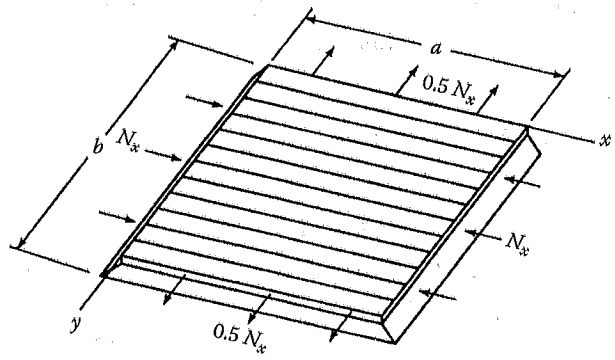

FIGURE 7.66
Simply supported, specially orthotropic plate under in-plane loads for problem 22.

21. Derive the coupled differential equations and the boundary conditions governing the small transverse deflections of a simply supported, rectangular, antisymmetric angle-ply laminate that is subjected to distributed loading. Propose solutions for the displacements u, v, and w that satisfy the differential equations and boundary conditions.
22. A simply supported, specially orthotropic plate is subjected to an in-plane compressive load per unit length N_x and an in-plane tensile load per unit length $N_y = -0.5\ N_x$, as shown in figure 7.66. Derive the expression for the critical buckling load.
23. Derive the differential equation and the boundary conditions governing the buckling of a simply supported, rectangular, symmetric angle-ply laminate that is subjected to a uniaxial in-plane load, N_x. Does a solution of the form given in equation (7.145) satisfy this differential equation and boundary conditions? Why?
24. Using the carpet plots of figure 7.51, select the percentages of 0°, ±45°, and 90° plies that are needed in a $[0_i/\pm45_j/90_k]$ laminate if the longitudinal modulus, E_x, is to be at least 20 GPa, the in-plane shear modulus, G_{xy}, is to be at least 10 GPa, and the longitudinal CTE, α_x, is equal to zero.

25. A symmetric [0/90/0] laminate is 0.75-mm thick and its full compliance matrix is given below.

$$\begin{bmatrix} A & B \\ B & D \end{bmatrix}^{-1} = \begin{bmatrix} A' & B' \\ B' & D' \end{bmatrix}$$

$$= \begin{bmatrix} 0.014 & -7.235x10^{-4} & 0 & 0 & 0 & 0 \\ -7.235x10^{-4} & 0.026 & 0 & 0 & 0 & 0 \\ 0 & 0 & 0.188 & 0 & 0 & 0 \\ 0 & 0 & 0 & 0.213 & -0.042 & 0 \\ 0 & 0 & 0 & -0.042 & 2.066 & 0 \\ 0 & 0 & 0 & 0 & 0 & 4.016 \end{bmatrix}$$

where the units of the matrix are

$$\begin{bmatrix} A' & B' \\ B' & D' \end{bmatrix} = \begin{bmatrix} [\text{GPa-mm}]^{-1} & [\text{GPa-mm}^2]^{-1} \\ [\text{GPa-mm}^2]^{-1} & [\text{GPa-mm}^3]^{-1} \end{bmatrix}$$

Determine the following effective engineering constants for the laminate, giving both magnitude and units; (a) the effective longitudinal Young's modulus, E_x, (b) the effective transverse Young's modulus, E_y, (c) the effective in-plane shear modulus, G_{xy}, (d) the effective longitudinal Poisson's ratio, ν_{xy}, and (e) the effective flexural modulus, E_{fx}.

26. The laminate described in problem 25 has laminae that are 0.25-mm thick and the stiffness matrix associated with the 0° lamina is given by

$$[Q] = \begin{bmatrix} 138.8 & 2.7 & 0 \\ 2.7 & 8.965 & 0 \\ 0 & 0 & 7.1 \end{bmatrix} \text{GPa}$$

If a single bending moment per unit length $M_x = 0.1$ GPa-mm^2 is applied to the laminate, (a) determine the stresses associated with the x and y axes on the top surface of the laminate and (b) determine the stresses associated with the x and y axes on the middle surface of the laminate.

27. The sensing element in many thermostats is a bimetallic strip (fig. 7.67), which is a nonsymmetric laminate consisting of two

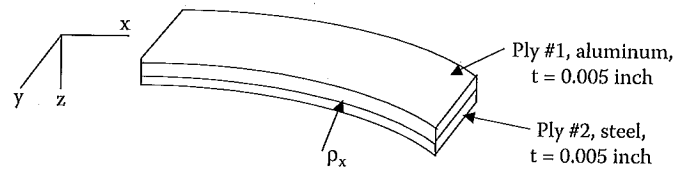

FIGURE 7.67
Bimetallic strip for problem 27.

plies made from different metals. If the strip is subjected to a temperature change ΔT, the differential thermal expansion of the two plies causes a corresponding change in the radius of curvature of the strip, ρ_x, and this motion activates the temperature control system. In the strip shown in figure 7.67, ply #1 is aluminum, ply #2 is steel, both plies are isotropic, and each ply is 0.005-in. thick. It has been determined that the effects of B_{ij}-type coupling on the thermal response of the strip can be neglected. Find the relationship between the temperature change ΔT and the radius of curvature ρ_x. Recall that the curvature $\kappa_x = 1/\rho_x$. The required properties are given below.

Ply thermal expansion coefficients:

$$\text{Aluminum: } \alpha_{Al} = 12.5 \times 10^{-6}/°\text{F}$$
$$\text{Steel: } \alpha_{St} = 6.6 \times 10^{-6}/°\text{F}$$

Laminate-bending compliances:

$$[D'] = \begin{bmatrix} 0.739 & -0.227 & 0 \\ -0.227 & 0.739 & 0 \\ 0 & 0 & 1.928 \end{bmatrix} (\text{psi} - \text{in.}^3)^{-1}$$

Ply stiffness matrices:

$$[Q]_{St} = \begin{bmatrix} 32.817 & 9.615 & 0 \\ 9.615 & 32.817 & 0 \\ 0 & 0 & 11.6 \end{bmatrix} 10^6 \text{psi}$$

$$[Q]_{Al} = \begin{bmatrix} 11.11 & 3.51 & 0 \\ 3.51 & 11.11 & 0 \\ 0 & 0 & 3.8 \end{bmatrix} 10^6 \text{psi}$$

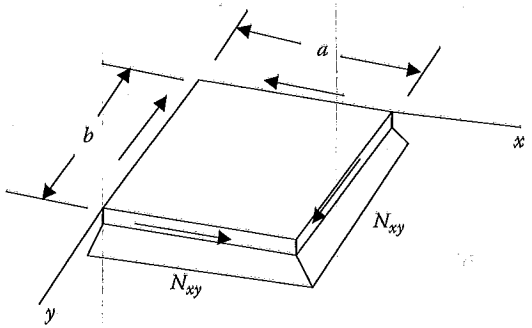

FIGURE 7.68
Simply supported laminated plate under in-plane shear loads for problem 28.

28. The plate in figure 7.68 has edge dimensions a and b and is made from a $[90/0/90]_s$ symmetric cross-ply laminate. The plate is simply supported on all edges and is subjected to a single in-plane shear load N_{xy} along its edges as shown. Answer the following questions below in terms of variables, not numerical values. Do not try to solve the equations, just set them up: (a) write the differential equation governing the buckling behavior of the plate, (b) write the boundary conditions for the plate, and (c) is a solution of the form shown in equation (7.145) in the textbook possible for this problem? If so, why? If not, why not?
29. The nonsymmetrically laminated beam shown in figure 7.69 consists of a substrate material having Young's modulus E_S and a coating material having Young's modulus E_C, and both materials are linear elastic, isotropic, and homogeneous. Using a modified

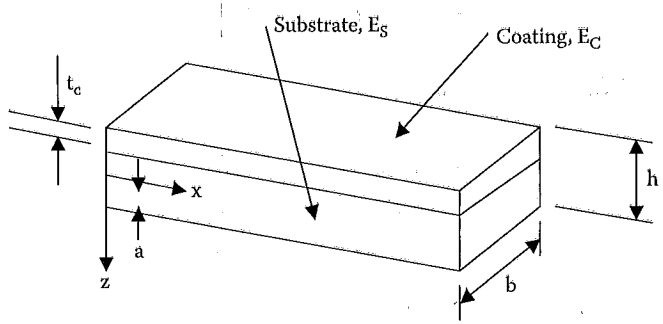

FIGURE 7.69
Nonsymmetrically laminated beam for problem 29.

laminated beam theory, derive the equation for the flexural modulus E_f for the beam. Your answer should be in terms of the given parameters. Hint: Assumption #2 for laminated beam theory in section 7.2 is violated here, so how must the derivation of the flexural modulus in section 7.2 be modified?

References

1. Pagano, N.J. 1967. Analysis of the flexure test of bidirectional composites. *Journal of Composite Materials*. 1, 336–342.
2. Higdon, A., Ohlsen, E.H., Stiles, W.B., Weese, J.A., and Riley, W.F. 1976. *Mechanics of Materials*, 3d ed. John Wiley & Sons, New York.
3. Smith, C.B. 1953. Some new types of orthotropic plates laminated of orthotropic material. *Journal of Applied Mechanics*, 20, 286–288.
4. Pister, K.S. and Dong, S.B. 1959. Elastic bending of layered plates, in *Proceedings of the American Society of Civil Engineers* (*Journal of Engineering Mechanics Division*), 85, EM4, 1–10.
5. Reissner, E. and Stavsky, Y. 1961. Bending and stretching of certain types of heterogeneous aeolotropic elastic plates. *Journal of Applied Mechanics*, 28, 402–408.
6. Stavsky, Y. 1964. On the general theory of heterogeneous aeolotropic plates. *Aeronautical Quarterly*, 15, 29–38.
7. Lekhnitskii, S.G. 1968. *Anisotropic Plates* (translation from the 2d Russian ed.) in Tsai, S.W. and Cheron, T. eds. Gordon and Breach Science Publishers, New York.
8. Stavsky, Y. and Hoff, N.J. 1969. Mechanics of composite structures, in Dietz, A.G.H. ed., *Composite Engineering Laminates*. MIT Press, Cambridge, MA.
9. Timoshenko, S.A. and Woinowsky-Krieger, S. 1959. *Theory of Plates and Shells*, 2d ed. McGraw-Hill, Inc., New York.
10. Whitney, J.M. 1987. *Structural Analysis of Laminated Plates*. Technomic Publishing Co., Inc., Lancaster, PA.
11. Christensen, R.M. 1979. *Mechanics of Composite Materials*. John Wiley & Sons, Inc., New York.
12. Halpin, J.C. 1984. *Primer on Composite Materials: Analysis*. Technomic Publishing Co. Lancaster, PA.
13. Tsai, S.W. 1964. *Structural Behavior of Composite Materials*. NASA CR-71.
14. Pipes, R.B. and Pagano, N.J. 1970. Interlaminar stresses in composite laminates under uniform axial extension. *Journal of Composite Materials*, 4, 538–548.
15. Wang, S.S. and Choi, I. 1982. Boundary layer effects in composite laminates. Part 1: Free edge singularities. *Journal of Applied Mechanics*, 49, 541–548.
16. Wang, S.S. and Choi, I. 1982. Boundary layer effects in composite laminates. Part 2: Free edge solutions and basic characteristics. *Journal of Applied Mechanics*, 49, 549–560.

17. Pipes, R.B. and Daniel, I.M. 1971. Moiré analysis of the interlaminar shear edge effect in laminated composites. *Journal of Composite Materials*, 5, 255–259.
18. Pipes, R.B. and Pagano, N.J. 1974. Interlaminar stresses in composite laminates — An approximate elasticity solution. *Journal of Applied Mechanics*, 41, Series E (3), 668–672.
19. Pagano, N.J. and Pipes, R.B. 1971. The influence of stacking sequence on laminate strength. *Journal of Composite Materials*, 5(1), 50–57.
20. Whitney, J.M. and Browning, C.E. 1972. Free-edge delamination of tensile coupons. *Journal of Composite Materials*, 6(2), 300–303.
21. Whitney, J.M. and Kim, R.Y. 1977. Effect of stacking sequence on the notched strength of laminated composites. *Composite Materials: Testing and Design (Fourth Conference)*, ASTM STP 617, pp. 229–242. American Society for Testing and Materials, Philadelphia, PA.
22. Rybicki, E.F. 1971. Approximate three-dimensional solutions for symmetric laminates under in-plane loading. *Journal of Composite Materials*, 5(3), 354–360.
23. Wang, A.S.D. and Crossman, F.W. 1977. Some new results on edge effect in symmetric composite laminates. *Journal of Composite Materials*, 11, 92–106.
24. Herakovich, C.T. 1981. On the relationship between engineering properties and delamination of composite materials. *Journal of Composite Materials*, 15, 336–348.
25. Hwang, S.J. and Gibson, R.F. 1992. Contribution of interlaminar stresses to damping in thick composites under uniaxial extension. *Composite Structures*, 20, 29–35.
26. Hwang, S.J. 1988. Characterization of the effects of three dimensional states of stress on damping of laminated composites. Ph.D. Dissertation, Mechanical Engineering Department, University of Idaho.
27. Whitney, J.M. 1973. Free edge effects in the characterization of composite materials. *Analysis of the Test Methods for High Modulus Fibers and Composites*, ASTM STP 521, pp. 167–180. American Society for Testing and Materials, Philadelphia, PA.
28. Conti, P. and De Paulis, A. 1985. A simple model to simulate the interlaminar stresses generated near the free edge of a composite laminate, in Johnson, W.S. ed. *Delamination and Debonding of Materials*, ASTM STP 876, pp. 35–51. American Society for Testing and Materials, Philadelphia, PA.
29. Hahn, H.T. and Tsai, S.W. 1974. On the behavior of composite laminates after initial failures. *Journal of Composite Materials*, 8(3), 288–305.
30. Tsai, S.W. 1965. *Strength Characteristics of Composite Materials*. NASA CR-224.
31. Kim, R.Y. and Soni, S.R. 1984. Experimental and analytical studies on the onset of delamination in laminated composites. *Journal of Composite Materials*, 18, 70–80.
32. Whitney, J.M. and Nuismer, R.J. 1974. Stress fracture criteria for laminated composites containing stress concentrations. *Journal of Composite Materials*, 8, 253–265.

33. Brewer, J.C. and Lagace, P.A. 1988. Quadratic stress criterion for initiation of delamination. *Journal of Composite Materials*, 22,1141–1155.
34. O'Brien, T.K. 1982. Characterization of delamination onset and growth in a composite laminate, in Reifsnider, K.L. ed. *Damage in Composite Materials*, ASTM STP 775, pp. 140–167. American Society for Testing and Materials, Philadelphia, PA.
35. Newaz, G.M. ed., 1991. *Delamination in Advanced Composites*. Technomic Publishing Co., Lancaster, PA.
36. Johnson, W.S. ed. 1985. *Delamination and Debonding of Materials*. ASTM STP 876, American Society for Testing and Materials, Philadelphia, PA.
37. Pagano, N.J. ed. 1989. *Interlaminar response of composite laminates*, vol. 5, *Composite Laminates Series*, Pipes, R.B. (series ed.). Elsevier Science Publishers, Amsterdam.
38. Vinson, J.R. and Sierakowski, R.L. 1986. *The Behavior of Structures Composed of Composite Materials*. Martinus Mijhoff Publishers, Dordrecht, The Netherlands.
39. Leissa, A.W. 1985. *Buckling of Laminated Composite Plates and Shell Panels*. AFWAL-TR-85-3069, Air Force Wright Aeronautical Laboratories, Wright-Patterson Air Force Base, OH.
40. Hatcher, D. and Tuttle, M. 1991. Measurement of critical buckling loads and mode shapes of composite panels, in Chung, H.H. and Kwon, Y.W. eds. *Recent Advances in Structural Mechanics*. PVP-Vol. 225/NE-Vol. 7, pp. 21–26. American Society of Mechanical Engineers, New York.
41. Jones, R.M. 1975. *Mechanics of Composite Materials*. Hemisphere Publishing Co., New York, pp. 264–270.
42. Dropek, R.K. 1987. Numerical design and analysis of structures, in Reinhart, T.J. ed. *Engineered Materials Handbook*, vol. 1, *Composites*, pp. 463–478. ASM International, Materials Park, OH.
43. Peters, S.T., Humphrey, W.D., and Foral, R.F. 1991. *Filament Winding Composite Structure Fabrication*, pp. 5–45. Society for Advancement of Materials and Process Engineering, Covina, CA.
44. Kelly, A. and Zweben, C. eds. 2000. *Comprehensive Composite Materials*, vols 1–6. Elsevier, Amsterdam.
45. Mallick, P.K. ed. 1997. *Composites Engineering Handbook*. Marcel Dekker, Inc., New York.
46. Harper, C.A., ed. 2002. *Handbook of Plastics, Elastomers and Composites*. McGraw-Hill Co., New York.
47. Donaldson, S.L. and Miracle, D.B. eds. 2001. *ASM Handbook, Composites*, vol. 21. ASM International.
48. U.S. Department of Defense, 2002. *MIL-HDBK-17, Handbook of Composites*, vols 1–5. Available online at http://assist.daps.dla.mil/quicksearch/ (type in MIL-HDBK-17 in the Document ID box and click on Submit).
49. Vinson, J.R. and Sierakowski, R.L. 2002. *The Behavior of Structures Composed of Composite Materials*, 2d ed. Kluwer Academic Publishers, Dordrecht, The Netherlands.
50. Kollar, L.P. and Springer, G.S. 2003. *Mechanics of Composite Structures*. Cambridge University Press, Cambridge.

51. Sun, C.T. 1998. *Mechanics of Aircraft Structures*. John Wiley & Sons, Inc., New York.
52. Vinson, J.R. 1999. *The Behavior of Sandwich Structures of Isotropic and Composite Materials*. CRC Press, Boca Raton, FL.
53. Steeves, C.A. and Fleck, N.A. 2004. Collapse mechanisms of sandwich beams with composite faces and a foam core, loaded in three-point bending. Part II: Experimental investigation and numerical modeling. *International Journal of Mechanical Sciences*, 46, 585–608.
54. Zenkert, D. 1995. *An Introduction to Sandwich Construction*. Chameleon, London.
55. Steeves, C.A. and Fleck, N.A. 2004. Collapse mechanisms of sandwich beams with composite faces and a foam core, loaded in three-point bending. Part I: analytical models and minimum weight design. *International Journal of Mechanical Sciences*, 46, 561–583.
56. Rehfield, L.W. 1999. A brief history of analysis methodology for grid-stiffened geodesic composite structures. *Proc. 44th International SAMPE Symposium*, CD-ROM.
57. Chen, H.J. and Tsai, S.W. 1996. Analysis and optimum design of composite grid structures. *Journal of Composite Materials*, 30(4), 503–534.
58. Huybrechts, S. and Tsai, S.W. 1996. Analysis and behavior of grid structures. *Composites Science and Technology*, 56(9), 1001–1015.

8

Analysis of Viscoelastic and Dynamic Behavior

8.1 Introduction

In the analyses of chapter 1 to chapter 7, it has been assumed that the applied loads are static in nature and that the composite and its constituents exhibit time-independent linear elastic behavior. However, composite structures are often subjected to dynamic loading caused by vibration or wave propagation. In addition, many composites exhibit time-dependent viscoelastic behavior under load; this is particularly true for composites having polymeric constituents. This chapter contains the basic information needed for the analysis of both viscoelastic and dynamic behavior of composites and their constituents.

The word "viscoelastic" has evolved as a way of describing materials that exhibit characteristics of both viscous fluids and elastic solids. Polymeric materials, which are known to be viscoelastic, may behave like fluids or solids, depending on the time scale or the temperature. For example, polycarbonate, a thermoplastic polymer, is a liquid during molding at processing temperatures, but is a glassy solid at service (ambient) temperatures. It will deform like a rubber at temperatures just above the glass transition temperature, T_g. At temperatures below T_g, however, it will deform just as much, and in the same way if the test time is long enough.

We know that ideal Hookean elastic solids are capable of energy storage under load, but not energy dissipation, whereas ideal Newtonian fluids under nonhydrostatic stresses are capable of energy dissipation, but not energy storage. Viscoelastic materials, however, are capable of both storage and dissipation of energy under load. Another characteristic of viscoelastic materials is memory. Perfectly elastic solids are said to have only "simple memory" because they remember only the unstrained state and the current strains depend only on the current stresses. Viscoelastic materials have what is often referred to as "fading memory" because they remember the past in such a way that the current strains depend more strongly on the recent stress–time history than on the more distant